OCRWM	MODEL COVER SHEET	1. QA: QA Page 1 of 144

2. Type of Mathematical Model

☒ Process Model ☐ Abstraction Model ☐ System Model

Describe Intended Use of Model

The purpose of this Model Report is to document drift-scale modeling of coupled thermal-hydrological-mechanical (THM) processes around a drift containing heat-releasing waste inventory, as well as to study the impact of THM processes on seepage and flow in the near-field rock.

3. Title

Drift Scale THM Model

4. DI (Including Rev. No. and Change No., if applicable)

MDL-NBS-HS-000017 REV00

5. Total Attachments	6. Attachment Numbers - No. of Pages in Each
3	I-4, II-3, III-2

	Printed Name	Signature	Date
7. Originator	J. Rutqvist	SIGNATURE ON FILE	8/6/03
8. CSO	J. Yamlow	SIGNATURE ON FILE	8-6-03
9. Checker	R.A. Wagner	SIGNATURE ON FILE	6 Aug 03
10. QER	W.F. Hoiub	SIGNATURE ON FILE	8-6-03
11. Responsible Manager/Lead	J.S.Y. Wang/ Y. Tsang	SIGNATURE ON FILE	8-6-03 8-6-03
12. Responsible Manager Per	P. Dixon Ernest Hardin	SIGNATURE ON FILE	8/6/03

13. Remarks

Initial Issue

Technical Error Report (TER) for numbers addressed in this model report

N/A. Note: TER-02-0074 and TER-02-0101 were assessed against ANL-NBS-HS-000037 and are not applicable to this model report (MDL-NBS-HS-000017 REV00)

MODEL REVISION RECORD

2. Model Title:
Drift Scale THM Model

3. DI (including Rev. No. and Change No., if applicable):
MDL-NBS-HS-000017 REV00

4. Revision/Change No.	5. Description of Revision/Change
	MDL-NBS-HS-000017 REV00 was previously issued as an analysis report entitled, Coupled Thermal-Hydrologic-Mechanical Effects on Permeability Analysis and Models Report, ANL-NBS-HS-000037 REV 00 (BSC 2001 [155957]).
REV00	Initial Issue

TABLE OF CONTENTS

TABLE OF CONTENTS (Continued)

LIST OF FIGURES

LIST OF FIGURES (Continued)

LIST OF FIGURES (Continued)

INTENTIONALLY LEFT BLANK

LIST OF TABLES

INTENTIONALLY LEFT BLANK

ACRONYMS

1-D	one-dimensional
2-D	two-dimensional
3-D	three-dimensional
AFM	Active Fracture Model
AMR	Analysis/Model Report
BSC	Bechtel SAIC Company, LLC
CDTT	Cross-Drift Thermal Test
CRWMS	Civilian Radioactive Waste Management System
DIRS	Document Input Reference System
DST	Drift Scale Test
DTN	Data Tracking Number
EBS	Engineered Barrier System
ESF	Exploratory Studies Facility
FEP	features, events, and proceses
GFM	Geological Framework Model
HM	hydrological-mechanical
LA	License Application
LBNL	Lawrence Berkeley National Laboratory
M&O	Management and Operating Contractor
MPBX	multiple-point borehole extensiometer
OCRWM	Office of Civilian Radioactive Waste Management
PA	Performance Assessment
QA	Quality Assurance
SCM	Software Configuration Management
SHT	Single Heater Test
TBD	to be determined
TBV	to be verified
TDMS	Technical Data Management System
TH	thermal-hydrological
THC	thermal-hydrological-chemical

ACRONYMS (Continued)

THM	thermal-hydrological-mechanical
TM	thermal-mechanical
TSPA	Total System Performance Assessment
TWP	Technical Work Plan
USGS	United States Geological Survey
UZ	unsaturated zone
UZ Model	Unsaturated Zone Flow and Transport Model
YMP	Yucca Mountain Project
YMRP	*Yucca Mountain Review Plan, Final Report*

Additional Geological Abbreviations

CHn	Calico Hills and Lower Painbrush nonwelded thermal mechanical unit
PTn	Upper Pantbrush Tuff nowelded thermal mechanical unit
TCw	Tiva Canyon welded thermal mechanical unit
Tptpmn	Topopah Spring tuff middle nonlithophysal unit
Tptpll	Topopah Spring tuff lower lithophysal unit
Tptpul	Topopah Spring tuff upper lithophysal unit
TSw1	Topopah Spring lithophysal-rich thermal mechanical unit
TSw2	Topopah Spring lithophysal-poor thermal mechanical unit
TSw3	Topopah Spring vitrophyre thermal mechanical unit

1. PURPOSE

The purpose of this Model Report is to document drift-scale modeling of coupled thermal-hydrological-mechanical (THM) processes around a drift containing heat-releasing waste packages, as well as to study the impact of THM processes on permeability and flow in the near-field rock. The heat generated by the decay of radioactive waste results in elevated rock temperatures for thousands of years after waste emplacement. Depending on the thermal load, these temperatures are high enough to cause boiling conditions in the rock, resulting in water redistribution and altered flow paths. These temperatures will also cause thermal expansion of the rock, with the potential of opening or closing fractures and thus changing fracture permeability in the near field. Understanding the THM coupled processes is important for the performance of the repository because the thermally induced permeability changes potentially affect the spatial distribution of percolation flux in the vicinity of the drift, and hence the seepage of water into the drift.

The main model outputs from this Model Report are the potential changes in permeability and their impact on the flow field around the drift. The results supplement thermal seepage results from thermal-hydrological (TH) simulations reported in the Model Report entitled *Drift-Scale Coupled Processes (DST and TH Seepage) Models*, MDL-NBS-HS-000015 REV 00 (BSC 2003 [161530]), which feeds the Model Report *Abstraction of Drift Seepage* (upcoming revision of MDL-NBS-HS-000019 REV 00) (CRWMS M&O 2001 [154291]) where probability distributions of ambient and thermal seepage shall be developed for use in TSPA. To ensure consistency between the present Model Report and the TH study (BSC 2003 [161530], Section 6.2), the same conceptual model and TH properties are used.

The present Model Report is not concerned with drift degradation effects, which require a discontinuum analysis for prediction of rock fall and block size distribution. The latter is the subject of a separate Model Report, *Drift Degradation Analysis* (BSC 2003 [164285]).

The analyses documented in this report were conducted under the *Technical Work Plan (TWP) for: Performance Assessment Unsaturated Zone,* TWP-NBS-HS-000003 REV 02 (BSC 2002 [160819]). The relevant TWP sections for this work are Section 1.12, entitled "Coupled Effects on Flow & Seepage" (Work Package [WP] AUZM08), and Attachment I, entitled "Model Validation Plans" (Section I-3-3-1). Note that this Model Report has a new ID, U0250 (it was previously identified as N0030 within the TWP). In accordance with the TWP, the work scope of this Model Report includes prediction of coupled THM effects on fracture permeability and flow field at the drift scale and validation against measurements from the ongoing Drift Scale Test.

The coupled THM model reported in this Model Report builds upon insight obtained in earlier studies involving a sequential snapshot approach, in which thermal-mechanical (TM) analyses were made on the results of TH simulations to obtain thermal stresses, which, in turn, were used in an independent analysis to calculate fracture permeability changes. More specifically, in the Analysis/Model Report (AMR) entitled *Calculation of Permeability Change Due to Coupled Thermal-Hydrological-Mechanical Effects* (CRWMS M&O 2000 [149040]) (and later updated in BSC (2001 [155957]), TM behavior of a region of fractured rock surrounding a section of a long horizontal emplacement drift was simulated. The effects of drift excavation, and of heating

and cooling cycles associated with the radioactive waste packages, on the directions and magnitudes of the principal stresses were calculated, using the distinct-element code 3 DEC V2.0 (Itasca Consulting Group 1998 [148865]). Results include rotation of the principal stress direction and separate changes in permeability values for the vertical and subvertical fractures and for horizontal fracture sets. Such changes appear to persist throughout the 1,000-year simulation period reported in that AMR.

The present Model Report involves development and application of a new, fully coupled THM methodology, based on joining two well-established codes through carefully designed linkage routines. The first is the TOUGH2 V1.6 code (LBNL 2003 [161491]), which uses the dual-permeability continuum (fracture and matrix continua) approach. This code has proven successful in predicting the temperature and moisture distribution of field experiments at Yucca Mountain, including the Single Heater Test (CRWMS M&O 1999 [129261], Section 8.7) and the Drift Scale Test (BSC 2001 [157330], Section 6). The second is the rock mechanics-standard FLAC3D V2.0 code, which can calculate fractured-rock mechanical processes in a continuum model. The two codes, TOUGH2 V1.6 and FLAC3D V2.0 (LBNL 2001 [154783]), are linked through two coupling functions, one that dictates TM coupling (TOUGH2 V1.6 to FLAC3D V2.0 coupling) and one that dictates hydrological-mechanical (HM) coupling (FLAC3D V2.0 to TOUGH2 V1.6 coupling).

The predictive simulations from the Drift-Scale THM Model are performed in two-dimensional vertical cross sections perpendicular to the axis of a representative waste emplacement drift. Different cross sections (model domains) are studied, depending on the location of the drifts. The Tptpmn model domain has the emplacement drift located in the Topopah Spring Tuff middle nonlithophysal unit (Tptpmn). The Tptpll model domain has the emplacement drift located in the Topopah Spring Tuff lower lithophysal unit (Tptpll). This Model Report considers a thermal load representative of the average thermal conditions for the current repository design, resulting in maximum rock temperatures close to emplacement drifts that are above the boiling point of water for several hundred years.

Relevant simulation results from the Drift-Scale THM Model are given in Sections 6.5 (Tptpmn model domain) and 6.6 (Tptpll model domain). The results include the distribution of calculated changes in hydraulic properties, in particular calculated changes in horizontal and vertical intrinsic permeability and their impact on the vertical percolation flux around the emplacement drift.

Measured data from the ongoing Drift Scale Test (DST) are used to evaluate and validate the Drift-Scale THM Model. The geometry of the DST Heated Drift is consistent with the current designs of the potential repository and can therefore provide a test of the Drift-Scale THM Model at a relevant scale. The simulation of the DST is conducted with the Drift-Scale THM Model on a model domain constructed for the DST—the DST model domain. Validation results are provided in Section 7.

The limitations of the Drift-Scale THM Model, as for all predictive models, are defined by the conceptual model (Section 6.2) and by the uncertainties and validity ranges of input data (Section 6.4 and Section 7). Because modeling of coupled processes is so computationally intensive, the TH Seepage Model is conducted in two-dimensional (2-D) vertical sections rather

than with a three-dimensional (3-D) representation. For the same reason, it is not feasible to conduct systematic sensitivity studies by variation of many input parameters over a wide range of values. Rather, a conservative estimate of key parameters for evaluating the impact of coupled THM effects on flow have been carefully selected (see Section 6.4).

INTENTIONALLY LEFT BLANK

2. QUALITY ASSURANCE

Development of this Model Report and the supporting modeling activities have been determined to be subject to the Yucca Mountain Project's quality assurance (QA) program as indicated in *Technical Work Plan for: Performance Assessment Unsaturated Zone,* TWP-NBS-HS-000003 REV 02 (BSC 2002 [160819], Section 8.2, Work Package (WP) AUZM08). Approved QA procedures identified in the TWP (BSC 2002 [160819], Section 4) have been used to conduct and document the activities described in this model report. The TWP also identifies the methods used to control the electronic management of data (BSC 2002 [160819], Section 8.4, WP AUZM08) during the modeling and documentation activities.

This Model Report provides drift-scale THM processes of a natural barrier that is important to the demonstration of compliance with the postclosure performance objectives prescribed in 10 CFR 63.113 [156605]. Therefore it is classified as a "Quality Level – 1" with regard to importance to waste isolation, as defined in AP-2.22Q, *Classification Criteria and Maintenance of the Monitored Geologic Repository Q-List*. The report contributes to the analysis and modeling data used to support performance assessment; the conclusions do not directly impact engineered features important to safety, as defined in AP-2.22Q.

INTENTIONALLY LEFT BLANK

3. USE OF SOFTWARE

A list of software codes and routines used in this Model Report is given in Table 3-1. The software codes and routines have been baselined in accordance with AP-SI.1Q, *Software Management*. All software used is considered appropriate for the intended use, has been applied in the range of the validation, and was obtained from the Software Configuration Management (SCM).

Commercial off-the-shelf software applications Tecplot Version 8.0 and MS Excel 97 SR-2 were used for graphic visualization. In a few cases, computations were performed using this commercial off-the-shelf software program and are exempt from AP-SI.1Q. All information to reproduce these computations using the standard software programs is included in this report, within the specified reference (i.e., the Scientific Notebooks listed in Table 6-1).

Table 3-1. Qualified Software and Routines Used in This Report

Item No.	Software Name	Version	Software Tracking Number (STN)	DIRS
1.	TOUGH2	1.6	10007-1.6-01	161491
2.	FLAC3D	2.0	10502-2.0-00	154783
3.	Gpzones.dat	1.0	10509-1.0-00	154792
4.	Tin	1.1	10889-1.1-00	162038
5.	Delb.dat	1.0	10507-1.0-00	154791
6.	2KGRIDV1.F	1.0	10244-1.0-00	147553
7.	EXT	1.0	10047-1.0-00	147562

INTENTIONALLY LEFT BLANK

4. INPUTS

4.1 DATA AND PARAMETERS

This section provides documentation for data input to the Model Report. Data input to the Model Report are referred to by Data Tracking Number (DTN) or by reference listed in Table 4.1-1 and 4.1-2. Section 4.1.1 provides details about input references to the predictive analysis with the Drift-Scale THM Model. Section 4.1.2 provides input references for the coupled THM analysis of the DST used as corroborative information for model validation, and Section 4.1.3 summarizes measured data from the DST and niches used as corroborative information for model validation.

Note that this Model Report uses the nomenclature for lithostratigraphic units defined in the Geologic Framework Model (BSC 2002 [159124]), while some DTNs refer to the same lithostratigraphic units using the nomenclature of the unsaturated zone (UZ) model reports. The relationship between these are given in several model reports, e.g., in BSC (2003 [160109], Table 11).

4.1.1 Input Data to Drift-Scale THM model used for Predictive Analysis

This subsection summarizes input data and provides references for input to the Drift-Scale THM Model used for predictive analysis of a repository drift located in the Tptpmn unit (Tptpmn model domain) and Tptpll unit (Tptpll model domain).

4.1.1.1 Rock Properties

Hydrological properties (such as permeability, van Genuchten parameters, residual saturation for both the fractures and the matrix, and the active fracture parameter for the fractures) used in the Drift-Scale THM Model are excerpted from the UZ drift-scale calibrated property set for the mean infiltration scenario (DTN: LB0208UZDSCPMI.002 [161243]). The procedures adopted in developing these properties can be found in *Calibrated Properties Model* (BSC 2003 [160240], Section 6.3.2). Other sources used for hydrological, thermal, and mechanical properties are consistent with current UZ analyses and analyses of coupled processes. This includes other hydrological properties such as fracture porosity, frequency, aperture, and interface areas obtained from DTN: LB0205REVUZPRP.001 [159525]. Thermal properties and matrix porosity are taken from DTN: LB0210THRMLPRP.001 [160799]. A more detailed description of thermal properties can be found in *Analysis of Hydrologic Properties Data* (BSC 2003 [161773], Section 6.3). Together, these hydrological and thermal properties will be referred to as the DS/AFM-UZ02-Mean property set in this Model Report. Mechanical properties of the rock mass (Young's Modulus and Poisson's ratio) are extracted from the 1999 TBV-332/TBD 325 Resolution Analysis: Geotechnical Rock Properties (DTN: MO9911SEPGRP34.000 [148524]). The Young's modulus and Poisson's ratio for TCw, PTn, TSw1, and TSw2 TM units are extracted from MO9911SEPGRP34.000 [148524], Table 10 and Table 11 for 40% cumulative frequency. The mechanical properties of TSw3 are assumed to be equal to TSw2 (Assumption 3 in Section 5) and the mechanical properties of CHn TM unit are extracted from intact rock values given in MO9911SEPGRP34.000 [148524], Table 8 (Assumption 4 in Section 5). Source DTNs for hydrological, thermal, and mechanical properties are given in Table 4.1-1. For quick reference,

values of these properties are listed in Table 4.1-3 for the stratigraphic units Topopah Spring Tuff middle nonlithophysal (Tptpmn or tsw34) and lower lithophysal (Tptpll or tsw35), in which the main part of the repository will be located. For the sake of completeness, properties for the upper lithophysal (Tptpul or tsw33) unit are also provided.

The open space of the emplacement drift is represented by an element of high permeability, high porosity, and small capillarity. The drift element is also assigned a large heat conductivity to simulate the effective radiative heat transfer within the drift. Since the flow and transport processes within the drift (including the waste packages) are not explicitly modeled in this Model Report, these input properties of the drift elements are part of the conceptual model for the simulation analyses; they are not direct inputs to this Model Report.

4.1.1.2 Boundary Conditions

The infiltration rates applied at the top of the TH Seepage Model are adopted from the mean infiltration scenario that includes present-day (0 to 600 years), monsoon (600 to 2,000 years), and glacial transition climates (more than 2,000 years), as described in the AMR *Simulation of Net Infiltration for Modern and Potential Future Climates* (USGS 2001 [160355], Sections 6.9 and 6.11). The specific infiltration values, 6, 16, and 25 mm/year for the present-day, monsoon, and glacial transition periods, respectively, represent repository-wide averages. These values have been calculated as the arithmetic average of the 31 repository locations considered in the *Multiscale Thermohydrologic Model* (BSC 2001 [158204], Section 6.3.1). Infiltration values at these 31 repository locations are provided in DTN: LL000114004242.090 ([142884], file chimney_infiltration_fluxes). The calculation for deriving the repository-wide averages is given in BSC (2003 [161530], Attachment II).

The top and bottom boundary conditions for the TH Seepage Model represent the conditions at the USW SD-9 borehole, at column “i64” of the Unsaturated Zone Flow and Transport Model (UZ Model) grid (for the Tptpmn Submodel), and the conditions at the center of the repository, at column “j34” of the UZ model grid (for the Tptpll Submodel), respectively. Values are given in DTN: LB991131233129.004 ([162183], file “pa99cal_ecm.out” in directory /AMR U0050 Data_1.6.00/LB991131233129.004-Charles). Elements with names “Tpi64” and “Bti64” provide pressure, saturation, and temperature conditions at the top and the bottom of the Tptpmn model domain, respectively. Elements with names “Tpj34” and “Btj34” provide pressure, saturation, and temperature conditions at the top and bottom of the Tptpll model domain, respectively. Further information on developing these boundary conditions can be found in BSC (2001 [158726], Section 6). The infiltration rates and the model boundary conditions used in this Model Report are identical to the ones used in the THC modeling described in BSC (2002 [158375], Tables 11 and 12). The specific values used in this Model Report are presented in Table 6.3-1 and Figure 6.3-1. Source DTNs for boundary conditions are given in Table 4.1-1.

4.1.1.3 Thermal Load

The thermal output of individual waste packages placed into drifts is represented by an average thermal line load, which is 1.45 kW/m according to current designs. After emplacement of all waste packages over 24 years, a 50-year ventilation period is planned, in which a significant fraction of the heat is removed from the repository. The thermal line load of 1.45 kW/m and the

50-year ventilation period are described in repository design drawing 800-IED-EBS0-00201-000-00A (BSC 2003 [164069], *Repository Design Project, Repository/PA IED Emplacement Drift Configuration*, *1 of 2* effective date 5/30/2003). Note that the value of 1.45 kW/m refers to the initial thermal line load at emplacement time. This value decreases with time as a result of radioactive decay. The time-dependent thermal-line-load values used in this report stems from the repository design drawing DWG-MGR-MD-000003 REV A (BSC 2002 [159527], *Repository Design, Repository/PA IED Subsurface Facilities Plan Sht. 5 of 5*, effective date 05/20/2002). BSC (2002 [159527]) has been superseded by 800-IED-WIS0-00204-000-00A (BSC 2003 [164136], *Repository Design Project, RPD/PA IED Typical Waste Package Assembly (4)*, effective date 06/30/2003, during the writing of this report. The values given in BSC (2003 [164136]) are within 1% of values given in BSC (2003 [164136]). The ventilation efficiency during the 50-year period is 86%, as given in Section 8.1 of BSC (2003 [164576]). Ventilation efficiency is the fraction of heat removed from the repository. In BSC (2003 [164576]) the calculated values of ventilation efficiency is 86% or 88% for an 800 m and 600 m drift, respectively. As noted in BSC (2003 [164576]), Section 8.1, the difference in ventilation efficiency between these two cases is small. Furthermore, adopting 86% is conservative for the aim of this Model Report since this result in a slightly higher actual heat load and a slightly higher temperature in the rock mass. All thermal load parameters are consistent throughout the UZ and coupled processes models. All source DTNs for thermal load are given in Table 4.1-1.

4.1.1.4 Grid Design Data

The data needed for grid design are the stratigraphy at the respective locations of the Tptpmn and the Tptpll model domain, and the data related to the configuration of emplacement drifts. For the Tptpmn model domain, the stratigraphy at borehole USW SD-9 is chosen as representative for the vertical profile. Geologic data from this borehole, as implemented in UZ Model grid (DTN: LB990501233129.004 [111475], file primary.mesh, column “i64”), were used as the basis to map geological contacts into the Tptpmn model domain. The stratigraphy of the Tptpll model domain is extracted at a location near the center of the potential repository (at approximately Nevada State Plane coordinates E170572, N233195), close to the area of the proposed Cross-Drift Thermal Test. Geologic data from column “j34” of the UZ Model grid (DTN: LB990501233129.004 [111475], file primary.mesh), are used to map geologic contacts into the 2-D mesh. Note that the stratigraphy of both submodels corresponds to an earlier version of the Geologic Framework Model (CRWMS M&O (2000 [138860]), as explained in Section 5, Assumption 1. Information on drift geometry and configuration are presented in this section because they are used as input for the grid design. The current drift configuration, as given in repository design drawing 800-IED-EBS0-00201-000-00A (BSC 2003 [164069], *Repository Design Project, Repository/PA IED Emplacement Drift Configuration 1 of 2*, effective date 5/30/2003), calls for a drift diameter of 5.5 m and a drift spacing of 81 m. There is no backfill in the drifts. The in-drift geometry for waste package and drip-shield configuration is not explicitly accounted for in the Drift-Scale THM, because effective radiative heat exchange is assumed within the open drift. Source DTNs for Grid Design Data are given in Table 4.1-1.

4.1.2 Input Data to DST Model Domain Used for Model Validation

This subsection summarizes input data and provides input references for the Drift-Scale THM Model applied to the DST model domain and used as corroborative information for model

validation against measurements at the DST. The values in Table 4.1-4 are properties used in the DST model domain. The validation method between the Drift-Scale THM Model simulation results and measured values in the DST includes (Section 7):

1. Checking that the simulated temperature field is in reasonable agreement with the observed temperature field to ensure that the THM model is properly implemented in terms of thermal behavior.

2. Checking that simulated rock-mass displacements capture the general trends and average magnitudes of observed displacements (validation of TM processes).

3. Checking that the simulated changes in air permeability capture the general trends and magnitudes observed in the field (validation of THM processes).

TM and HM properties of the rock mass developed in this analysis are used in the validation (i.e. initial hydraulic aperture, parameters for the stress-aperture function, and thermal expansion coefficient). Sections 4.1.2.4 through 4.1.3.4 describe observed measurements associated with DST. The DST measurements shown in Table 4.1-5 include data acquired for validation of the THM model. Source DTNs for all inputs related to the model validation are given in Table 4.1-2.

4.1.2.1 Rock Properties

The DST model domain is designed for comparative model analysis with the measured data from the DST, utilizing a TH property set partially based on site-specific characterization of the DST test block. This data set, referred to as DKM-TT99, is described in the previous *Thermal Tests Thermal-Hydrological Analyses/Model Report* (BSC 2001 [157330], Section 4.1, Table 5). The DKM-TT99 property set is selected because it is more representative of the rock at the DST than the alternative UZ drift-scale calibrated properties. The fracture frequency, noted as N/A in BSC 2001 [157330], Section 4.1, Table 5 for the DKM-TT99, is extracted from the current estimates given in LB0205REVUZPRP.001 [159525]. Mechanical properties of the rock mass (Young's Modulus and Poisson's ratio) are extracted from the 1999 TBV-332/TBD 325 Resolution Analysis: Geotechnical Rock Properties (DTN: MO9911SEPGRP34.000 [148524]). The Young's modulus and Poisson's ratio for TSw1 and TWw2 TM units are extracted from MO9911SEPGRP34.000 [148524], Table 10 and Table 11 for 40% cumulative frequency, and are identical to those in the Predictive Drift-Scale THM Analysis (Section 4.1.1.1). TH properties of the DKM-TT99 property set and mechanical properties are summarized in Table 4.1-4 for the three geological units comprising the DST model domain, namely the Tptpul, the Tptpmn, and the Tptpll. Fracture frequency and other hydrological properties are obtained from other sources, but are consistent with mean input values used in the UZ and other coupled process models, including predictive analyses.

4.1.2.2 Boundary Conditions

The top and bottom model boundary conditions are identical to the ones used in the *Thermal Tests Thermal-Hydrological Analyses/Model Report* (BSC 2001 [157330], Section 6.1.2). The boundary condition values are given in DTN: LB000300123142.001 ([148120], file "Incon.heat" in directory /LBNL_DST_AMR_DKMTT99). Elements with names "Tt001" and "tt001" provide pressure, saturation, and temperature conditions at the top, while elements with names

"Bb001" and "bb001" provide pressure, saturation, and temperature conditions at the bottom of the model domain (for both fracture and matrix continua). These boundary values were developed from simulations of a one-dimensional (1-D) column extending from the land surface to the water table, mapped to the location of the top and bottom of the model domain.

4.1.2.3 Thermal Load

In the DST, heat is provided by nine canister heaters, located on the floor of the Heated Drift. Additional heating is provided by 50 wing heaters (see Section 7.2.1). The total output power from both the canister and the wing heaters has been continuously collected. Average values of these total powers over certain time periods have been used in the DST model domain (see Section 7.3.4 for more details.). Table 4.1-2 provides a list of DTNs for the total canister and wing heater powers at various times.

4.1.2.4 Borehole and Sensor Location Data

Passive monitoring of thermal-hydrological-mechanical (THM) data (such as temperature, pressure, and displacement) from the DST are carried out with measurement sensors located in a number of boreholes (see Figure 7.2.1-2). Active monitoring of data (such as periodic air-injection tests) are carried out in boreholes specifically designed for such purposes. Results from the model simulation are compared directly against these measured data from the DST. Though the boreholes and the sensors have not been explicitly modeled in the DST model domain, the 3-D numerical grid has been developed in such a way that simulated THM data can be easily interpolated to specific sensor location. The DTN containing these design parameters of the DST is listed in Table 4.1-2.

4.1.3 Measurements at the DST and Niches

The data presented in this subsection is considered as corroborative information (other input information), since it is used for model validation purposes. In Section 7, the Drift-Scale THM Model is validated by comparison to measured data at DST and niches. The input information on measurement data used for validation are explained below and summarized in Table 4.1.5.

4.1.3.1 Temperature Measurements at DST

Temperature data, similar to heater power in Section 4.1.2.3, have been continuously collected from the DST. For model validation, these measured temperatures are directly compared against simulated temperatures. The DTNs for the measured temperature data are listed in Table 4.1-5.

4.1.3.2 Air-Permeability Measurements at DST

Periodic air-permeability-measurement testing has been carried out at the DST. The air permeability at the DST also includes a pre-test baseline test to capture the ambient condition in the fractures. Subsequent air-permeability measurements during heating and cooling at the DST are used to determine fractional changes in air permeability. These measured air-permeability ratios are compared against simulated air-permeability ratios. The DTNs for measured air-permeability ratios are listed in Table 4.1-5.

4.1.3.3 Displacement Measurements at DST

Displacement data have been continuously collected from multiple-point borehole extensometers (MPBX) at the DST. For model validation, these measured displacements are directly compared against simulated displacements from the model simulation. The DTNs for the measured displacement data are listed in Table 4.1-5.

4.1.3.4 Air-Permeability Measurements at Niches

Air-permeability measurements were conducted at several excavated niches to study permeability changes near a drift wall caused by excavation effects (i.e., mechanical unloading of the rock mass near the drift wall, causing fracture opening and consequently permeability increase). These types of tests were conducted at three excavated niches located in the Tptpmn unit and one excavated niche located in the Tptpll unit. For model validation, the measured changes in permeability induced by the excavation of the niches (air-permeability ratio) are compared to model simulations. The DTNs for measured air-permeability ratios are listed in Table 4.1-5.

Table 4.1-1. Data Tracking Numbers for Sources of Data Input to the Drift-Scale THM Model Used for Predictive Analysis

DTNs/Reference	Description	TDMS Input	Design Input	Other Analyses/
Rock Properties (Section 4.1.1.1)				
LB0205REVUZPRP.001 [159525]	Fracture parameters such as porosity, aperture, frequency and interface area (Table 4.1-3)	X		
LB0208UZDSCPMI.002 [161243]	Fracture and matrix calibrated parameters—Mean Infiltration (Table 4.1-3)	X		
LB0210THRMLPRP.001 [160799]	Matrix thermal data and porosity	X		
MO9911SEPGRP34.000 [148524] MOL.19991005.0235 Table 10 and Table 11 for 40% cumulative frequency	Rock mass mechanical properties (Young's modulus and Poisson's ratio in Table 4.1-3)	X		
Boundary Conditions (Section 4.1.1.2)				
BSC 2003 [161530], Attachment II[1]	Infiltration rates for present day, monsoon, and glacial periods (Table 6.3-1 and Figure 6.3-1) The median infiltration case is used in this report for both Tptpmn and Tptpll model domains			X
LB991131233129.004 [162183] File "pa99cal_ecm.out" in directory /AMR U0050 Data_1.6.00/LB991131233129.004 -Charles: Elements Tpi64 and Bti64 for top and bottom of Tptpmn model domain Elements Tpj34 and Btj34 for top and bottom of Tptpll model domain	Top and bottom boundary temperatures, pressure, liquid/gas saturations (Table 6.3-1 and Figure 6.3-1) At borehole USW SD-9 for Tptpmn model domain At center of the repository for Tptpll model domain (Nevada State Plane coord. E170572, N233195)	X		
Thermal Load (Section 4.1.1.3)				
800-IED-WIS0-00204-000-00A BSC 2003 [164136]	Thermal decay (Figure 6.5.2-1)		X	
800-IED-EBS0-00201-000-00A (BSC 2003 [164069])	Heat load (1.45 kW/m)		X	
BSC 2003 [164576], Section 8.1	Ventilation efficiency (86%)			X
Grid Design Data (Section 4.1.1.4)				
LB990501233129.004 [111475] File primary.mesh Column i64 for Tptpmn model domain Column j34 for Tptpll model domain	Stratigraphy taken from UZ model grid At borehole USW SD-9 for Tptpmn model domain At center of the repository for Tptpll model domain (Nevada State Plane coord. E170572, N233195)	X		
800-IED-EBS0-00201-000-00A (BSC 2003 [164069])	Drift geometry (diameter and spacing)		X	

NOTE: [1] Infiltration rates calculated from DTN: LL000114004242.090 [142884]

Table 4.1-2. Data Tracking Numbers for Sources of Data Input to the Drift-Scale THM Model Used for Corroborative Information in Model Validation

DTNs/Reference	Description	TDMS Input	Design Input	Other Analyses/
Rock Properties (Section 4.1.2.1)				
ANL-NBS-TH-000001 REV 00 ICN 02 (BSC 2001 [157330], Section 4.1, Table 5)	Matrix and fracture thermal and hydrological properties for simulations with the DKM-TT99 property set (Table 4.1-4)			X
LB0205REVUZPRP.001 [159525]	Fracture frequency (Table 4.1-4)	X		
MO9911SEPGRP34.000 [148524] MOL.19991005.0235 Table 10 and Table 11 for 40% cumulative frequency	Rock-mass mechanical properties (Young's modulus and Poisson's ratio in Table 4.1-4)	X		
Boundary Conditions (Section 4.1.2.2)				
LB000300123142.001 [148120] File "Incon.heat" in directory /LBNL_DST_AMR_DKMTT99) Elements Tt001 and tt001 for top Elements Bb001 and bb001 for bottom	Top and bottom boundary temperature, pressure, saturation (Figure 7.3-1)	X		
Thermal Load (Section 4.1.2.3)				
BSC 2003 [161530], Table 7.3.4-1[1]	Drift Scale Test average heating phase power (Table 7.3-1)			X
DST Borehole and Sensor Locations (Section 4.1.2.4)				
MO0002ABBLSLDS.000 [147304]	Coordinates of borehole collar and bottom; coordinates of sensor locations (Figures 7.4.1-1, 7.4.2-1, 7.4.3-1)	X		

NOTE: [1] Average heat power was calculated from DTN: MO0208RESTRDST.002 [161129]

Table 4.1-3. Summary of Rock Properties of Geologic Units Tptpul, Tptpmn, and Tptpll in the Drift-Scale THM Model Applied to the Tptpll and Tptpmn Model Domains for Predictive Analysis

Stratigraphic Unit >		***Tptpul***	***Tptpmn***	***Tptpll***	**Source**
Matrix Thermal and Hydrological Properties					
Hydrogeological Unit > (Label for matrix properties)>		***Tsw33 (TswM3)***	***Tsw34 (TswM4)***	***Tsw35 (TswM5)***	
Permeability	k_m (m^2)	6.57E-18	1.77E-19	4.48E-18	LB0208UZDSCPMI.002 [161243]
Porosity	f_m (-)	0.1425	0.1287	0.1486	LB0210THRMLPRP.001 [160799]
Van Genuchten α	α_m (1/Pa)	6.17E-6	8.45E-6	1.08E-5	LB0208UZDSCPMI.002 [161243]
Van Genuchten m (or λ)	m_m (-)	0.283	0.317	0.216	LB0208UZDSCPMI.002 [161243]
Residual saturation	S_{lrm} (-)	0.12	0.19	0.12	LB0208UZDSCPMI.002 [161243]
Rock grain density	ρ (kg/m3)	2358	2466	2325	LB0210THRMLPRP.001 [160799]
Specific heat Capacity	C_p (J/kg K)	985	985	985	LB0210THRMLPRP.001 [160799]
Dry thermal conductivity	λ_{dry} (W/m K)	1.164	1.419	1.278	LB0210THRMLPRP.001 [160799]
Wet thermal conductivity	λ_{wet} (W/m K)	1.675	2.074	1.890	LB0210THRMLPRP.001 [160799]
Fracture Hydrological Properties					
Hydrogeological Unit > (Label for fracture properties)>		***Tsw33 (TswF3)***	***Tsw34 (TswF4)***	***Tsw35 (TswF5)***	
Permeability	k_f (m^2)	7.80E-13	3.30E-13	9.10E-13	LB0205REVUZPRP.001 [159525]
Porosity	f_f (-)	5.8E-3	8.5E-3	9.6E-3	LB0208UZDSCPMI.002 [161243]
Van Genuchten α	α_f (1/Pa)	1.59E-3	1.04E-4	1.02E-4	LB0208UZDSCPMI.002 [161243]
Van Genuchten m (or λ)	m_f (-)	0.633	0.633	0.633	LB0208UZDSCPMI.002 [161243]
Residual saturation	S_{lrf} (-)	0.01	0.01	0.01	LB0208UZDSCPMI.002 [161243]
Fracture frequency	f (m^{-1})	0.81	4.32	3.16	LB0205REVUZPRP.001 [159525]
Active fracture model coefficient	γ (-)	0.600	0.569	0.569	LB0208UZDSCPMI.002 [161243]
Rock-Mass Mechanical Properties					
Thermal mechanical Unit >		***TSw1***	***TSw2***	***TSw2***	
Young's Modulus	E (GPa)	19.40	14.77	14.77	MO9911SEPGRP34.000 [148524] MOL.19991005.0235 Table 10 for 40% cumulative frequency
Poisson's Ratio	ν (-)	0.23	0.21	0.21	MO9911SEPGRP34.000 [148524] MOL.19991005.0235 Table 11 for 40% cumulative frequency

Table 4.1-4. Summary of Rock Properties of Geologic Units Tptpul, Tptpmn and Tptpll in the Drift-Scale THM Model Applied to the DST Model Domain Used for Model Validation

Stratigraphic Unit >		***Tptpul***	***Tptpmn***	***Tptpll***	**Source**
Matrix Thermal and Hydrological Properties					
Hydrogeological Unit > ***(Label for matrix properties)>***		***Tsw33 (TswM3)***	***Tsw34 (TswM4)***	***Tsw35 (TswM5)***	
Permeability	k_m (m^2)	5.25E-18	1.24E-17	2.47E-16	ANL-NBS-TH-000001 REV 00 ICN 02 (BSC 2001 [157330], Table 5)
Porosity	f_m (-)	0.154	0.11	0.13	ANL-NBS-TH-000001 REV 00 ICN 02 (BSC 2001 [157330], Table 5)
van Genuchten α	α_m (1/Pa)	1.06E-5	2.25E-6	2.82E-6	ANL-NBS-TH-000001 REV 00 ICN 02 (BSC 2001 [157330], Table 5)
van Genuchten m (or λ)	m_m (-)	0.243[1]	0.247[1]	0.207[1]	ANL-NBS-TH-000001 REV 00 ICN 02 (BSC 2001 [157330], Table 5)
Residual saturation	S_{lrm} (-)	0.06	0.18	0.13	ANL-NBS-TH-000001 REV 00 ICN 02 (BSC 2001 [157330], Table 5)
Rock grain density	ρ (kg/m3)	2510	2530	2540	ANL-NBS-TH-000001 REV 00 ICN 02 (BSC 2001 [157330], Table 5)
Specific heat capacity	C_p (J/kg K)	917	953	953	ANL-NBS-TH-000001 REV 00 ICN 02 (BSC 2001 [157330], Table 5)
Dry thermal conductivity	λ_{dry} (W/m K)	1.15	1.67	1.59	ANL-NBS-TH-000001 REV 00 ICN 02 (BSC 2001 [157330], Table 5)
Wet thermal conductivity	λ_{wet} (W/m K)	1.7	2.0	2.29	ANL-NBS-TH-000001 REV 00 ICN 02 (BSC 2001 [157330], Table 5)
Fracture Hydraulic Properties					
Hydrogeological Unit > ***(Label for fracture properties)>***		***Tsw33 (TswF3)***	***Tsw34 (TswF4)***	***Tsw35 (TswF5)***	
Permeability	k_f (m^2)	6.353E-13	1.00E-13	1.87E-13	ANL-NBS-TH-000001 REV 00 ICN 02 (BSC 2001 [157330], Table 5)
Porosity	f_f (-)	0.171E-3	0.263E-3	0.392E-3	ANL-NBS-TH-000001 REV 00 ICN 02 (BSC 2001 [157330], Table 5)
van Genuchten α	α_f (1/Pa)	1.57E-4	9.73E-5	1.66E-5	ANL-NBS-TH-000001 REV 00 ICN 02 (BSC 2001 [157330], Table 5)
van Genuchten m[1] (or λ)	m_f (-)	0.492[1]	0.492[1]	0.492[1]	ANL-NBS-TH-000001 REV 00 ICN 02 (BSC 2001 [157330], Table 5)
Residual saturation	S_{lrf} (-)	0.01	0.01	0.01	ANL-NBS-TH-000001 REV 00 ICN 02 (BSC 2001 [157330], Table 5)
Fracture frequency	f (m^{-1})	0.81	4.32	3.16	LB0205REVUZPRP.001 [159525]
Rock-Mass Mechanical Properties					
Thermal mechanical Unit >		***TSw1***	***TSw2***	***TSw2***	
Young's Modulus	E (GPa)	19.40	14.77	14.77	MO9911SEPGRP34.000 [148524] MOL.19991005.0235 Table 10, 40% cumulative freq.
Poisson's Ratio	ν (-)	0.23	0.21	0.21	MO9911SEPGRP34.000 [148524] MOL.19991005.0235 Table 11, 40% cumulative freq.

NOTE: [1] Denoted β_m in ANL-NBS-TH-000001 REV 00 ICN 02 (BSC 2001 [157330], Table 5).

Table 4.1-5. Data Tracking Numbers for Sources of Measured Data at DST and Niches Used for Model Validation

DTNs	Description
Temperature Measurements at DST (Section 4.1.3.1)	
MO0208RESTRDST.002 [161129]	Restructured Drift Scale Test (DST) heating phase temperature measurements
Air-Permeability Measurements at DST (Section 4.1.3.2)	
LB0208AIRKDSTH.001 [160897]	Measured air-permeability data during heating at the DST
MPBX Displacement Measurements at DST (Section 4.1.3.3)	
SN0207F3912298.037 [162046]	Smoothed measurements of displacement during heating at the DST
Air-Permeability Measurements at Niches (Section 4.1.3.4)	
LB0110AIRK0015.001 [162179]	Measured air-permeability change ratio during excavation of Niche 3107, Niche 3650, Niche 4788 and Niche CD 1620

4.2 CRITERIA

Technical requirements to be satisfied by performance assessment (PA) are based on 10 CFR 63.114 [156605] (*Requirements for Performance Assessment*) and identified in the Yucca Mountain *Project Requirements Document* (Canori and Leitner 2003 [161770]). The acceptance criteria that will be used by the Nuclear Regulatory Commission (NRC) to determine whether the technical requirements have been met are identified in the *Yucca Mountain Review Plan, Final Report* (YMRP; NRC 2003 [163274]). Pertinent requirements and acceptance criteria for this Model Report are summarized in Table 4.2-1.

Table 4.2-1. Project Requirements and YMRP Acceptance Criteria Applicable to This Model Report

Requirement Number[a]	Requirement Title[a]	10 CFR 63 Link	YMRP Acceptance Criteria
PRD-002/T-015	Requirements for Performance Assessment	10 CFR 63.114(a-c) [156605]	Criteria 1 to 5 for *Quantity and Chemistry of Water Contacting Engineered Barriers and Waste Forms* [b] Criteria 1 to 4 for *Flow Paths in the Unsaturated Zone* [c] Criteria 1 to 3 for *System Description and Demonstration for Multiple Barriers* [d]

NOTES: [a] from Canori and Leitner (2003 [161770])
[b] from NRC (2003 [163274], Section 2.2.1.3.3.3)
[c] from NRC (2003 [163274], Section 2.2.1.3.6.3)
[d] from NRC (2003 [163274], Section 2.2.1.1.3)

The acceptance criteria are given below, followed by a short description of their applicability to this Model Report. The criteria from Section 2.2.1.3.6.3 *Acceptance Criteria*, [for Section 2.2.1.3.6, *Flow Paths in the UZ*] are:

- Acceptance Criterion 1, *System Description and Model Integration Are Adequate (Addressed in Section 6.1 through 6.4)*:

The process-level model of drift-scale coupled thermal-hydrological-mechanical (THM) effects adequately incorporates important physical phenomena and couplings, and uses consistent and appropriate assumptions throughout the flow paths in the UZ abstraction process.

The aspects of geology, hydrology, physical phenomena, and couplings that may affect flow paths in the UZ are adequately considered.

Adequate spatial and temporal variability of model parameters and boundary conditions are employed in process-level models to estimate flow paths in the UZ, percolation flux and seepage flux.

Average parameter estimates used in process-level models are representative of the temporal and spatial discretizations considered in the model.

- Acceptance Criterion 2, *Data Are Sufficient for Model Justification (Addressed in Sections 4.1, 6.4, 7.3, 7.4, 7.6):*

  Hydrological and thermal-hydrological-mechanical-chemical values used in the license application are adequately justified. Adequate descriptions of how data were used, interpreted, and appropriately synthesized into the parameters are provided.

  Input data used in this report is collected in appropriate thermal-hydrological-mechanical tests, so that critical thermal-hydrological-mechanical processes were observed, and values for relevant parameters estimated.

  Accepted and well-documented procedures are used to construct and calibrate numerical models.

  Reasonably complete process-level conceptual and mathematical models are used in the analyses. In particular: (1) mathematical models are provided that are consistent with conceptual models and site characteristics; and (2) the robustness of results from different mathematical models is compared.

- Acceptance Criterion 3, *Data Uncertainty Is Characterized and Propagated Through the Model Abstraction (Addressed in Sections 6.1, 6.4, 6.8.4, 6.8.5, 8.2)*:

  Models use parameter values, assumed ranges, probability distributions, and/or bounding assumptions that are technically defensible, and reasonably account for uncertainties and variabilities.

  The initial conditions, boundary conditions, and computational domain used in sensitivity analyses and/or similar analyses are consistent with available data. Parameter values are consistent with the initial and boundary conditions and the assumptions of the conceptual models for the Yucca Mountain site.

  Coupled THM processes are adequately represented

Uncertainties in the characteristics of the natural system are considered.

- Acceptance Criterion 4, *Model Uncertainty Is Characterized and Propagated through the Model Abstraction (Addressed in Section 6.8, 6.9, 7.6, 8.2)*:

  Alternative modeling approaches of features, events, and processes, consistent with available data and current scientific understanding, are investigated;

The criteria from Section 2.2.1.3.3.3 *Acceptance Criteria*, [for Section 2.2.1.3.3 *Quantity and Chemistry of Water Contacting Engineered Barriers and Waste Forms*] are:

- Acceptance Criterion 1, *System Description and Model Integration Are Adequate (Addressed in Section 6.1 through 6.4, 6.8)*:

  Adequate technical bases are provided, including activities such as field data or sensitivity studies, for inclusion of any thermal-hydrological-mechanical couplings and features, events, and processes.

  Performance-affecting processes that have been observed in thermal-hydrological-mechanical tests and experiments are included within the performance assessment.

- Acceptance Criterion 2, *Data Are Sufficient for Model Justification (Addressed in Sections 4.1, 6.4, 7.3, 7.4, 7.6)*:

  Geological and hydrological values used in the license application are adequately justified. Adequate descriptions of how data were used, interpreted, and appropriately synthesized into the parameters are provided.

  Data on the characteristics of the natural system are sufficient to establish initial and boundary conditions for conceptual models of thermal-hydrological-mechanical coupled processes that affect seepage and flow.

  Input data used in this report are sufficient to verify that thermal-hydrological-mechanical conceptual models address important thermal-hydrological-mechanical phenomena.

- Acceptance Criterion 3, *Data Uncertainty Is Characterized and Propagated through the Model Abstraction (Addressed in Sections 6.1, 6.4, 6.8.4, 6.8.5, 8.2):*

  Models use parameter values, assumed ranges, probability distributions, and/or bounding assumptions that are technically defensible, and reasonably account for uncertainties and variabilities.

  Adequate representation of uncertainties in the characteristics of the natural system is provided in parameter development for process-level models.

- Acceptance Criterion 4, *Model Uncertainty Is Characterized and Propagated through the Model Abstraction (Addressed in Sections 6.8, 6.9, 7.6, and 8.2)*:

Alternative modeling approaches of features, events, and processes, consistent with available data and current scientific understanding, are investigated.

Alternative modeling approaches are considered, and the selected modeling approach is consistent with available data and current scientific understanding. The results, limitations, and uncertainties of the chosen model are provided.

Adequate consideration is given to effects of thermal-hydrological-mechanical coupled processes in the assessment of alternative conceptual models.

- Acceptance Criterion 5, *Model Abstraction Output Is Supported by Objective Comparison: (Addressed in Sections 7, 8.2)*:

  This model provides results consistent with output from empirical observations (field testing).

  Simulations of THM-induced changes in hydrological properties are adequately justified by comparison with direct observations and field studies;

  Accepted and well-documented procedures are used to construct and test the numerical models that stimulate coupled thermal-hydrological-mechanical effects on flow, numerical models are appropriately supported.

The criteria from Section 2.2.1.1.3 *Acceptance Criteria*, [for Section 2.2.1.1 *System Description and Demonstration of Multiple Barriers*] are:

- Acceptance Criterion 1, *Identification of Barriers Is Adequate: (Addressed in Section 6.8, 8.1)*:

  Barriers relied on to achieve compliance with 10 CFR 63.113 [156605] (b), as demonstrated in the total system performance assessment, are adequately identified, and are clearly linked to their capability. The barriers identified are part of the natural system.

- Acceptance Criterion 2, *Description of Barrier Capability to Isolate Waste Is Acceptable: (Addressed in Section 6.8, 8.1)*:

  The capability of the identified barriers to prevent or substantially reduce the rate of water movement from the Yucca Mountain repository to the accessible environment is adequately identified and described.

- Acceptance Criterion 3, *Technical basis for Barriers Capability Is Adequately Presented: (Addressed in Section 6.8, 6.9, 8.1)*:

  The technical bases are consistent with the technical basis for the performance assessment. The technical basis for assertions of barrier capability is commensurate with the importance of each barrier's capability and the associated uncertainties.

Note that only Acceptance Criterion 1 from Section 2.2.1.3.6.3 of NRC (2003 [163274]) was identified for this model report in BSC (2002 [160819], Table 3.1). The other Acceptance Criteria identified here are also applicable to this model report.

4.3 CODES AND STANDARDS

No specific formally established standards have been identified as applying to this modeling activity.

INTENTIONALLY LEFT BLANK

5. ASSUMPTIONS

This section contains the basic assumptions of the Drift-Scale THM model used in this Model Report. Each statement of an assumption is followed by the rationale for why the assumption is considered valid or reasonable.

1. The stratigraphy layers represented in the Tptpmn and Tptpll model domains in Section 6.3 follow the earlier revision of the Geologic Framework Model as described in CRWMS M&O (2000 [138860]) and are based on data of status 1999 (DTN: MO9901MWDGFM31.000 [103769]), corresponding to an earlier revision of the Geologic Framework Model as described in CRWMS M&O (2000 [138860]). The modifications presented in the most current revision, as described in BSC (2002 [159124]), have not been implemented, in order to use layering that is consistent with the TH Seepage Model applied in the *Drift-Scale Coupled Processes (DST and TH Seepage) Models* Report (BSC 2003 [161530], Section 6.2), which this analysis supplements.

   Basis:
   The stratigraphy modifications in the current revision of the Geologic Framework Model are small for the repository units. It is noted in *Geologic Framework Model (GFM 2000)* (BSC 2002 [159124], Section 6.1) that the changes between the earlier and the new revision of the Geologic Framework Model relating to the elevation in geologic layers are relatively small in magnitude, rarely as large as 25 feet, and are primarily near the edges of the GFM boundary. Therefore, changes in thickness and contact elevations in the repository are minor, much smaller than the extent of the host rock units considered in Section 6. Since this study is focused on THM in the repository unit around an emplacement drift, the results of this model report are not affected by these changes. This assumption is considered adequate and requires no further confirmation.

2. The initial vertical stress field is assumed to be $\sigma_v = -\rho g z_d = -2{,}200 \times 9.81 \times z_d = -21{,}582 \times z_d$, where z_d is depth. Horizontal stresses are assumed to be $\sigma_H = 0.6 \times \sigma_v$ (least compressive horizontal stress) and $\sigma_h = 0.5 \times \sigma_v$ (maximum compressive horizontal stress). This assumption is consistently used for all simulation cases in the Model Report, including the Tptpmn and Tptpll model domains (Section 6.3), and for the simulation of the DST (Section 7.3).

   Basis:
   The assumed initial stress field represents the best estimate of the stress field at the repository horizon. Vertical stress is estimated based on the weight of the overburden rock with an average density of 2,200 kg/m^3 (See Section 6.3). The horizontal stresses represent the best estimate at the repository horizon (CRWMS M&O 1997 [103564], Table 3-2, p. 3–23). This estimate of the initial stress is considered sufficiently accurate because this Model Report concerns itself with thermally induced stresses, which are largely independent of the initial stress field. This assumption is considered adequate and requires no further confirmation.

3. The TSw3 TM unit is assigned rock-mass mechanical properties (Young's modulus and Poisson's rate) that are equal to that of the TSw2 TM unit. This assumption is needed for complete definition of mechanical material properties in the Tptpmn and Tptpll subdomains (Section 6.4).

   Basis:
   Rock-mass properties of the TSw3 TM unit are not listed in the qualified data source (MO9911SEPGRP34.000 [148524], Tables 10 and 11) and have to be derived. Assigning the TSw3 TM unit to have mechanical properties equivalent to the TSw2 TM unit is considered to be a good estimate for the following reasons: (1) the Young's modulus measured on intact rock samples from TSw3 and TSw2 TM units are similar (MO9911SEPGRP34.000 [148524], Table 8); (2) the mean fracture spacing of the two TM units are similar. This estimate is considered sufficiently accurate, considering that the TSw3 TM unit is located below and away from the repository units. For the THM analysis conducted in the Model Report, concerns are focused on THM processes primarily in the repository units and secondarily on units located above the repository. This assumption is considered adequate and requires no further confirmation.

4. The rock-mass mechanical properties (Young's modulus and Poisson's rate) of the CHn TM unit are assumed to be equivalent to the intact rock mechanical properties (Young's modulus and Poisson's rate). This assumption is needed for complete definition of mechanical material properties in the Tptpmn and Tptpll subdomains (Section 6.4).

   Basis:
   Rock-mass properties of the CHn TM unit are not listed in the qualified data source (MO9911SEPGRP34.000 [148524], Tables 10 and 11) and have to be derived. Assuming the rock properties of the CHn TM unit to be equal to its intact rock properties is justified as follows: (a) for the CHn TM unit, the measured values of Young's modulus of intact rock samples is very low (5.63 GPa with 1.55 GPa standard deviation according to MO9911SEPGRP34.000 [148524], Table 8). This indicates that the rock-mass deformability is controlled by the deformability of the intact rock matrix rather than by the deformability of rock fractures; (b) The intact rock modulus provides an upper limit for the rock-mass modulus of deformation, which can be considered a conservative estimate giving the maximum possible TM impact. This estimate is considered sufficient, considering that the CHn TM unit is located far below the repository units. For the THM analysis, concern is focused on THM processes primarily in the repository units and secondarily in units located above the repository. This assumption is considered adequate and requires no further confirmation.

5. Appropriate values of the tortuosity parameter are selected based on the parameter range given in de Marsily (1986 [100439], p. 233) and Jury et al. (1991 [102010], p. 203). Jury et al. (1991 [102010], p. 203) presents results of diffusion tests through packed soil core samples with recommended average value of 0.66 ($\approx$0.7) for the tortuosity parameter. This is done for rock properties in both the Tptpmn and Tptpll subdomains as well as for the DST model domain (Sections 6.2 and 7).

Basis:
The tortuosity parameter is used for calculating vapor-air diffusion processes. These processes are of minor importance to modeling results, because their impact on TH conditions in the rock is very small compared to conductive and convective processes. Thus, exact quantification or even calibration of this parameter is not needed; instead, appropriate tortuosity values are taken from the literature. From the range of values given in de Marsily (1986 [100439], p. 233), a value of 0.7 is selected for the rock matrix. Fracture tortuosities of the fracture continuum are further modified for fracture-fracture connections by multiplication of the tortuosity by the fracture porosity of the bulk rock. This operation yields the appropriate value for the fracture-to-fracture interconnection area. This assumption is considered adequate and requires no further confirmation.

INTENTIONALLY LEFT BLANK

6. MODEL

In this section, a fully coupled thermal-hydrological-mechanical (THM) analysis is conducted to investigate the impact of THM processes on the drift-scale performance of a repository at Yucca Mountain. A model denoted the Drift-Scale THM Model is developed in Section 6.3 and 6.4, based on the coupled THM simulator TOUGH2-FLAC3D (Rutqvist et al. 2002 [162048]), which is presented in Section 6.2. This model is applied to predict coupled THM processes around an emplacement drift, first for an emplacement drift located in the Tptpmn unit (Tptpmn model domain) presented in Section 6.5, and then for an emplacement drift located in the Tptpll unit (Tptpll model domain) presented in Section 6.6. For both cases, the fully coupled THM analysis is complemented by a partially coupled TH analysis, leading to a total of four simulations. Simulation results are summarized in Sections 6.7, followed by a discussion of uncertainties and an alternative conceptual model in Sections 6.8 and 6.9, respectively. The key scientific notebooks (with relevant page numbers) used in the study are presented in Table 6-1.

Table 6-1. Scientific Notebooks Used in This Model Report

LBNL Scientific Notebook ID	M&O Scientific Notebook ID	Relevant Pages	Citation
YMP-LBNL-JR-1	SN-LBNL-SCI-204-V1	14–18, 104–148	Rutqvist 2002 [162047]
YMP-LBNL-JR-2	SN-LBNL-SCI-204-V2	9–148, 168–184	Wang 2003 [162654]

The following table (or list) of features, events, and processes (FEPs) were taken from the LA FEP List (DTN: MO0301SEPFEPS1.000 [161496]). The LA FEP List is a revision to the previous project FEP list (Freeze et al. 2001 [154365]) used to develop the list of included FEPs in the *Technical Work Plan for: Performance Assessment Unsaturated Zone* (BSC 2002 [160819], Table 2-6). The selected FEPs are those taken from the LA FEP list that are associated with the subject matter of this report, regardless of the anticipated status for exclusion or inclusion in TSPA-LA as represented in BSC (2002 [160819]). The results of this model are part of the basis for the treatment of FEPs as discussed in the *Total System Performance Assessment-License Application Methods and Approach* (BSC 2002 [160146], Section 3.2.2). The cross-reference for each FEP to the relevant sections of this report is also given below.

The UZ Department's documentation for the FEPs listed in Table 6-2 is compiled from this and other model reports and can be found in the model abstraction reports as described in Section 2.4 of the TWP (BSC 2002 [160819]) for any included FEPs. These abstraction reports include: *Abstraction of Drift Seepage* (MDL-NBS-HS-000019, BSC 2003 [162268]) and upcoming revision on *Abstraction of Drift-Scale Coupled Processes* (refer to current version, ANL-NBS-HS-000029, CRWMS M&O 2000 [123916]). The documentation for any excluded FEPs listed in Table 6-2 can be found in the UZ FEPs AMR as described in Section 2.4 of the TWP (BSC 2002 [160819]).

Table 6-2. FEPs Addressed in this Model Report

FEP No.	FEP Name	Summary Description
1.1.02.00.0B	Mechanical effects of the excavation/construction in EBS (Engineered Barrier System)	Mechanical effects of the excavation/construction of the emplacement drift and its impact on the percolation flux are analyzed in Sections 6.5.1 and 6.6.1. Rock fall at the drift wall is discussed in Sections 6.8.3 and 8.2.
1.1.02.02.0A	Preclosure ventilation	Preclosure ventilation is considered (see Section 6.3).
1.2.02.01.0A	Fractures	Fracture characteristics are described by appropriate parameters that are based on site characterization, calibration and underground testing (see Sections 4.1.1.1, Table 4.1-3, 6.4, 7.4 and 7.5)
1.3.01.00.0A	Climate change, global	Potential effects of climate change on the amount of infiltration and percolation at Yucca Mountain are taken into account by appropriate infiltration boundary conditions (see Section 6.3).
1.4.01.01.0A	Climate modification increases recharge	Potential effects of climate change on the amount of infiltration and percolation at Yucca Mountain are taken into account by appropriate infiltration boundary conditions (see Table 6.3-1).
2.1.08.01.0A	Water influx at the repository	The potential increase in the magnitude of percolation flux at the repository as a result of climate changes is accounted for in this report by appropriate flux variation (see Table 6.3-1).
2.1.08.02.0A	Enhanced influx at the repository	The impact of an underground opening on the unsaturated flow field (including capillary barrier effect and flow diversion around the drifts) is captured in the process model by using appropriate rock properties and appropriate boundary conditions at the drift wall (see Section 6.3 and 6.4).
2.2.01.01.0A	Mechanical effects of excavation/construction in the near field	Mechanical effects of excavation/construction on the hydraulic properties in the near field are analyzed in Sections 6.5.1 and 6.6.1.
2.2.01.02.0A	Thermally induced stress changes in the near field	Thermally induced stress changes in the near field are analyzed in Sections 6.5.3, 6.6, and discussed in Section 6.7.
2.2.01.03.0A	Changes in fluid saturations in the excavation-disturbed zone	Changes in fluid saturation caused by drying and wetting around the excavation are accounted for by the unsaturated flow model and appropriate boundary conditions at the drift wall (Section 6.3). TM-induced changes in fracture saturation caused by fracture closure or opening with associated changes in the capillary pressure are analyzed (see Sections 6.5.4 and 6.6.1).
2.2.03.01.0A	Stratigraphy	The stratigraphy of geological units at Yucca Mountain is represented in the drift-scale models (see Section 6.3).
2.2.03.02.0A	Rock properties of host rock and other units	Rock properties are described by appropriate parameters based on site characterization, calibration, and underground testing (see Sections 4, 6.4, and 7.3).
2.2.07.02.0A	Unsaturated groundwater flow in the geosphere	Unsaturated flow processes are accounted for in the conceptual and mathematical model (Section 6.2).
2.2.07.04.0A	Focusing of unsaturated flow (fingers, weeps)	The potential impact of THM on flow focusing of unsaturated flow in a heterogeneous permeability field is discussed in Section 6.8.5.
2.2.07.08.0A	Fracture flow in the UZ	The coupled flow of fluid, gas, and heat is explicitly included in the process model (see Sections 6.2, 6.5, 6.6, and 7.4)
2.2.07.09.0A	Matrix imbibition in the UZ	Matrix imbibition is accounted for in the conceptual and mathematical model (Section 6.2).
2.2.07.10.0A	Condensation zone forms around drifts	The coupled TH processes of vapor condensation forming a condensation cap above the drifts are explicitly simulated with appropriate process model described in Section 6.2. The condensation cap can be seen in the model results in Sections 6.5.5, 6.6.2, and 7.4.3.
2.2.07.11.0A	Resaturation of geosphere dryout zone	Resaturation of the dryout zone around drifts, and the potential of return flow from the condensation zone back to the drifts, are explicitly simulated with appropriate process models described in Section 6.2. The resaturation of the dryout zone can be seen in the model results in Sections 6.5.5 and 6.6.2.

Table 6-2. FEPs Addressed in this Model Report (Continued)

FEP No.	FEP Name	Summary Description
2.2.07.20.0A	Flow diversion around repository drifts	Flow diversion around repository drifts as a result of capillary-strength differences is captured in the process model by using appropriate boundary conditions at the drift wall (see Section 6.3).
2.2.10.04.0A	Thermal-mechanical stresses alter characteristics of fractured near repository	THM induced changes in fracture permeability and fracture capillary pressure function are analyzed in Sections 6.5, 6.6, and 7.4.3, and discussed in Sections 6.8, 6.9, 8.1, and 8.2.
2.2.10.10.0A	Two-phase buoyant flow / heat pipes	Coupled TH processes causing heat-pipe behavior—including boiling and convection of heat with vapor flow—are explicitly simulated with appropriate process models. Heat-pipe effects can be seen in the model results (Sections 6.2 and 7.4.1) as well as in the measured temperature data (Section 7.4.1).
2.2.10.12.0A	Geosphere dryout due to waste heat	Changes in fluid saturation caused by TH-induced drying and wetting in the excavation-disturbed zone are analyzed (see Sections 6.5.5, 6.6.2, and 7.4.3).

6.1 INTRODUCTION TO COUPLED THM ANALYSIS

Coupled THM processes in the fractured rock around a waste emplacement drift can impact the spatial distribution of percolation flux through stress-induced changes in porosity, permeability and capillary pressure. Stress-induced changes can occur as a result of tunneling excavation and heating of the rock mass surrounding the waste emplacement drifts. Tunneling excavation can affect the permeability through opening or closing of existing fractures and potentially through formation of new fractures near the drift wall. After waste emplacement, the heating of the rock mass will induce thermal expansion and thermal stresses that will tend to close existing fractures, leading to a general decrease in fracture permeability. However, permeability changes that occur during the thermal period could be fully reversible, meaning that the permeability would recover to pre-emplacement conditions after the temperature has declined to ambient. Thermal stresses could also induce permeability enhancement through fracture shear slip with accompanying shear dilation. Such permeability changes would be irreversible and remain after the temperature has declined to ambient.

The analysis performed in this Model Report aims at assessing coupled THM processes and their impact on fracture permeability and percolation flux around a waste emplacement drift. Changes in fracture permeability and percolation flux can impact the potential for drift seepage (liquid water entering a drift). Drift seepage is usually analyzed with hydrological models or thermal-hydrological (TH) models, using stochastic modeling with multiple realizations of heterogeneous rock properties, which requires a larger number of simulation runs (CRWMS M&O 2001 [154291]; BSC 2003 [161530], Section 6.2). In simulations of drift seepage, the impact of coupled THM processes are evaluated by assigning THM-induced changes in mean value of fracture permeability around the drift, while the variability of permeability field is kept the same. To assess the impact of the THM processes on the flow field, it is sufficient to calculate changes in the mean value of the permeability for a conservative case of relative strong THM-induced changes in permeability. The conservative case is realized by adopting a conservative estimate of the coupled THM material properties. This includes a conservative estimate of the thermal expansion coefficient (leading to the maximum possible thermal stress) and a conservative estimate of a stress versus permeability function (leading to maximum possible permeability

change). Thus, assuming a homogeneous mean permeability is reasonable for showing changes between fully coupled THM analyses and partially coupled TH analyses, which is the basis for conclusions drawn in this Model Report. The use of mean values is adequately justified in both the predictive and validation analyses as a basis for assessing impact and validating the conceptual model.

In this Model Report, a fully coupled THM analysis is conducted first for the case of an emplacement drift located in the Tptpmn unit (Tptpmn submodel), and then for the case of an emplacement drift located in the Tptpll unit (Tptpll submodel). These two analyses are then compared to a partially coupled TH analysis ("partially coupled" because it does not account for the full THM coupling). The output in the form of THM-induced changes in mean permeability can be input to the above-mentioned hydrological or coupled TH multiple realization analyses as a correction factor for permeability. Furthermore, the comparison of the flow field obtained in this Model Report for the fully coupled THM analysis and partially coupled TH analysis can be used to assess the impact of THM processes on the flow field.

The analysis in this Model Report focuses on the impact of stress-induced permeability changes in the rock mass surrounding the repository drift and does not include the impact of drift collapse, which is covered in *Drift Degradation Analysis* (BSC 2003 [164285]).

6.2 DESCRIPTION OF THE COUPLED THM PROCESS MODEL

The two computer codes TOUGH2 V1.6; (LBNL 2003 [161491]) and FLAC3D V2.0; (LBNL 2001 [154783]) have been coupled for the analysis of coupled multiphase flow, heat transport, and rock deformations in fractured porous media (Rutqvist et al. 2002 [162048]). The TOUGH2 (Pruess et al. 1999 [160778]) code is designed for hydrological analysis of multiphase, multicomponent fluid and heat transport, while FLAC3D (Itasca Consulting Group 1997 [156788]) is designed for rock and soil mechanics. TOUGH2 has been successfully applied in the Yucca Mountain Project (YMP) to predict the temperature and moisture distribution of field experiments, including the Single Heater Test (Tsang and Birkholzer 1999 [137577]) and the Drift Scale Test (DST) (BSC 2001 [157330], Section 6). TOUGH2 can simulate relevant coupled TH processes—including evaporation of liquid water to vapor with transfer of latent heat during boiling, advection of moisture and dissolved air with gas and liquid phase flow, heat convection with water transport, vapor diffusion, and condensation of vapor to liquid water upon cooling. With these capabilities, the TOUGH2 code can simulate the evolution of temperature and moisture around a repository drift, including the formation and resaturation of a dryout zone. FLAC3D has the capability to analyze coupled hydrological-mechanical (HM) and thermal-mechanical (TM) responses of soil, rock, or other types of materials that may undergo plastic flow when their yield limit is reached. It contains various constitutive models suitable for mechanical analysis of geological materials. This includes Mohr-Coulomb elasto-plastic and ubiquitous joint models. Using appropriate mechanical constitutive models, it is capable of simulating relevant rock mechanical aspects, including stress and strain redistribution and the possibility of rock mass failure around a repository drift.

In this analysis, FLAC3D and TOUGH2 are coupled through external modules: one that calculates changes in effective stress as a function of multiphase pore pressure and thermal expansion, and one that corrects porosity, permeability, and capillary pressure as a function of

stress (Figure 6.2-1). Because these coupling parameters are material specific, specially designed coupling modules have been constructed and qualified for Yucca Mountain. The coupling modules are contained in qualified software routines Tin V1.1 (STN: 10889-1.1-00; LBNL 2002 [162038]), Delb.dat V1.0 (STN: 10507-1.0-0.0; LBNL 2001 [154791]), and Gpzones.dat V1.0 (STN: 10509-1.0-00; LBNL 2001 [154792]), the functions of which are described in more detail below.

For modeling of the unsaturated zone at Yucca Mountain, the linkage function from TOUGH2 to FLAC3D, considers only the effect of thermally induced strain and stresses. The changes in effective stress and bulk density caused by the multiphase fluid pressure and saturation changes are neglected. This is defensible considering that the fracture system is unsaturated, with a capillary pressure of less than 0.01 MPa. This is a very small pressure for a system that has *in situ* stresses and thermal stresses with magnitudes on the order of several to tens of MPa. Thus, the coupling module for the link from TOUGH2 to FLAC3D transfers the temperature field from TOUGH2 nodes to FLAC3D nodes. This coupling is provided by the FLAC3D FISH routine Tin V1.1 (LBNL 2002 [162038]) and with volume interpolation factors calculated by Gpzones.dat V1.0 (LBNL 2001 [154792]).

At Yucca Mountain, the two main stratigraphic units in which the emplacement drifts may be located (middle nonlithophysal [Tptpmn] and the lower lithophysal [Tptpll] units of the Topopah Spring Tuff) are both highly fractured, and the fractures are well connected (CRWMS M&O 2000 [153314], Section 6.7 and Figure 8). In these rock units, three dominant sets of fractures are oriented almost orthogonal to each other (BSC 2001 [156304], Table 5), two subvertical and one subhorizontal, and the mean fracture spacing is on the order of or less than 0.4 m (BSC 2001 [156304], Tables 7 and 8). Because of the high density and connectivity of the fracture network, the conceptual model used is a dual-permeability continuum model with interacting fractured and matrix continua, consistent with the UZ Flow Model and other coupled analyses. The dual-permeability continuum model appropriately accounts for the difference in water retention between the fractures and matrix necessary to capture important fracture-matrix interaction processes such as matrix imbibition. Previous analyses of TM-induced displacements at two major heater tests at Yucca Mountain (the Single Heater Test (SHT) and DST) have shown that mechanical deformations in the Tptpmn unit can be reasonably well captured with a linear-elastic or nonlinear-elastic mechanical model (Sobolik et al. 1998 [162049]; BSC 2001 [155957]; pp. 115–125; Sobolik et al. 1999 [163202], p. 735). Furthermore, previous comparisons of the discrete-fracture approach and continuum approach for the modeling of mechanical displacements in the DST show minor differences, indicating that the continuum approach is sufficient for accurately representing the *in situ* TM behavior at Yucca Mountain (BSC 2001 [155957], p. 125). This implies that the bulk-rock mass behavior is essentially elastic, although locally a small slip may occur on fracture planes. Next to the drift wall, on the other hand, more significant inelastic shear slip or tensile fracturing may occur because of the strong stress redistribution and a lack of confinement in that region (Figure 6.2-2a). Because the fractured porous medium is always in a static equilibrium, the three-dimensional stress is equivalent in the fracture and matrix continua. Therefore, the mechanical dual-continuum model reduces to a lumped fracture-matrix continuum model (equivalent continuum model). For fluid and heat transport, the dual continuum stills exists, but with fracture and matrix continua that may not be in equilibrium, and hence can have different fluid pressure and temperature.

To couple changes in the three-dimensional stress field to rock-mass permeability, a cubic-block conceptual model is utilized (Figure 6.2-2b). Although the fracture orientation in the cubic-block model is roughly consistent with common fracture orientations in at Yucca Mountain, it is a simplified representation of the *in situ* fracture network. For example, in some rock units, the subhorizontal fracture set may be less frequent and there may also be randomly oriented fractures. Furthermore, trace distributions of fractures mapped along ESF for the Tptpmn unit makes them discontinuous in nature, with fractures frequently terminating against an intersecting fracture (BSC 2003 [164285], Section 6.1.4.1). However, the conceptual model shown in Figure 6.2-2b is consistent with established hydrological and TH process models for the Yucca Mountain UZ. The hydrological properties of those models are largely derived directly from *in situ* permeability measurements and through model calibration against *in situ* hydrological data such as liquid saturation profiles along vertical boreholes (e.g. BSC 2003 [160240], Section 6.3.2). The fracture density is basically used for deriving parameters for the fracture-matrix interaction behavior, such as interface area and connection length between fracture elements and matrix blocks in the underlying conceptual model. Using this underlying conceptual model, the hydraulic properties such as the water retention curve are calibrated against field measurements. Thus, for deriving hydrological properties and for analysis of hydrological and TH processes in the unsaturated zone of Yucca Mountain, detailed information distribution of fracture length, orientation, and aperture are not explicitly incorporated, except for a generic value of mean fracture spacing in each rock unit. The underlying conceptual model for stress-versus-permeability coupling shown in Figure 6.2-2b is justified as being consistent with the established hydrological models of the Yucca Mountain unsaturated zone. In these hydrological models, the permeability field is heterogeneous, but isotropic, leading to an underlying conceptual model with equal fracture spacing and properties for vertical and horizontal fractures.

The conceptual model in Figure 6.2-2 is appropriate for estimating the impact of mechanical processes on the established hydrological models at Yucca Mountain. This is because it can capture all relevant THM processes observed at several *in situ* experiments conduced at Yucca Mountain (Section 7). The simplified conceptual model can capture relevant THM processes because the rock at Yucca Mountain is highly fractured, forming a network that is well connected for fluid flow. This conceptual model may not be generally acceptable for all types of fracture rock, (for example, at sparsely fracture rock sites where fluid flow is dominated by a few discrete hydraulic conducting fractures). Thus, the conceptual model is selected specifically for Yucca Mountain based on field evidence of intense fracturing and a well-connected fracture network. For the Tptpmn and Tptpll units, a mean fracture spacing of less than 0.4 (Table 4.1.3) has been derived, using mappings of fractures with a trace length larger then one meter. However, as pointed out in the *Drift Degradation Analysis* (BSC 2003 [164285], Section 6.1.4.1), 80% of the fractures have a trace length of less than one meter, and therefore, counting all fractures, the fracture spacing should be less than 0.4 meters. The concept of a well-connected fracture network for fluid flow is confirmed by air-permeability measurements conduced in boreholes with short (1 foot) packer intervals at several excavated niches at Yucca Mountain (BSC 2001 [158463], Section 6.1). In these tests, the permeability at each 0.3-meter interval of the boreholes is several orders larger than the matrix permeability, indicates that at least one hydraulic conductive fracture intersects every 0.3 meters and is connected to a network of hydraulic conducting fractures. For such intensively fractured rock, the detailed fracture

geometry does not impact the coupled THM behavior significantly, and hence, the adopted conceptual model is appropriate.

Although, a two-dimensional analysis is conducted in this Model Report, the permeability field in the plane of the model depends on the three-dimensional stress field (Figure 6.2-2b). The three-dimensional stress field is calculated in the 2-D plane-strain mechanical analysis performed in FLAC3D. Using the conceptual model in Figure 6.2-2b, the porosity, permeability, and capillary pressure in the fractured continuum are corrected for any change in the stress field according to:

$$\phi = F_{\phi} \times \phi_i \quad \text{(Eq. 6.2-1)}$$

$$k_x = F_{kx} \times k_{ix},\ k_y = F_{ky} \times k_{iy},\ k_z = F_{kz} \times k_{iz} \quad \text{(Eq. 6.2-2)}$$

$$P_c = F_{Pc} \times P_{ci} \quad \text{(Eq. 6.2-3)}$$

where F denotes various correction factors and subscript i denotes initial conditions. Porosity and permeability correction factors are calculated from the initial and current apertures, b, in Fracture Sets 1, 2, and 3 according to:

$$F_{\phi} = \frac{b_1 + b_2 + b_3}{b_{1i} + b_{2i} + b_{3i}} \quad \text{(Eq. 6.2-4)}$$

$$F_{kx} = \frac{b_2^3 + b_3^3}{b_{2i}^3 + b_{3i}^3},\ F_{ky} = \frac{b_1^3 + b_3^3}{b_{1i}^3 + b_{3i}^3}, F_{kz} = \frac{b_1^3 + b_2^3}{b_{1i}^3 + b_{2i}^3} \quad \text{(Eq. 6.2-5)}$$

where fractures in Fracture Sets 1, 2, and 3 are equally spaced and oriented normal to x, y, and z directions, respectively, and a parallel-plate fracture flow model (Witherspoon et al. 1980 [123506]) is adopted. The capillary pressure is corrected with porosity and permeability changes according to the Leverett (1941 [100588]) function:

$$F_{Pc} = \sqrt{\frac{F_{\phi}}{F_k}} \quad \text{(Eq. 6.2-6)}$$

where

$$F_k = \sqrt[3]{F_{kx} \times F_{ky} \times F_{kz}} \quad \text{(Eq. 6.2-7)}$$

Thus, in areas where permeability increases by fracture opening, the capillary pressure tends to decrease. In this study, the current fracture aperture b depends on the current effective normal stress σ'_n, according to the following exponential function (Rutqvist and Tsang 2003 [162584]):

$$b = b_r + b_m = b_r + b_{\max}\left[\exp\left(\alpha\sigma'_n\right)\right] \quad \text{(Eq. 6.2-8)}$$

where b_r is a residual aperture, b_m is mechanical aperture, b_{max} is the maximum mechanical aperture, and α is a parameter related to the curvature of the function (Figure 6.2-3). This relationship can also be expressed in terms of an initial aperture, b_i, and changes in aperture, Δb, as:

$$b = b_i + \Delta b = b_i + b_{\max}\left[\exp(\alpha\sigma_n) - \exp(\alpha\sigma_{ni})\right] \quad \text{(Eq. 6.2-9)}$$

where σ_{ni} is the initial stress normal to the fractures. This expression can be inserted into Equation (6.2-5) to derive expressions for rock-mass permeability-correction factors in x, y, and z directions. In this formulation, the permeability changes as a function of normal stress across each fracture set, while no shear induced permeability changes are considered. It is expected to be sufficient because closure of vertical fractures caused by thermally induced horizontal stresses are expected to have a dominating impact on permeability changes. Furthermore, the potential for shear induced permeability changes can be evaluated indirectly from the results of the stress analysis. The calculation of fracture aperture changes is conducted in the qualified software routine Delb.dat V1.0 (LBNL 2001 [154791]), which is then transferred into the TOUGH2 code for the correction of hydrological properties.

The most important parameter for estimating stress-induced changes in hydraulic properties is the relationship between fracture aperture and stress defined in Equation 6.2-8. For a well-connected fracture network, fracture spacing and fracture orientation has little importance on the stress-versus-permeability relationship in comparison with the fracture-aperture-versus-stress function. The relationship between fracture hydraulic aperture and stress has been determined, both from laboratory samples and in the field for various types of rock. This relationship depends on fracture characteristics such as roughness and degree of mineral filling (Rutqvist and Stephansson 2003 [162583]). However, aperture versus normal stress relationships derived from small-scale laboratory samples are generally not applicable in the field. A size effect on the permeability and normal stiffness of fractures has been confirmed in both theoretical and experimental studies (Rutqvist and Stephansson 2003 [162583]). Because of the potential effects of size and nonrepresentative sampling, it is important to determine the stress-versus-aperture relationship *in situ* (Rutqvist and Stephansson 2003 [162583]). An *in situ* determination of the stress-aperture relationship for Yucca Mountain is performed in Section 6.4 of this Model Report. Such *in situ* determination seeks to determine the basic parameters b_{max} and α for fractures in the underlying conceptual model. The same conceptual model with the corresponding parameters b_{max} and α is then used in the predictive analysis of coupled THM processes around an emplacement drift in Section 6.5 and 6.6. Finally, the conceptual model shown in Figure 6.2-2 and the adopted stress-versus-aperture function is validated against field measurements in Section 7.

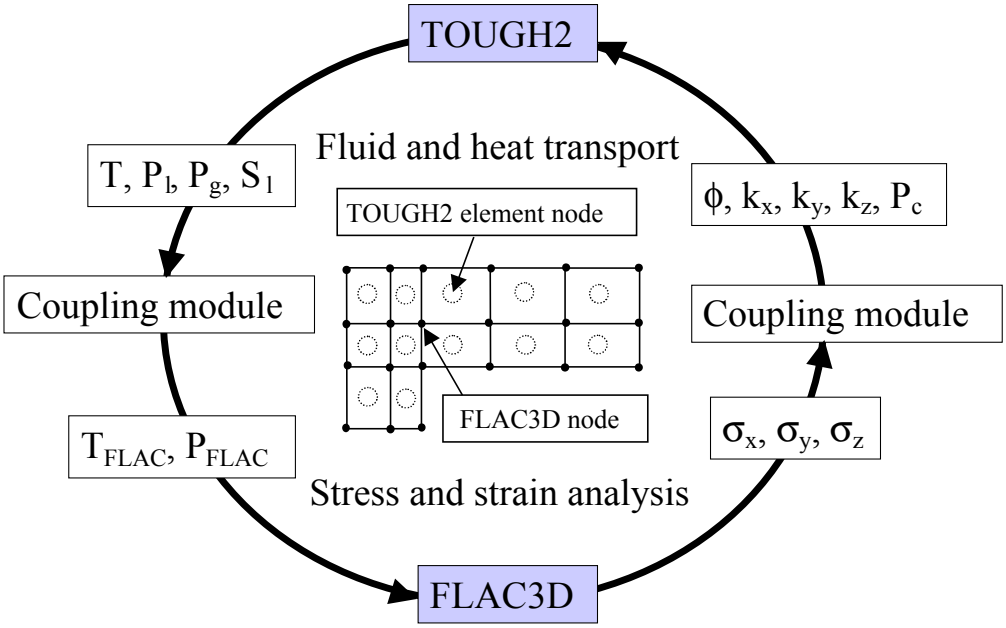

NOTE: T = Temperature, P_l = liquid fluid pressure, P_g = gas pressure, T_{Flac} = temperature at FLAC3D node, P_{FLAC} = pressure at FLAC3D node, ϕ = porosity, k_x, k_y, and k_z are permeabilities in x, y and z-directions, respectively, P_c is capillary pressure and σ_x, σ_y, and σ_x are stresses in x, y and z-directions, respectively. In the special case of Yucca Mountain, the illustrated transfer of multiphase fluid pressure from TOUGH2 to FLAC3D is not significant and therefore neglected. Only temperature has to be transferred from TOUGH2 to FLAC3D.

Figure 6.2-1. Schematic of Coupling between TOUGH2 and FLAC3D

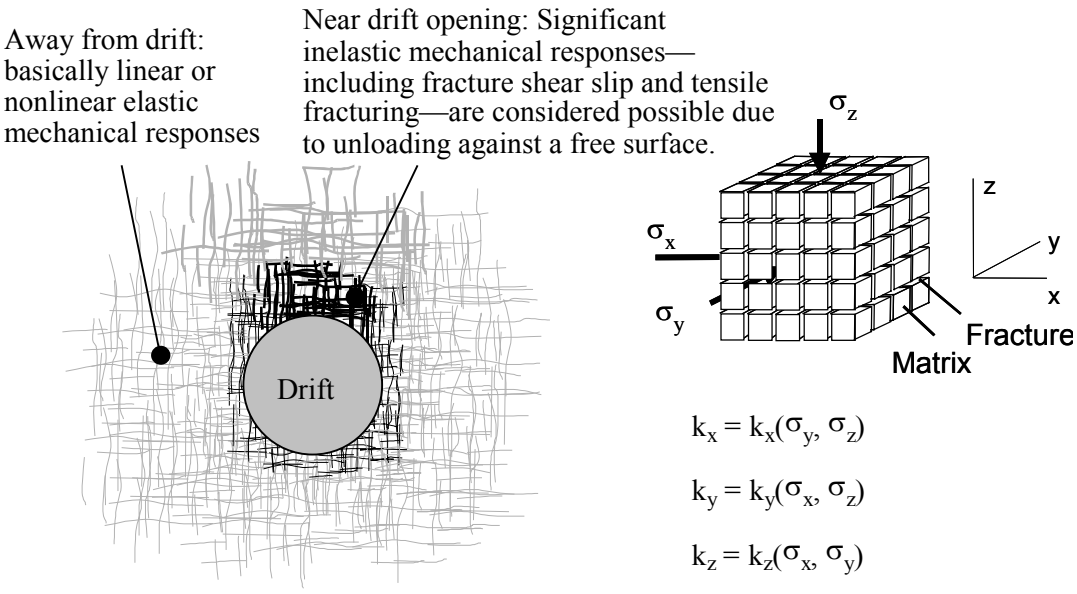

(a) Fractured rock-mass system (b) Conceptual stress-permeability model

NOTE: σ_x, σ_y, σ_x and k_x, k_y, k_z are stresses and permeabilities in x, y and z-directions, respectively. The illustrated inelastic zone near the drift wall may or may not exist depending on rock mass strength properties.

Figure 6.2-2. Schematic of the Fracture Rock System near a Drift and the Conceptual Model Use

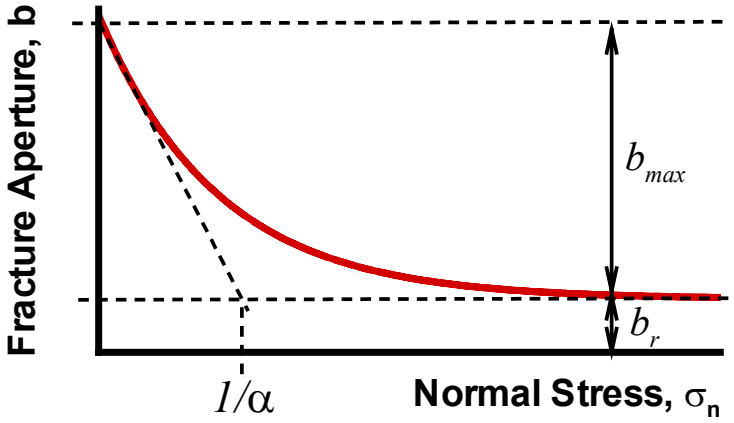

NOTE: b_{max} and α are parameters that determine the shape of the exponential function, and b_r is the residual aperture when the fracture is completely compressed from a mechanical point of view at a high normal stress.

Figure 6.2-3. Schematic for Normal Stress versus Aperture Relation

6.3 TPTPMN AND TPTPLL MODEL DOMAINS

The Drift-Scale THM model is a two-dimensional model that extends from the ground surface down to the groundwater table. It includes one-half of the emplacement drift, as a result of lateral symmetry (Figure 6.3-1a). Coupled THM simulation was conducted on two model domains, representing two different vertical two-dimensional cross sections through the interior of the repository at Yucca Mountain. The first one, the Tptpmn model domain, considers a waste emplacement drift located in the Topopah Spring Tuff middle nonlithophysal unit (Tptpmn unit). The second one, the Tptpll model domain, has a drift located in the Topopah Spring lower lithophysal unit (Tptpll unit). The two sections are selected to account for the two main host rock units of the repository and are the same sections being considered in both the *Drift-Scale Coupled Processes (DST and TH Seepage) Models* Report (BSC 2003 [161530], Section 6.2) and *Drift-Scale Coupled Processes (DST and THC Seepage) Model* Report (BSC 2003 [163506], Sections 6.5 and 6.7). A TOUGH2 dual-permeability mesh of both the Tptpmn and Tptpll model domains were constructed using the qualified software 2KGRIDV1.F V1.0 (STN: 10244-1.0-00; LBNL 1999 [147533]).

The Tptpmn model domain is a multiple-layered column extending 555.4 m vertically from the ground surface down to the water table, with the repository located in the Tptpmn unit at a depth of 220.1 m. The vertical layering for the model was chosen to correspond to the vertical contacts at borehole USW SD-9, as implemented in the three-dimensional Yucca Mountain UZ Model grid (DTN: LB990501233129.004 [111475]).

The Tptpll model domain extends 716.6 m vertically from the ground surface down to the water table, with the repository located in the Tptpll unit at a depth of 363.8 m. The stratigraphy of the Tptpll model domain was taken at the location near the center of the repository at Nevada State Plane Coordinates 170572.39 m (Easting) and 233194.536 m (Northing), close to the proposed Cross-Drift Thermal Test (CDTT). The geological data are derived from the "j34"column of three-dimensional Yucca Mountain UZ model grid (DTN: LB990501233129.004 [111475]).

The ground-surface boundary was set at a constant temperature and atmospheric pressure, mechanically free, and the water table boundary was set at constant temperature and mechanically fixed (Figure 6.3-1 and Table 6.3-1). Specific boundary values used for the Tptpmn model domain represent observations at the locations of the USW SD-9 borehole. The Tptpll model domain uses values representative of the center of the repository, at column "j34" of the UZ99_2_3-D mesh (DTN: LB9905012331329.004 [111475]). A varying yearly infiltration rate was applied at the ground surface according to the mean infiltration scenario described in the entitled AMR *Simulation of Net Infiltration for Modern and Potential Future Climates* (USGS 2001 [160355], Section 6.9 and 6.11) (Table 6.3-1). Horizontally, by symmetry, only half of the distance between the two drifts (40.5 m) was modeled because the drift spacing is 81 m. Thus, the left boundary was at the middle plane vertically through a drift, and the right boundary was mid-distance between two drifts. Both lateral boundaries of the model were mechanically fixed and closed for heat and fluid flow by symmetry.

The pre-excavation ambient thermal and hydrological conditions are derived by running a TH model to steady state, using the prescribed boundary conditions at the ground surface and water table and the present-day infiltration rate of 6 mm/year. The initial stress field represents the best

estimate of the stress field at the repository horizon (See Section 5, Assumption 2). The initial vertical stress is estimated based on the weight of the overburden rock mass, with an average saturated bulk rock density of 2,200 kg/m^3. This is the average value of the bulk rock density that was calculated for the rock mass overlying the repository drifts, using values of saturated rock densities given in 1999 TBV-332/TBD 325 Resolution Analysis: Geotechnical Rock Properties, Table 9 (DTN: MO9911SEPGRP34.000 [148524]). The magnitude of maximum and minimum principal compressive horizontal stresses are a factor of 0.6 and 0.5 of the vertical stress, with the maximum stress oriented perpendicular to the emplacement drift (CRWMS M&O 1997 [103564], Table 3-2, p. 3–23).

A repository drift of 5.5 m diameter was simulated as being excavated in the Tptpmn model domain at a depth of 220.1 m and in the Tptpll model domain at a depth of about 363.8 m. The waste emplacement was designed for a heat load of 1.45 kW (initial heat power) per meter emplacement drift (BSC 2003 [164069]). The time-varying heat-load values are given in *Repository Design, Repository/PA IED Subsurface Facilities Plan Sht. 5 of 5* (BSC 2002 [159527]). It is assumed that emplacement occurs all at once followed by a ventilation period of 50 years. During the ventilation period, ventilation of the drift will remove an estimated 86% to 88% of the time varying heat load (BSC 2003 [164576], Section 8.1). In this Model Report, a conservative estimate of 86% is adopted leading to an actual heat load as illustrated in Figure 6.5.2-1. Adopting 86% rather than 88% is conservative since it will result in a slightly higher actual heat load, and hence, a slightly higher rock temperature. This is also consistent with the reference-mode heat load studied in the Drift Scale Processes (TH Seepage and DST) Model Report (BSC 2003 [161530], Sections 1, 4.1.1.3, 6.2.1.3.3), which this analysis supplements. The condition that emplacement of all waste occurs at once provides a conservative case for estimating the impact of THM processes, because it leads to the highest possible heat load and therefore the highest possible thermal stress. In reality, all the waste cannot be emplaced at once but is planned to end in 24 years, followed by 50 more years of continuous ventilation.

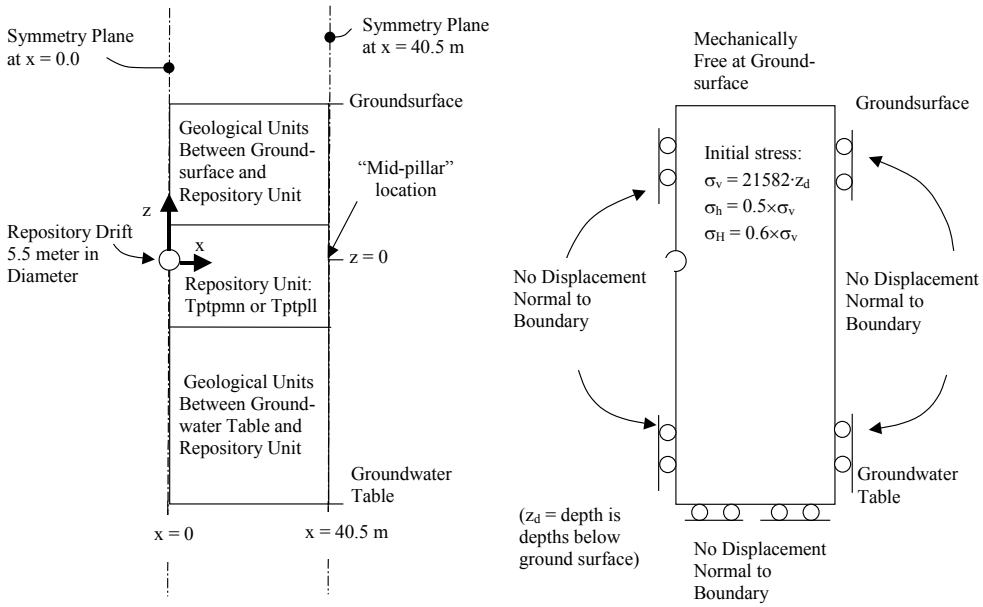

Figure 6.3-1. Domain and Boundary Conditions for the Drift-Scale THM Model

Table 6.3-1. THM Model Boundary Conditions

Boundary	Boundary Condition	Reference
Top of Tptpmn model domain which represents the conditions at the groundsurface near borehole USW SD-9	T = 17.68 °C S_l = 0.01 P = 86339 Pa Infiltration rate: 6 mm/year 0-600 years 16 mm/year 600-2000 years 25 mm/year >2000 years	Table 4.1-1 Table 4.1-1 Table 4.1-1 Table 4.1-1
Bottom Tptpmn model domain which represents the conditions at the groundwater table near borehole USW SD-9	T = 31.68 °C S_l = 0.99999 P = 92000 Pa	Table 4.1-1 Table 4.1-1 Table 4.1-1
Top Tptpll mode domain which represents the conditions at the groundsurface near the center of the repository	T = 16.13 °C S_l = 0.01 P = 84725 Pa Infiltration rate: 6 mm/year 0-600 years 16 mm/year 600-2000 years 25 mm/year >2000 years	Table 4.1-1 Table 4.1-1 Table 4.1-1 Table 4.1-1
Bottom Tptpll model domain which represents the conditions at the groundwater table near the center of the repository	T = 32.60 °C S_l = 0.99999 P = 92000 Pa	Table 4.1-1 Table 4.1-1 Table 4.1-1
Sides	No flux of water, gas, heat Mechanically fixed for normal displacement	Not Applicable Not Applicable
Drift Wall	Open boundary for water, gas, heat Mechanically free	Not Applicable Not Applicable
Waste Package Thermal Load	Initial heat of 1.45 kW/m decreasing with time (due to radioactive decay), and reduced by 86.3% during the first 50 years (due to removal by ventilation)	Table 4.1-1

NOTES: T = Temperature, S_l = liquid saturation, P = pressure

6.4 MATERIAL PROPERTIES

The THM properties used as direct input into the Drift-Scale THM Model and their sources are summarized in Section 4. The hydrological property set was developed in the mountain-scale calibration runs for the present-day ambient conditions at Yucca Mountain (BSC 2003 [160240], Section 6.3.2, Table 4): this property set is referred in this Model Report as the DS/AFM-UZ02-Mean Property set. The mechanical rock-mass properties are extracted from the qualified data set in the 1999 TBV-332/TBD 325 Resolution Analysis: Geotechnical Rock Properties (DTN: MO9911SEPGRP34.000 [148524], Tables 10 and 11) for 40% cumulative frequency. These elastic parameters, which represent the bulk rock mass (including the effect of fractures) have been estimated using an empirical method based on the Geological Strength Index (GSI). The adopted rock-mass Young's modulus for the rock in the repository units (Tptpmn and Tptpll) is about 50% lower than the Young's modulus of intact rock determined on core samples from the site. Assumptions 3 and 4, in Section 5, justify the choice of mechanical properties for TSw3 and CHn TM units located below the repository drift. The elastic properties of the CHn is taken from measurements on intact core samples (DTN: MO9911SEPGRP34.000 [148524], Table 8),

according to Assumption 4, in Section 5. TM and HM properties of the rock mass are developed within this Model Report as described below in this section.

As described in Section 6.1, to assess the impact of the THM processes on the flow field, it is sufficient to calculate changes in the mean value of the permeability for a conservative case of relative strong THM-induced changes in permeability. The conservative case is realized by adopting a conservative estimate of the coupled THM material properties. This includes a conservative estimate of the thermal expansion coefficient (leading to the maximum possible thermal stress) and a conservative estimate of a stress versus permeability function (leading to maximum possible permeability change).

The thermal expansion coefficient adopted for the Drift-Scale THM Model is derived from laboratory measurements on intact rock samples (Figure 6.4-1). The thermal expansion coefficient in the field could theoretically be equal to or lower than the intact value because of the presence of fractures. At the Single Heater Test (SHT), the *in situ* thermal expansion coefficient was determined to be slightly lower than the corresponding values for intact rock (CRWMS M&O 1999 [129261], p. 9-10). On the other hand, analysis of MPBX displacements at the early part of the DST by Sobolik et al. (1999 [163202], p. 741) and BSC (2001 [155957], pp. 21 and 115–125) indicate that the displacements are well predicted if intact-rock thermal expansion coefficient is used. In addition, both laboratory and field measurements have shown that the thermal expansion coefficient increases with temperature (Brodsky et al. 1997 [100653], Tables 4-4 through 4-7, pp. 30–33; DTN: SNL01B05059301.006 [129168]). Adopting a thermal expansion coefficient that closely represents the intact rock values can be considered as a conservative estimate for the purpose of this Model Report. The intact rock value is an upper bound of the possible *in situ* thermal expansion coefficient, which should give an upper bound of TM impact in the Drift-Scale THM Model. Figure 6.4-1 shows that the adopted function closely represents intact-rock thermal expansion coefficients for various rock units at Yucca Mountain. Therefore, the linear function shown in Figure 6.4-1 is adopted for all rock units in the Drift-Scale THM Model.

The parameters b_{max} and α in the stress-aperture function (Equation 6.2-9) are estimated through model calibration against air-permeability measurements conducted at several field experiments at Yucca Mountain. It is essential that these parameters are determined *in situ*, at a relevant scale, because of possible size dependency of the coupled HM properties of rock fractures (Rutqvist and Stephansson 2003 [162583]). The parameters b_{max} and α are uniquely determined from three air-permeability measurements, conducted at different stress levels, that represent three points on the stress-aperture function (Figure 6.4-2). The first data point on the stress-aperture function is defined by the initial aperture (back-calculated from the measured initial permeability) and the initial stress (estimated from *in situ* stress measurements). The initial aperture is estimated from the mean fracture frequency, f, and isotropic initial permeability, for an ideal cubic block model, leading to the formula (See Attachment I):

$$b_i = \sqrt[3]{6 \times k_i / f} \qquad \text{(Eq. 6.4-1)}$$

The second point on the stress-aperture function represents the conditions at high stress, when fractures are completely closed from a mechanical standpoint but still open to conduct water due

to their residual aperture. This point is abstracted from observed air-permeability changes at the DST (Figure 6.4-2). At the DST, the temperature in the rock increases up to 200°C, inducing strong thermal stresses expected to compress fractures to a smaller aperture. Air-permeability measurements show that the permeability decreases at most by a factor of about 0.15 at the end of the heating period (DTN: LB0208AIRKDSTH.001 [160897], borehole section 59-4 at 1/10/02 8:11 PM) and BSC 2003 [161530], Figure 7.4.3.3-2a). The factor 0.15 includes the effects of both TH-induced permeability changes (caused by changes in fracture moisture contents) and TM-induced permeability changes (caused by mechanical closure of fractures). BSC 2003 [161530], Figure 7.4.3.3-2a shows that TH-induced changes in permeability results in a permeability correction factor of 1.2. The TM-induced permeability correction factor can be estimated as 0.15/1.2 = 0.125. Hence, a residual permeability correction factor, F_{kr} = 0.125 is used for calibration of the stress-aperture function in this Model Report.

No numerical analysis is required for matching the stress-aperture function to the residual aperture. Applying a very high normal stress, σ_n to Equation (6.2-9), the residual aperture in each of the three fracture sets can be calculated directly. In this calculation, the initial aperture, b_i, is estimated to 51.8 μm, using Equation (6.4-1), an initial hydraulic permeability of 1e-13 m^2, and a mean fracture frequency of 4.32, both taken from Table 4.1-4. The initial stresses are calculated as described in Section 5, Assumption 2, for a depth of about 260 m. The calculated residual aperture is then inserted into Equation (6.2-5) to calculate the residual permeability-correction factors F_{kx}r, F_{ky}r, F_{kzr} in the x, y, and z direction, respectively. Finally, the geometric mean of the residual permeability correction factors is calculated as:

$$F_{kr} = \sqrt[3]{F_{kxr} \times F_{kyr} \times F_{kzr}} \qquad \text{(Eq. 6.4-2)}$$

A third data point on the stress-aperture curve (Figure 6.4-2) is obtained from numerical back-analyses of air-permeability measurements conducted at three excavated niches in the Tptpmn unit and one excavated niche in the Tptpll unit. These tests were conducted to study permeability changes near a drift wall caused by excavation effects (i.e., mechanical unloading of the rock mass near the drift wall causing fracture opening and consequent permeability increase). In the Tptpmn unit, the air permeability was measured before and after excavation in 0.3-meter packer-isolated sections along three boreholes located about 0.65 meters above the niches (BSC 2001 [158463], Section 6.1). In general, the permeability at the niche tests was found to increase by a factor of about 1 (no change) to 1,000 (an increase by three orders of magnitude) averaging about one orders of magnitude (BSC 2001 [158463], Section 6.1). It was also found that permeability generally changes more in initially lower-permeability sections.

In this study, the niche excavations were modeled using the FLAC3D V2.0 (LBNL 2001 [154783]) code to calculate changes in the stress field. Thus, the stress relief illustrated in Figure 6.4-2 was calculated with the FLAC3D V2.0 (LBNL 2001 [154783]) code model of the niches and using the mechanical properties of the rock mass given in Table 4.1.4. The FLAC3D V2.0 (LBNL 2001 [154783]) code model of the niches is described in Rutqvist (2002 [162047], pp. 14–18). Based on the calculated stress field, new fracture apertures for each fracture set can be calculated from Equation (6.2-9). The new apertures are then inserted into Equation (6.2-5) to calculate the excavation permeability correction factors F_{kx}e, F_{ky}e, F_{kze} in the x, y and z direction. Finally, the geometric mean of the excavation permeability correction factors are calculated as:

$$F_{ke} = \sqrt[3]{F_{kxe} \times F_{kye} \times F_{kze}} \quad \text{(Eq. 6.4-3)}$$

As a matching point, a permeability correction factor of F_{ke} = 9 is abstracted from BSC (2001 [158463], Figures 6.1.2-11 to 6.1.2-15). In these figures, a permeability correction factor of F_{ke} = 9 is in good agreement with the observed trend lines for the measured data at Niche 3107, 4788, and CD 1620 at an initial permeability of 1e-13 m^2.

Figure 6.4-3 presents the results of calibrating the parameters b_{max} and α. The two curves in Figure 6.4-3 shows different combinations of b_{max} and α that satisfy the condition of F_{kr} = 0.125 (red curve) and F_{ke} = 9 (blue curve). The red curve is determined by a trial-and-error iterative calculation in which b_{ma} is kept fixed at different discrete values between 100 to 400 μm, and for each $b_{max,}$ α is adjusted until the condition F_{kr} = 0.125 is satisfied. Similarly, the blue curve is determined by keeping b_{max} fixed and then adjusting α until the condition F_{ke} = 9 is satisfied. This calculation, resulting in the red and blue line of Figure 6.4-2 was conducted using an MS Excel spreadsheet as described in Attachment I. A unique solution, satisfying both the condition of F_{kr} = 0.125 and F_{ke} = 9, is obtained for b_{max} = 200 μm and α = 0.52 MPa^{-1} (Figure 6.4-3). These values of b_{max} and α are adopted for all rock units in the Drift-Scale THM model.

Table 6.4-1 summarizes the model parameters developed in this section of the Model Report.

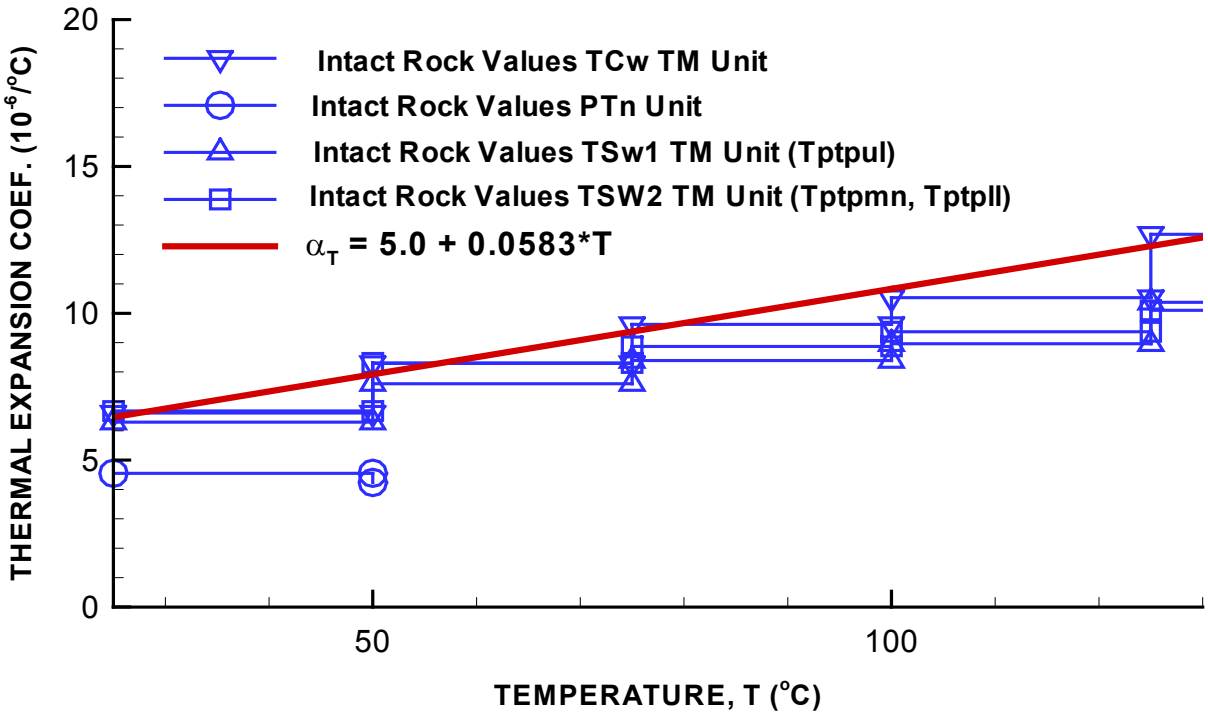

NOTE: Laboratory values are taken from MO0004RIB00035.001 [153848], Table 13 and represents values determined during heat-up on specimens from NRG boreholes. The red line is matched visually to the maximum values of thermal expansion coefficient at each temperature. The line was matched to maximum values of intact-rock thermal expansion because maximum thermal expansion represents a conservative case of maximum possible thermal-mechanical impact in a THM analysis.

Figure 6.4-1. Temperature-Dependent Thermal Expansion Coefficient in the DST Model Domain with Comparison to Values of Intact Rock Samples for Various TM Units

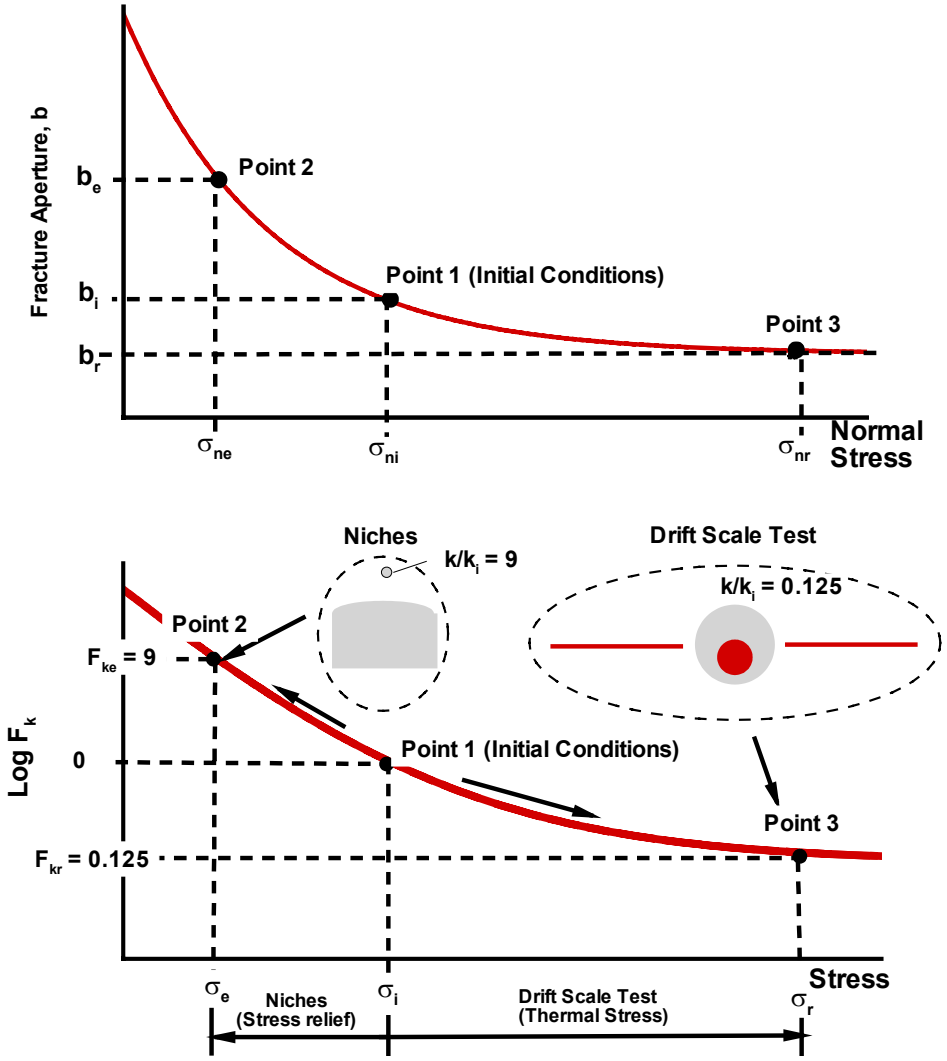

NOTE: The three data points can uniquely constrain the stress-aperture function resulting in determination of parameters b_{max} and α.

Subscripts n = normal, i = initial conditions, e = conditions after excavation and subscript r represents conditions at high stress when fracture aperture and fracture permeability is close to their residual values. Hence, F_{ke} is permeability correction factor after excavation and F_{kr} is permeability factor at high stress when fracture aperture and fracture permeability is close to their residual values.

Figure 6.4-2. Schematic of Calibration of Stress-Aperture Function Using Three Air-Permeability Measurements Conducted at Three Different Stress Levels

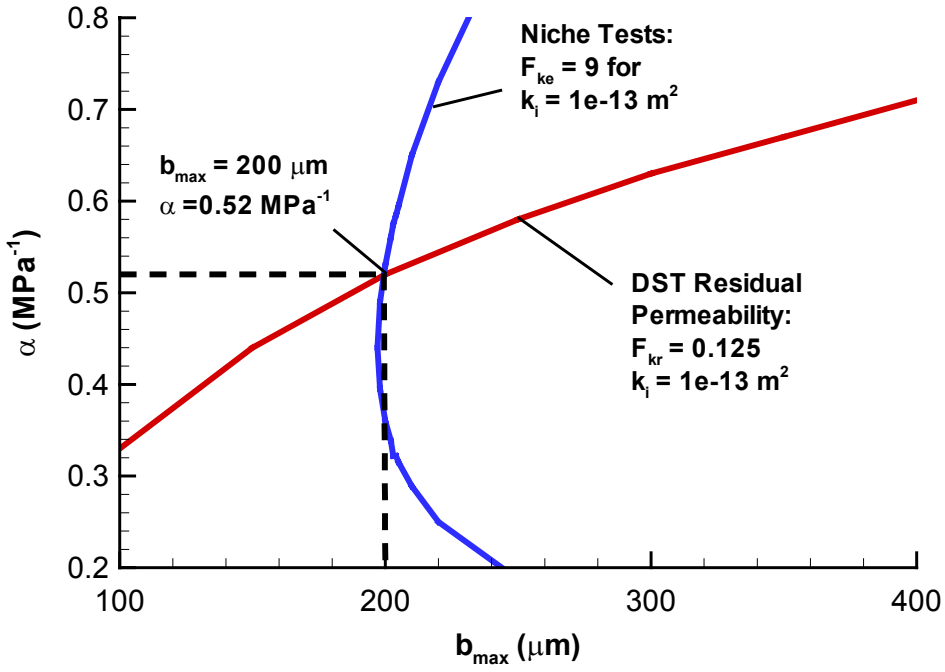

Output - DTN: (calculation of red and blue line) LB0306DSTTHMVL.002

NOTE: F_{ke} = Permeability correction factor (k/k_i) as a result of stress relief after excavation of a niche

F_{kr} = Permeability correction factor (k/k_i) as a results of stress increase cause by thermal stress at the DST

k_i = Initial fracture permeability

The red and blue lines shows combinations of b_{max} and α that satisfy the conditions of F_{ke} = 9 and F_{kr} = 0.125, respectively. The calculations leading to the red and blue lines are described in detail in Attachment I. Both conditions of F_{ke} = 9 and F_{kr} = 0.125 are only satisfied at the intersection of the blue and red line for b_{max} = 200 and α = *0.5*2 MPa^{-1}.

Figure 6.4-3. Determination of Parameters b_{max} and α by Model Calibration against Air-Permeability Measurements from the DST and Niche Tests

Table 6.4-1. Summary of TM and HM Parameters and Properties of the Rock Mass Developed in this Model Report for the Drift-Scale THM Model

	Geol. Unit >	Tptpul	Tptpmn	Tptpll	Source
Initial hydraulic aperture	b_i (μm)	179	77	120	Calculated using Equation (6.4-1) using values of frequency and permeability given in Table 4.1-4
Maximum joint closure for Equation (6.2-9)	b_{max} (μm)	200	200	200	Developed by model calibration against field experiments (Figure 6.4.3)
Exponent for α for Equation (6.2-9)	α (1/Pa)	5.2E-7	5.2E-7	5.2E-7	Developed by model calibration against field experiments (Figure 6.4.3)
Thermal Expansion Coefficient	α_T (10^{-6}/°C)	5.0+0.0583×T	5.0+0.0583×T	5.0+0.0583×T	Derived from laboratory tests (Figure 6.4.1)

NOTE: T = Temperature in °C

6.5 SIMULATION RESULTS FOR THE TPTPMN MODEL DOMAIN

This subsection presents modeling results for a representative drift located in the Tptpmn unit. Discussion is focused on permeability changes in the vicinity of the repository drift and its impact on the flow field. The impact on the flow field is evaluated by a comparison of fully coupled THM simulation results with partially coupled TH simulation results.

6.5.1 Excavation of the Repository Drift

The simulation was conducted by first excavating the drift and then emplacing a thermal waste package into the drift. Excavation of the drift caused stress and permeability changes in the rock mass immediately around the drift (Figure 6.5.1-1a and b). Most changes occurred near the top and bottom of the drift, where the horizontal permeability increases by about one order of magnitude. Near the springline of the drift, vertical permeability increased while horizontal permeability decreased, resulting in much smaller changes in mean permeability. The increased permeability at the top of the drift is consistent with measured permeability changes at three excavated niches located in the Tptpmn unit (BSC 2001 [158463], Table 6.1.2-1).

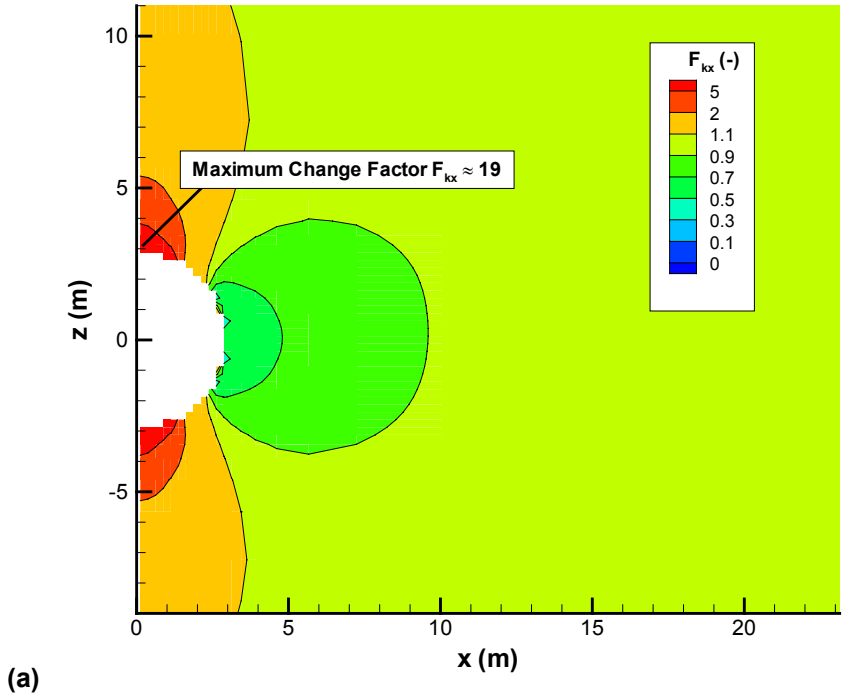

(a)

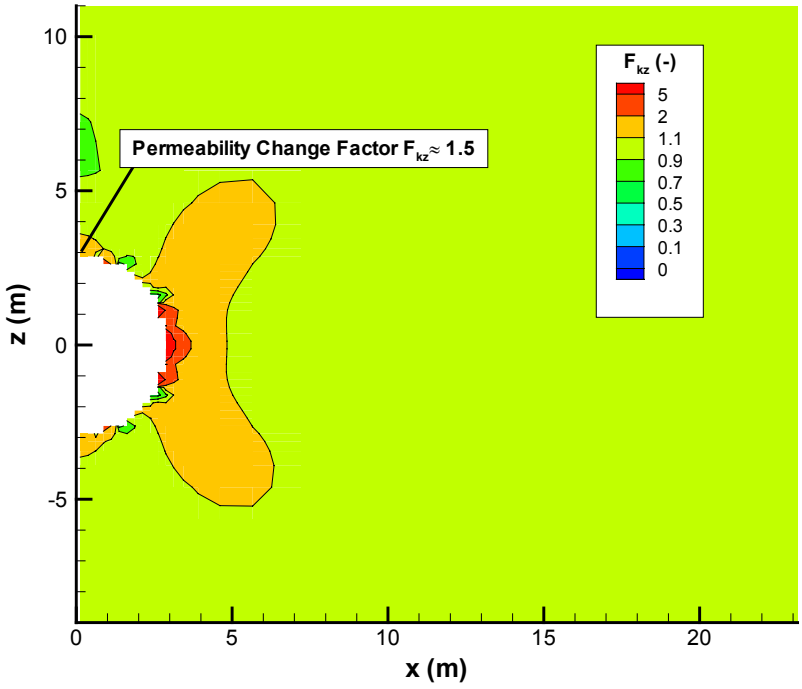

(b)

Output - DTN: LB0306DRSCLTHM.002

Figure 6.5.1-1. Permeability Correction Factor Caused by Stress Redistribution during Excavation of the Emplacement Drift: (a) Correction Factor (F_{kx} = kx/ki) for Horizontal Permeability; (b) Correction Factor (F_{kz} = kz/ki) for Vertical Permeability (Tptpmn Model Domain)

6.5.2 Evolution of Temperature

After emplacement of the waste in the excavated drift, the temperature in the drift wall rises rapidly and peaks at about 80 years, a few tens of years after the end of the forced ventilation period (Figures 6.5.2-1). As explained in Section 6.3, the emplacement is conditioned to take place all at once in the entire repository. In reality, the emplacement will end in 24 years followed by 50 more years of ventilation. Thus, the peak temperature will not occur at the same time at all drifts, but is likely after more than 80 years from the drift emplacement of the first waste package. Nevertheless, as shown in Figure 6.5.2-1, the simulated temperature in the rock mass away from the drift continues to rise, and the mid-pillar temperature peaks at about 89°C after 800 years (see location of mid-pillar in Figure 6.3-1a). After about 1,000 years, a general decline in temperature at the repository level takes place. At the same time, the thermal gradient around the repository becomes smaller with the declining temperature difference between the drift wall and the mid-pillar. However, at 10,000 years, the temperature is about 45 to 50°C, which is still significantly higher than the initial temperature of 24°C. The calculated evolution of temperature and peak-temperature is consistent and almost identical for a partially coupled TH and a fully coupled THM analysis. Thus, the THM coupling does not significantly impact the temperature evolution.

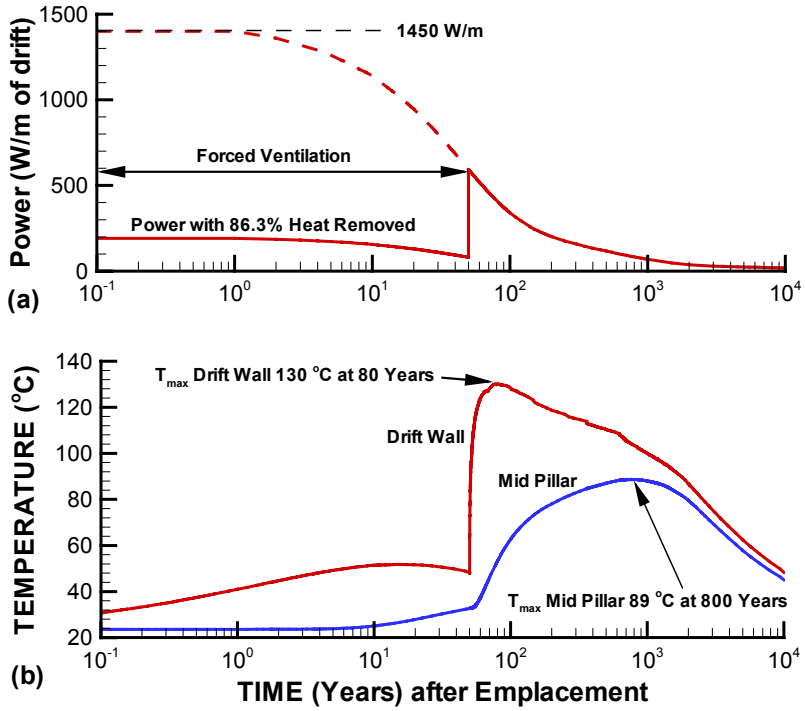

Output - DTN: LB0306DRSCLTHM.002

NOTE: Mid-pillar is a point located at the mid-distance between neighboring repository drifts as defined in shown in Figure 6.3-1a. Time 0 is at emplacement of the waste package into the drift which is assumed to take place all at once for the entire repository.

Figure 6.5.2-1. Evolution of Thermal Power from Waste Package (a) and Temperature at Two Points on the Level of the Emplacement Drifts (b)

6.5.3 Evolution of Thermal Stress

The evolution of thermal stress is important for evaluation of the potential for stress-induced rock failure for prediction of stress-induced changes in fracture permeability. Stress-induced rock failure would first be initiated near the drift wall, where large differences between maximum and minimum principal stresses can occur. Large differences in principal stress can occur near the drift wall because of a lack of confinement in a direction normal to the drift wall. Moreover, redistribution of compressive stresses around the drift implies that high tangential compressive stress will occur at the drift wall. Changes in permeability caused by thermal stresses can occur both near the drift wall and away from the drift wall. It is therefore important to evaluate the thermal stresses near the drift wall as well as in the rock mass away from the drift wall.

Figure 6.5.3-1 and 6.5.3-2 shows that the increased rock temperature causes thermal expansion of the rock mass with accompanying deformations and increased compressive stresses. The magnitude of thermally induced stresses generally depends on the thermal expansion coefficient, the modulus of elasticity, and the degree of confinement. Consequently, the highest thermal stresses are created in the horizontal direction because of the confinement of the model between the fixed lateral boundaries (see mechanical boundary conditions in Figure 6.3-1b). Note that the condition of fixed lateral boundaries results from the condition that emplacement of all waste occurs at once, providing a repetitive symmetry of no displacements normal to the lateral boundaries. The lateral fixed boundaries is a conservative case for estimating the impact of THM processes because it leads to the highest possible heat load and therefore the highest possible thermal stress. Figure 6.5.3-1 shows that high horizontal stress develops at the repository level at 100 years (green contour level around z = 0). At 1,000 years, a zone of increased horizontal stress extends more than one hundred meters below and above the repository. This zone of significantly increased thermal stress extends over the TSw1, TSw2, and Tsw3 TM units, which have a relatively high modulus of elasticity. The thermal stresses are much smaller in the PTn and CHn units because of the much smaller modulus of elasticity in these units. The zone of increased compressive stress has contracted somewhat at 10,000 years. Figure 6.5.3-2 shows that smaller thermal stresses developed in the vertical direction. This is a result of the free-moving ground surface, and hence, a lack of mechanical confinement in the vertical direction. The maximum compressive stress occurs at the drift crown as a result of high thermal stress in the horizontal direction and stress concentration at the drift walls (Figure 6.5.3-3a). Figure 6.5.3-4 shows that the maximum horizontal stress is about 31 MPa at the drift crown and occurs 100 to 500 years after emplacement, whereas the stresses at mid-pillar reach about 14 MPa. The mid-pillar stress is lower than the stress at the drift crown, but is relevant for assessing the general permeability changes at the repository level in areas away from the immediate surrounding of the drift. This calculated stress evolution is in general agreement with the *Drift Degradation Analysis* (BSC 2003 [164285], Section 6.2), with a maximum horizontal stress of about 30 MPa at the drift wall.

The evolution of the hydraulic properties as a result of these thermally induced stress changes is presented in the next section. The potential for thermally induced rock failure at the drift crown is discussed in Section 6.8.2.

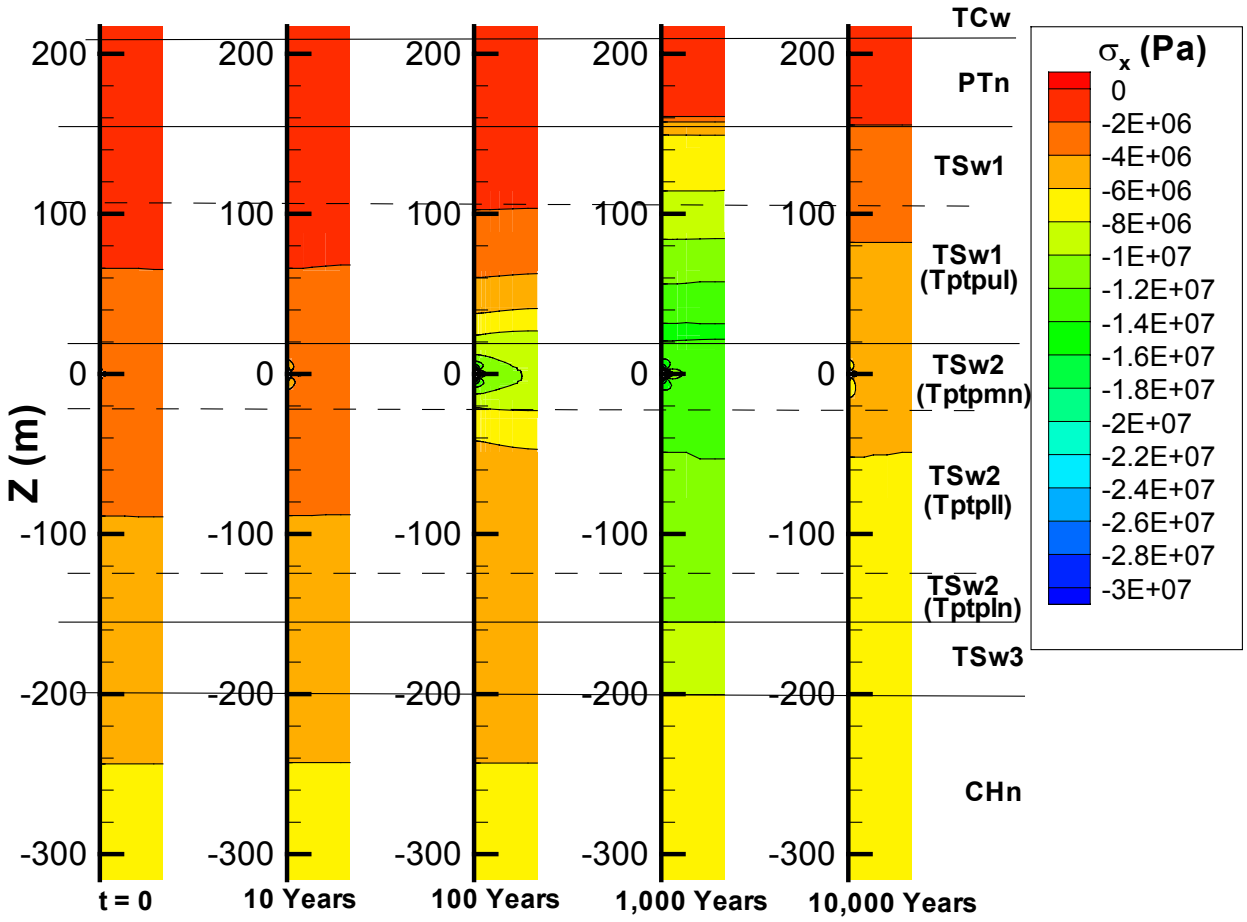

Output - DTN: LB0306DRSCLTHM.002

NOTE: The width of each column is 40.5 meters. The top is the ground surface and the bottom is the water table.

Figure 6.5.3-1. Evolution of Horizontal Stress (σ_x) in the Tptpmn Model Domain

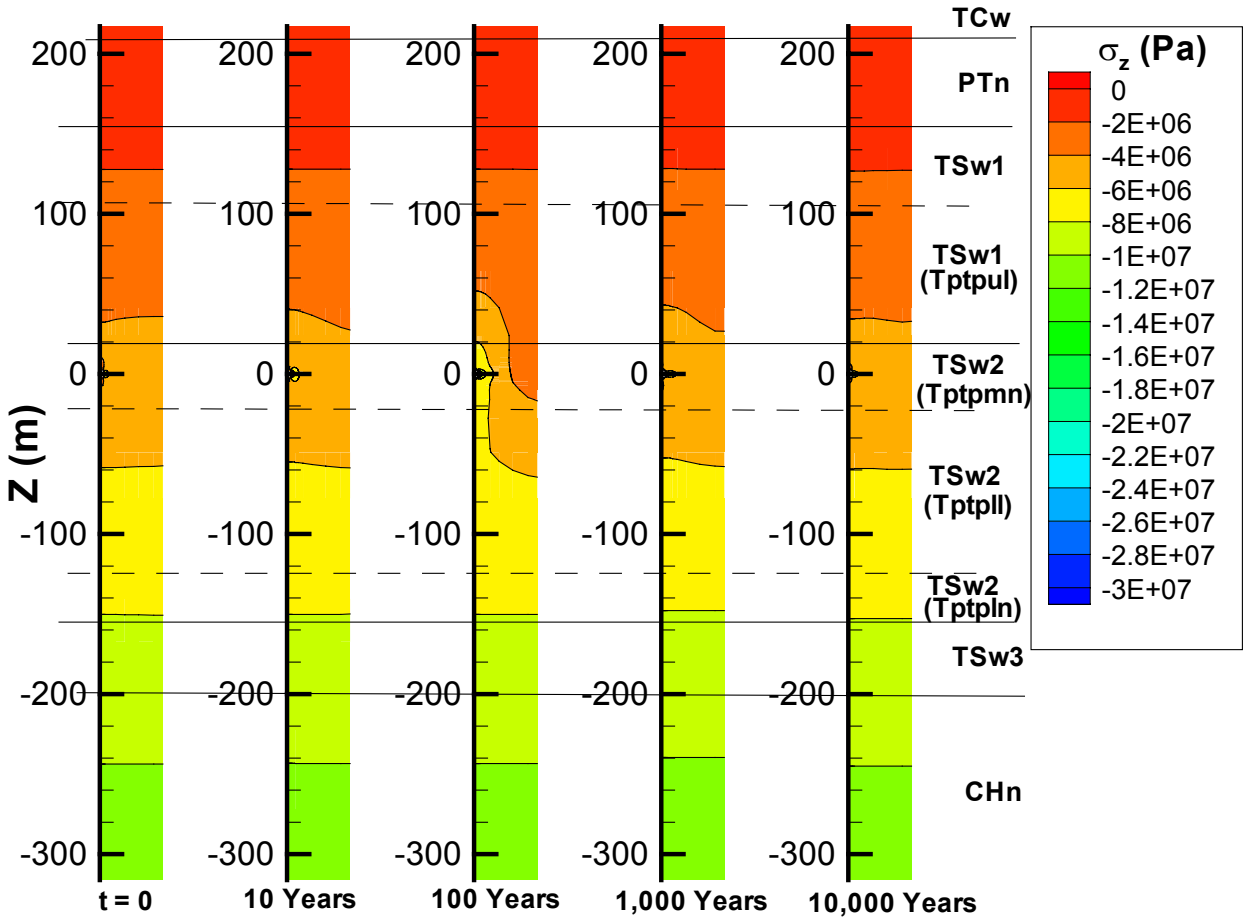

Output - DTN: LB0306DRSCLTHM.002

NOTE: The width of each column is 40.5 meters. The top is the ground surface and the bottom is the water table.

Figure 6.5.3-2. Evolution of Vertical Stress (σ_z) in the Tptpmn Model Domain

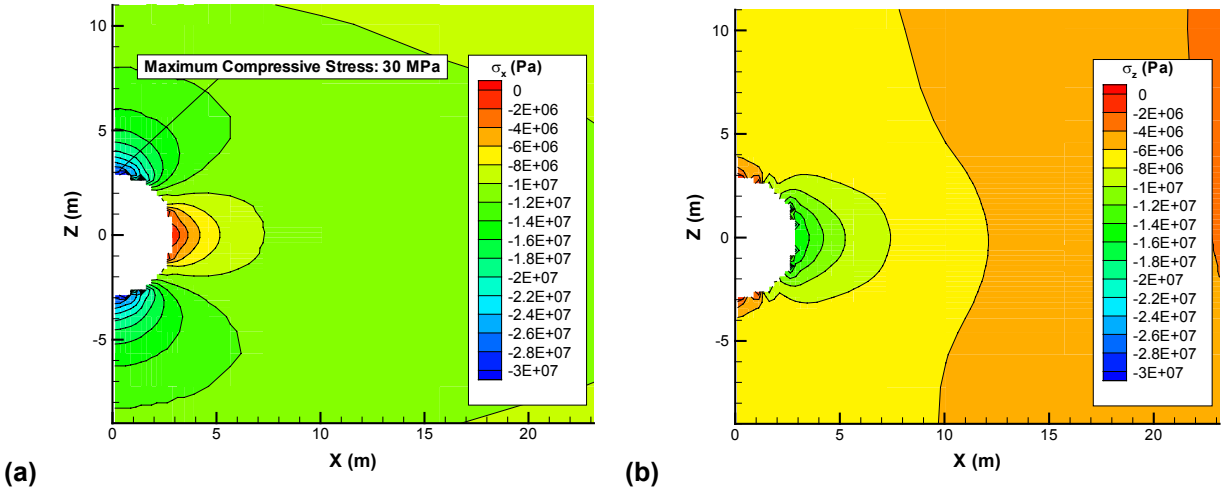

Output - DTN: LB0306DRSCLTHM.002

Figure 6.5.3-3. Distribution of (a) Horizontal Stress (σ_x) and (b) Vertical Stress (σ_z) at 100 Years after Emplacement (Tptpmn Model Domain)

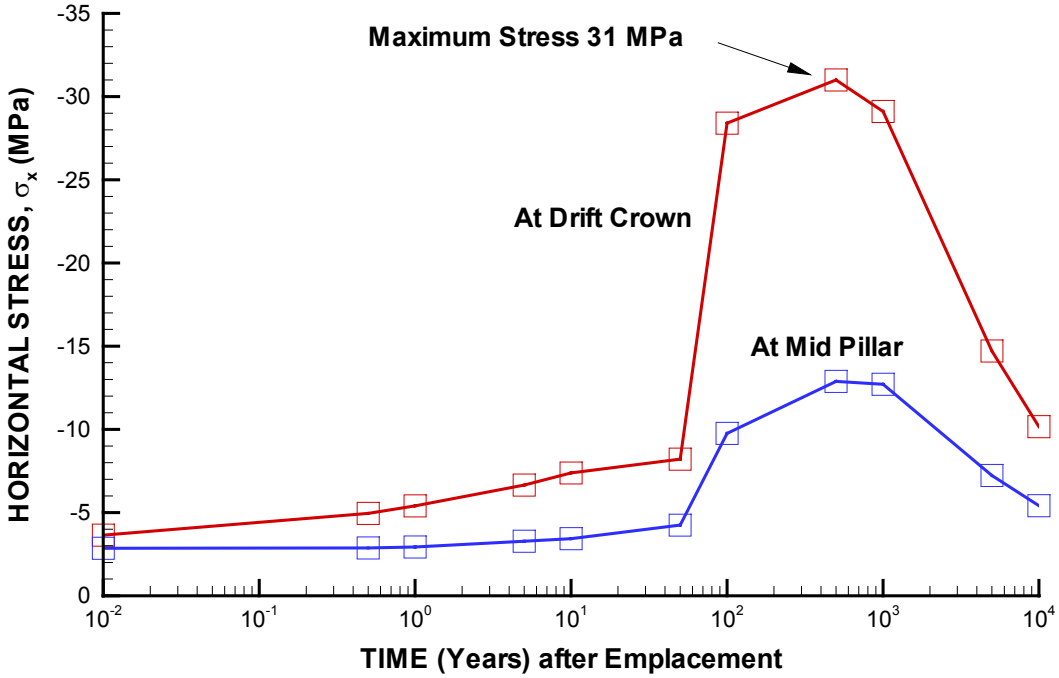

Output - DTN: LB0306DRSCLTHM.002

NOTE: Mid-pillar is a point located at the mid-distance between neighboring repository drifts as defined in shown in Figure 6.3-1a.

Figure 6.5.3-4. Evolution of Horizontal Stress in the Drift Crown and at the Mid-Pillar Location

6.5.4 Evolution of Hydraulic Properties

Figures 6.5.4-1 to 6.5.4-6 present evolution of hydraulic properties at 10, 100, 1,000 and 10,000 years. These times are selected because they represent the following conditions: (1) preclosure conditions (10 years), (2) maximum drift-wall temperature (100 years), (3) maximum thermal-mechanical impact at the repository level (1,000 years) and (4) the end of the licensing period. These times represent various extremes in the THM conditions at the drift scale and are therefore sufficient for evaluating what impact of THM processes have on hydraulic properties and percolation flux.

TM processes induce compressive stresses that act across fractures, closing them to a smaller aperture with an associated decrease in permeability and an increase in capillary pressure. In general, the calculation shows that the vertical permeability (Figure 6.5.4-1) changes much more than the horizontal (Figure 6.5.4-2), corresponding to the result that horizontal fractures stay open during the entire heating cycle, whereas vertical fractures tighten to their residual aperture. The horizontal fractures remain open because no significant thermal stress can develop in the vertical direction, on account of the free-moving ground surface. Vertical fractures, on the other hand, close because thermal stresses develop in the horizontal direction as a result of the confinement (no displacement conditions) at lateral boundaries. For example, at 1,000 years, the results show that horizontal stresses have generally increased from 2.9 to 14 MPa at drift level (see stress at mid-pillar location in Figure 6.5.3-4), while vertical stresses remain almost unchanged.

Figures 6.5.4-1 and 6.5.4-2 show how the zone of decreased permeability extends farther away from the repository over time. At 10 years, this zone extends about 20 m above and below the repository drift. At 1,000 years, permeability changes are observed several hundred meters below the drift and all the way up to the ground surface. The changes are relatively larger in the area above the repository, towards the ground surface, compared to regions below the repository. These trends are associated with different initial fracture permeability in different hydrological units and a small initial stress toward the ground surface. Furthermore, relatively strong permeability changes occur in the Tptpmn unit surrounding the repository ($z = \pm 20$ m) and in the tsw31–33 units ($z = 100$–160 m). The relatively stronger permeability changes in these units are also associated with a relatively small initial fracture aperture.

Figures 6.5.4-3 and 6.5.4-4 present the evolution of permeability around the drift in the Tptpmn unit. At 10 years, this decrease is able to overcome the initial excavation-induced permeability increases, except possibly in areas very close to the crown of the drift (Figure 6.5.4-4a). With time, the permeability decreases further and the zone of decreased permeability propagates farther from the drift. At 100 and 1,000 years, the permeability has decreased to a residual value of around 0.03 to 0.06 of the original permeability, because vertical fractures have closed to their residual aperture values. At 10,000 years, the declining rock temperature and thermal stresses cause the previously decreasing permeability to recover somewhat. However, at the drift crown, the vertical permeability still remains at one order of magnitude below its original value.

Figure 6.5.4-5 and 6.5.4-6 presents the changes in fracture capillary pressure, which are calculated according to the Leverett correction function in Equation (6.2-6). In general, the capillary pressure increases because of fracture closure, except very close to the drift, where the

capillary pressure decreases because of fracture opening. The calculated changes range between a factor of 0.6 to 2.

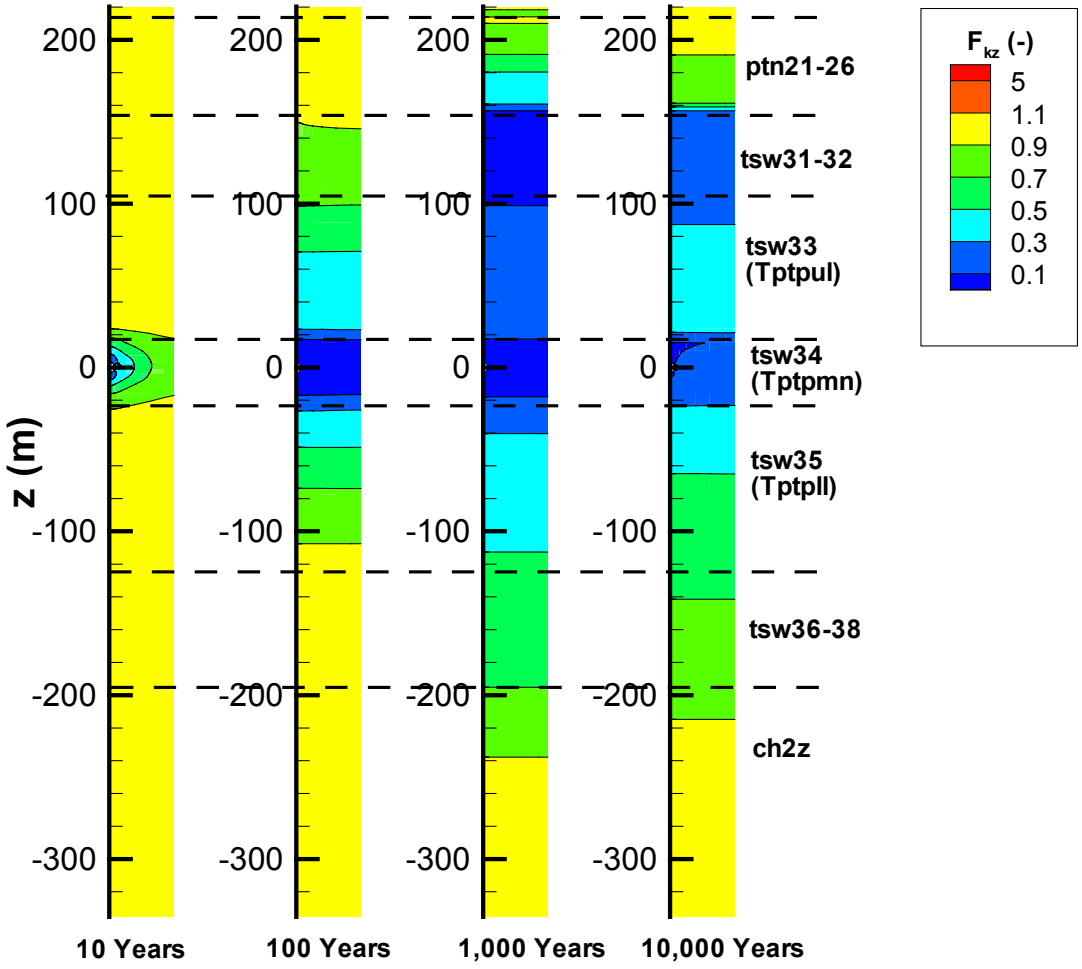

Output - DTN: LB0306DRSCLTHM.002

NOTE: The width of each column is 40.5 meters. The top is the ground surface and the bottom is the water table.

Figure 6.5.4-1. Evolution of Vertical Permeability Correction Factor ($F_{kz} = k_z/ki$) Relative to Pre-Excavation Permeability in the Tptpmn Model Domain

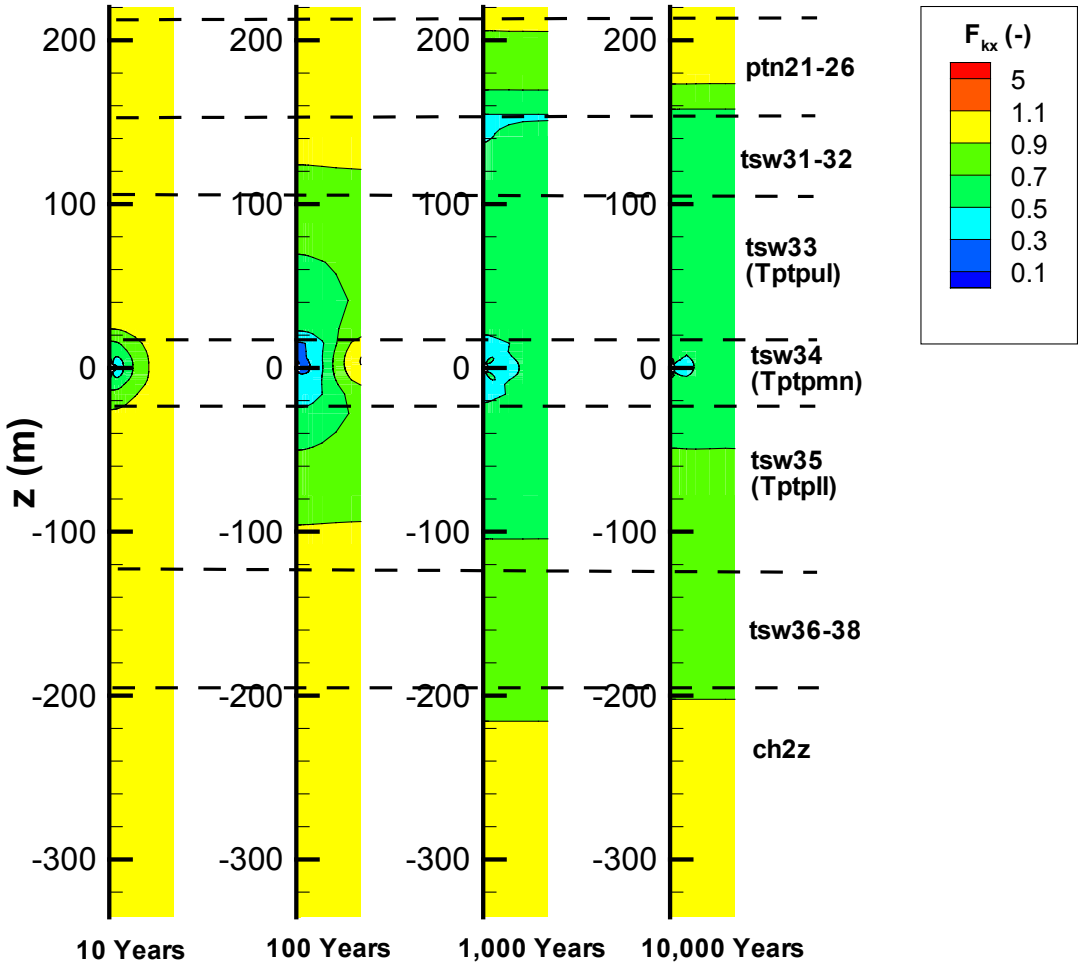

Output - DTN: LB0306DRSCLTHM.002

NOTE: The width of each column is 40.5 meters. The top is the ground surface and the bottom is the water table.

Figure 6.5.4-2. Evolution of Horizontal Permeability Correction Factor ($F_{kx} = k_x/k_l$) Relative to Pre-Excavation Permeability in the Tptpmn Model Domain

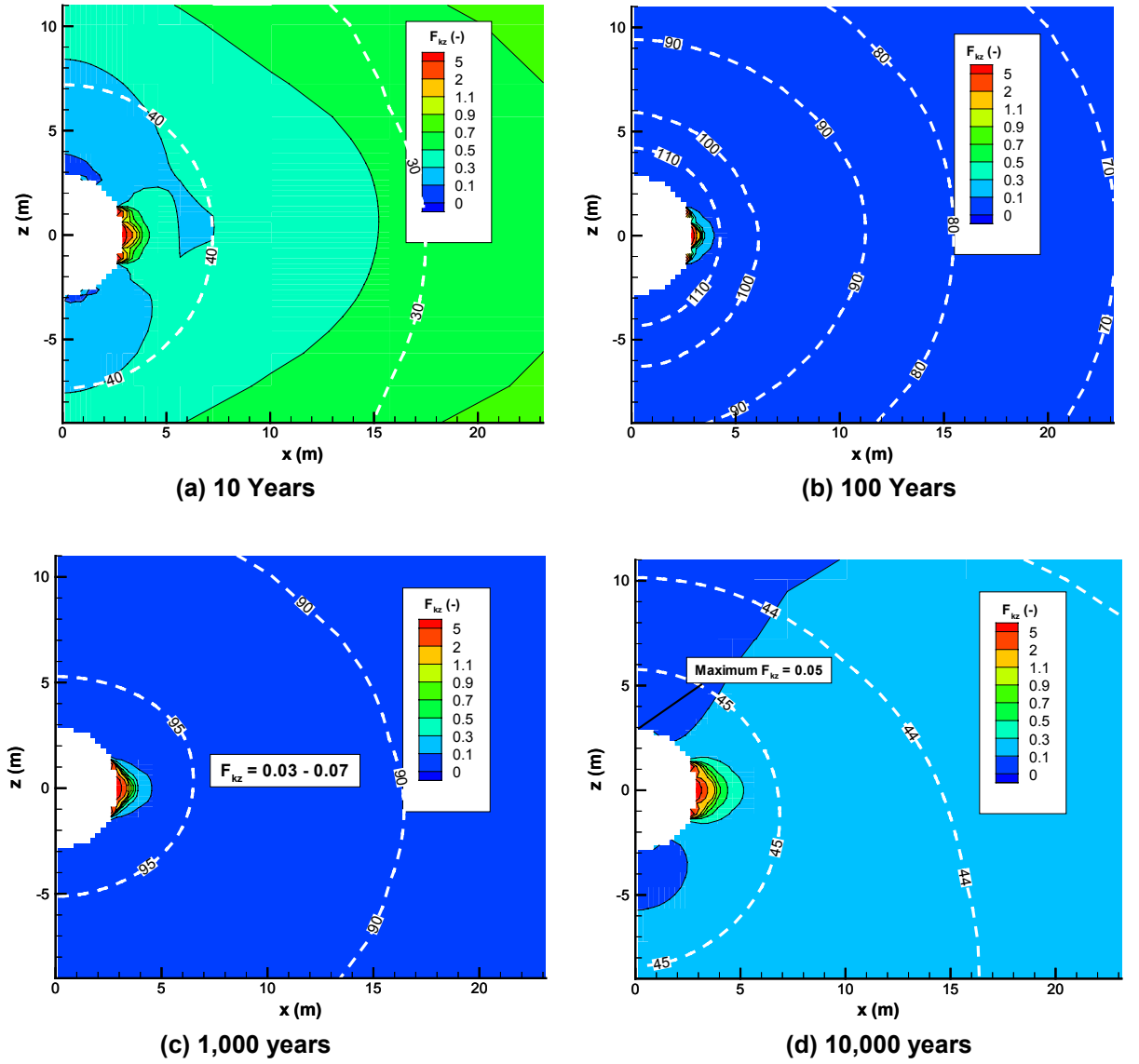

Output - DTN: LB0306DRSCLTHM.002

Figure 6.5.4-3. Evolution of Vertical Permeability Correction Factor ($F_{kz} = k_z/k_l$) Relative to Pre-Excavation Permeability around the Emplacement Drift in the Tptpmn Unit

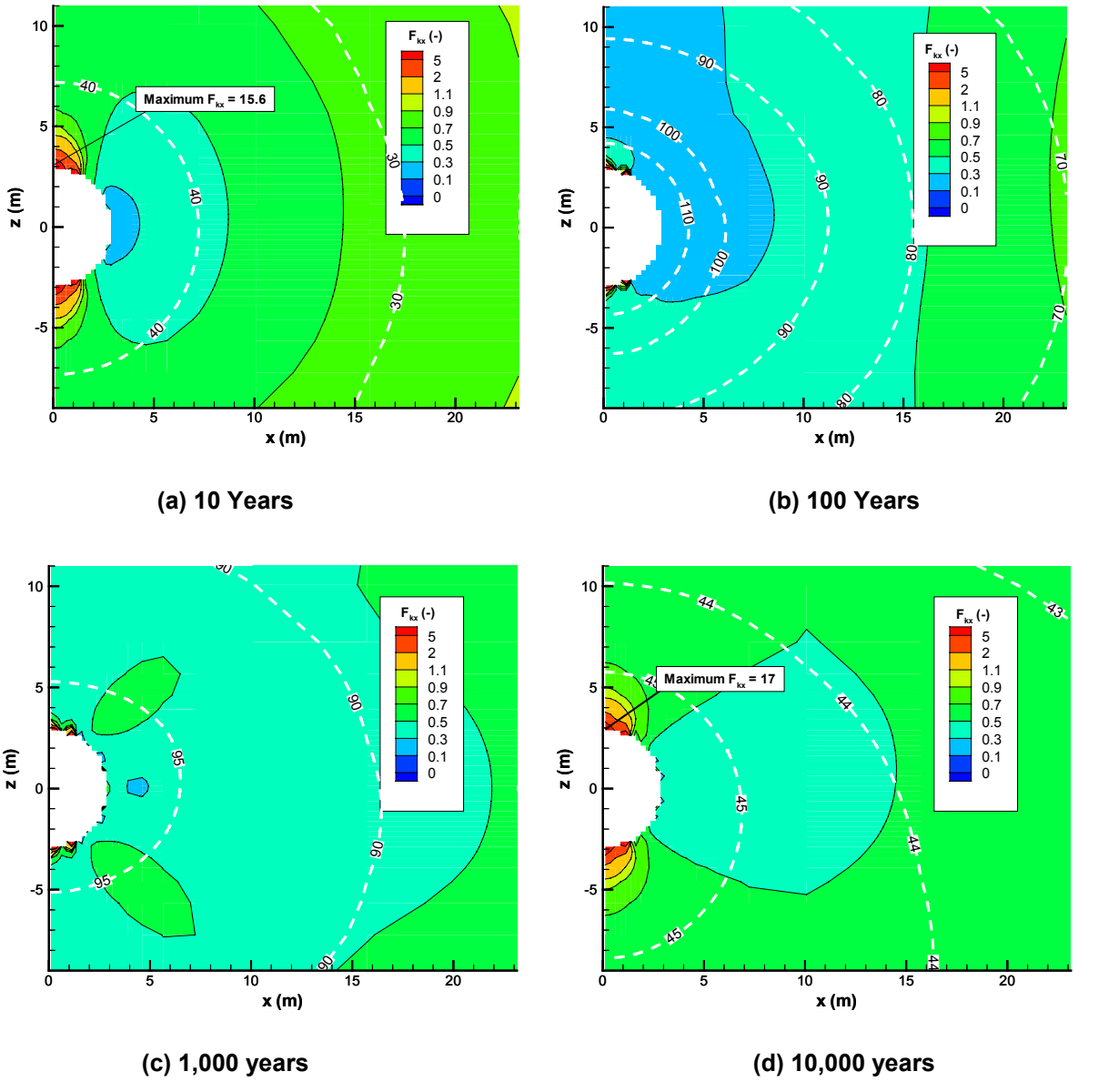

Output - DTN: LB0306DRSCLTHM.002

Figure 6.5.4-4. Evolution of Horizontal Permeability Correction Factor ($F_{kx} = k_x/k_l$) Relative to Pre-Excavation Permeability around the Emplacement Drift in the Tptpmn Unit

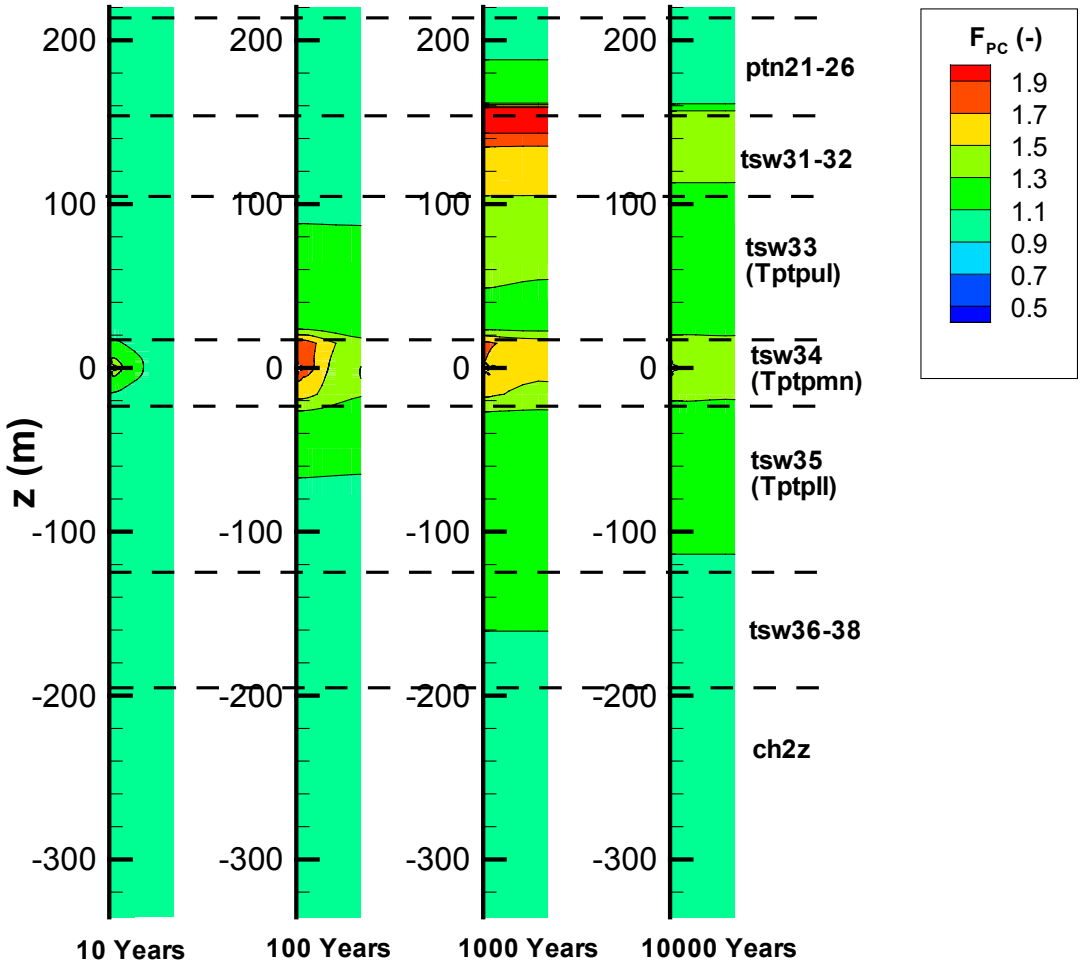

Output - DTN: LB0306DRSCLTHM.002

NOTE: The width of each column is 40.5 meters. The top is the ground surface and the bottom is the water table.

Figure 6.5.4-5. Evolution of Stress-Induced Capillary-Pressure Correction Factor ($F_{PC} = P_c/P_{ci}$) Relative to Pre-Excavation Value in the Tptpmn Model Domain

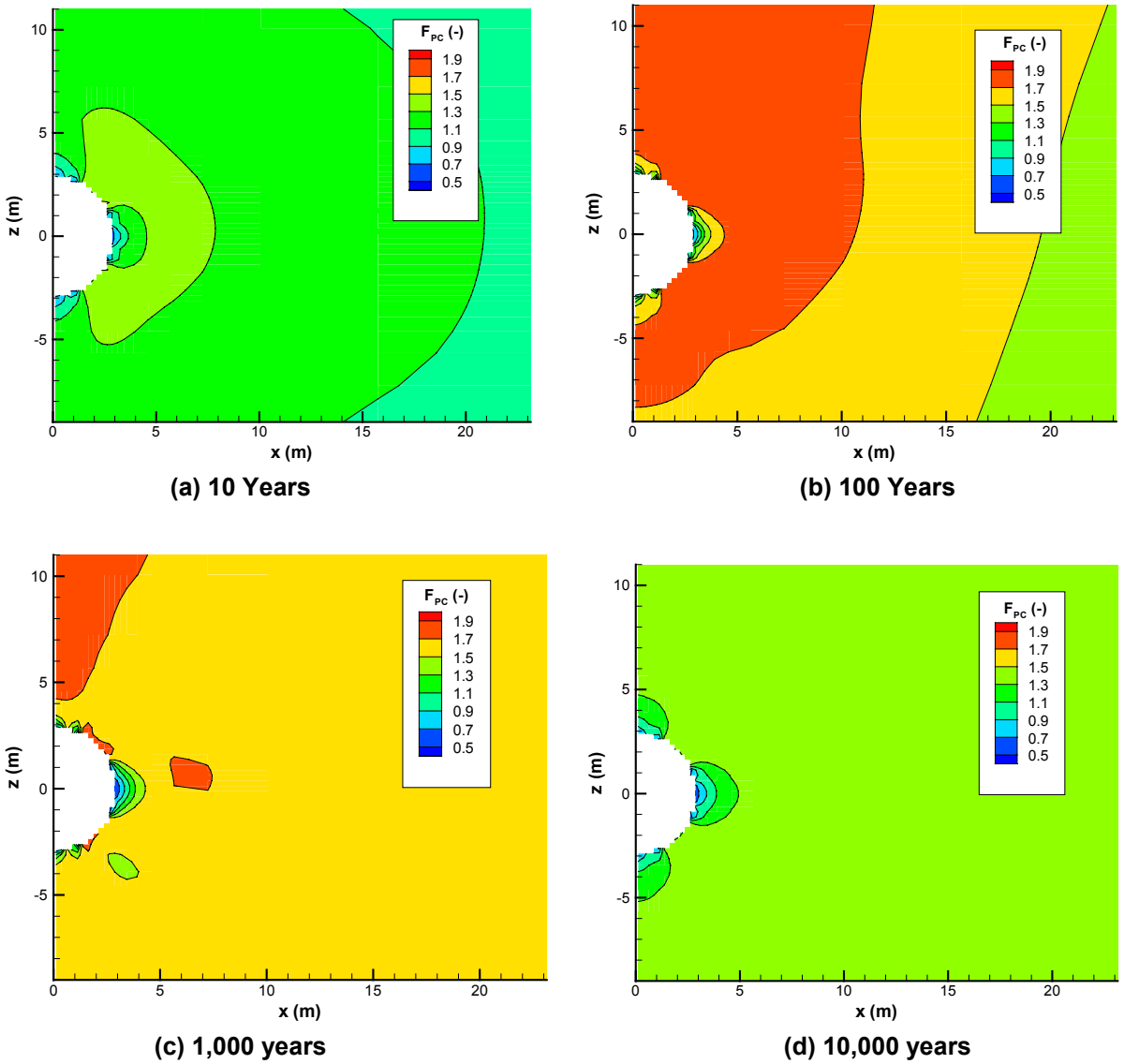

Output - DTN: LB0306DRSCLTHM.002

Figure 6.5.4-6. Evolution of Stress-Induced Capillary-Pressure Correction Factor ($F_{PC} = P_c/P_{ci}$) Relative to Pre-Excavation Values around the Emplacement Drift in the Tptpmn Unit

6.5.5 Impact on Fluid Flow Field

The impact of HM coupling is investigated by comparing a fully coupled THM simulation with a TH simulation. In the TH simulation, the hydrological properties of the rock mass are constant in time, which means that the coupling between hydraulic and mechanical processes—the HM coupling—is neglected. The impact on the flow field is investigated by comparison of vertical liquid flux in the fractured continuum and fracture liquid saturation. Saturation and vertical percolation flux distributions at 10, 100, 1,000, and 10,000 years, with and without HM coupling (TH and THM), are shown in Figure 6.5.5-1 and 6.5.5-2, for the entire Tptpmn model domain. The main difference in saturation profiles between TH and THM results is a slightly higher saturation in the Tptpmn unit at z = -20 to 20 m (Figure 6.5.5-1) and in Tsw31 and 32 at z = 100 to 140 m. These changes appear to be associated with changes in the capillary pressure function (as shown in Figure 6.5.4-5). The liquid flow patterns, on the other hand, are quite similar between the TH and THM cases (Figure 6.5.5-2). One reason for the similarity is that the reduced permeability is accompanied by a higher relative permeability from the increased liquid saturation, which may have compensated for part of its impact. Another reason may be that permeability reduction is constant horizontally across the flow domain. Since the vertical downward flux cannot flow around regions of reduced permeability, it is thus forced to take the same flow pattern. Only in the area close to the repository does a noticeable change in the flow pattern occur.

Figures 6.5.5-3 to 6.5.5-5 present a comparison between the TH and THM flow fields in the Tptpmn unit around the repository drift. At 100 years, the formation of a dryout zone and a condensation cap above the drift is apparent for both TH and THM results (Figure 6.5.5-3). It is shown that vertical liquid flow is redirected around the dryout zone. In Figures 6.5.5-3 to 6.5.5-5, there are some differences in the distribution of the vertical liquid flux between TH and THM results, which appear to be related to calculated changes in capillary pressure as shown in Figure 6.5.4-6. However, the main impact of the THM processes is that the dryout zone around the repository drift is smaller (e.g., Figure 6.5.5-4). In the THM modeling, the dryout zone has contracted to the drift wall at about 1,000 years. This smaller dryout zone is caused primarily by a significantly smaller fracture permeability, which reduces the convection of heat and thereby reduces the heat-pipe effect, leading to an accelerated rewetting of the dryout zone.

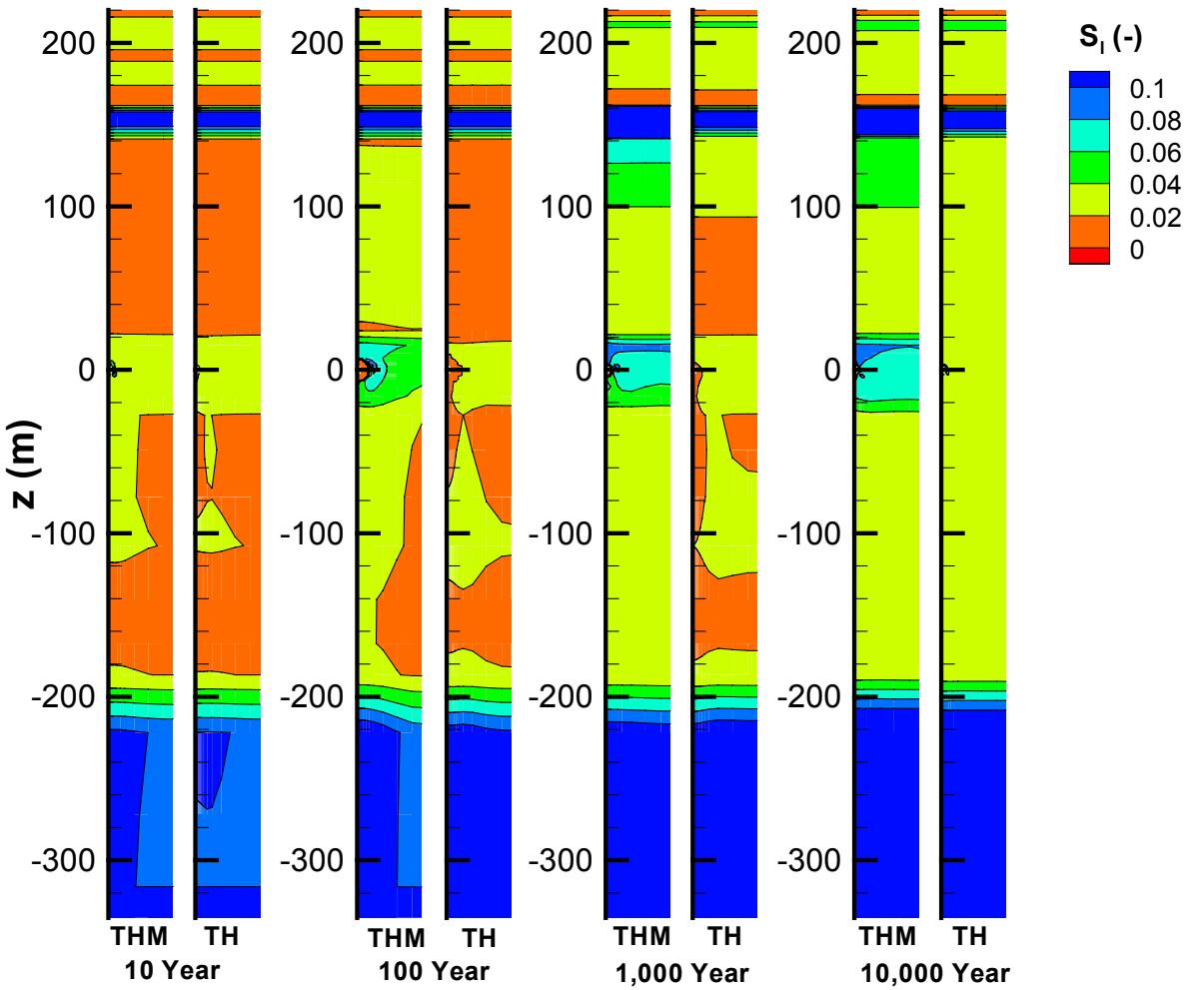

Output - DTN: LB0306DRSCLTHM.002

NOTE: The difference between the color regions such as orange and pale green is only 0.02 Sl.

Figure 6.5.5-1. Comparison of the Distribution of Liquid Saturation (S_l) in the Fractures for a Fully Coupled THM Simulation and TH Simulation (Tptpmn Model Domain)

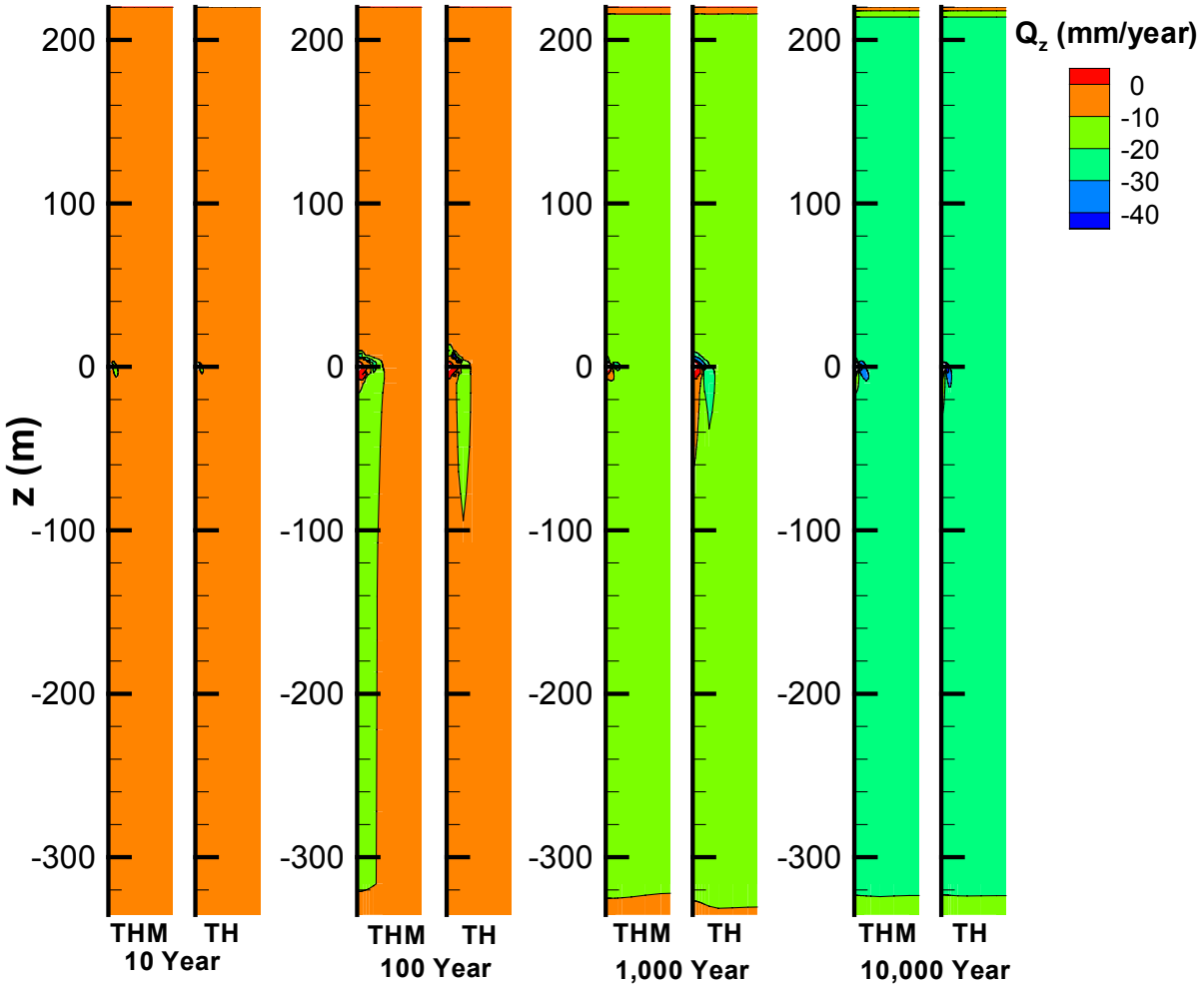

Output - DTN: LB0306DRSCLTHM.002

NOTE: The width of each column is 40.5 meters. The top is the ground surface and the bottom is the water table.

Figure 6.5.5-2. Comparison of the Distribution of Vertical Liquid Flux (Q_z) for a Fully Coupled THM Simulation and TH Simulation (Tptpmn Model Domain)

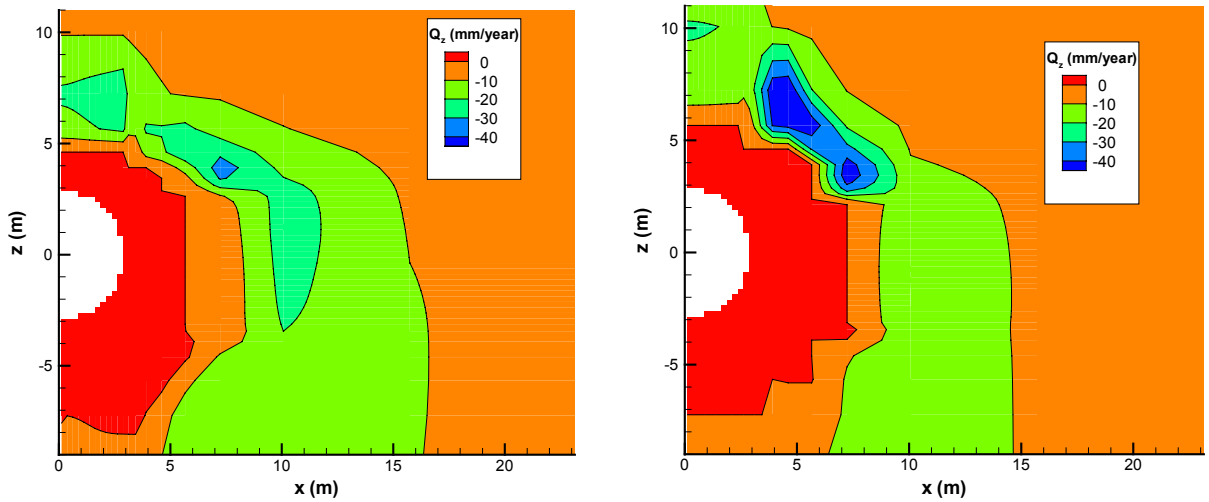

Output - DTN: LB0306DRSCLTHM.002

Figure 6.5.5-3. Comparison of the Distribution of Vertical Percolation Flux (Q_z) in Fractures at 100 Years for a Fully Coupled THM Simulation and TH Simulation (Tptpmn Model Domain)

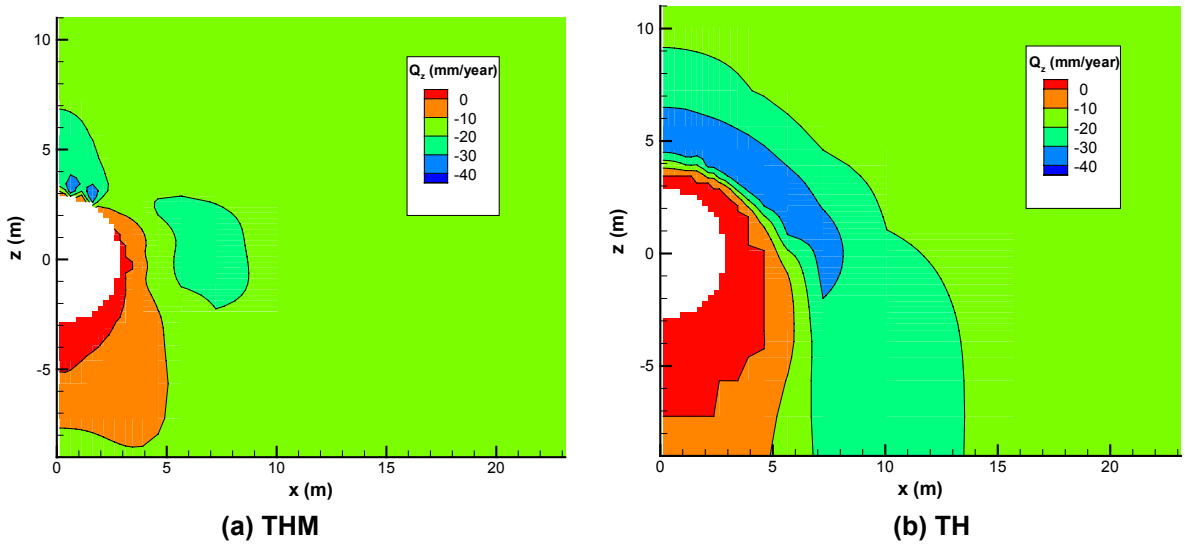

Output - DTN: LB0306DRSCLTHM.002

Figure 6.5.5-4. Comparison of the Vertical Percolation Flux (Q_z) in Fractures at 1,000 Years for a Fully Coupled THM Simulation and TH Simulation (Tptpmn Model Domain)

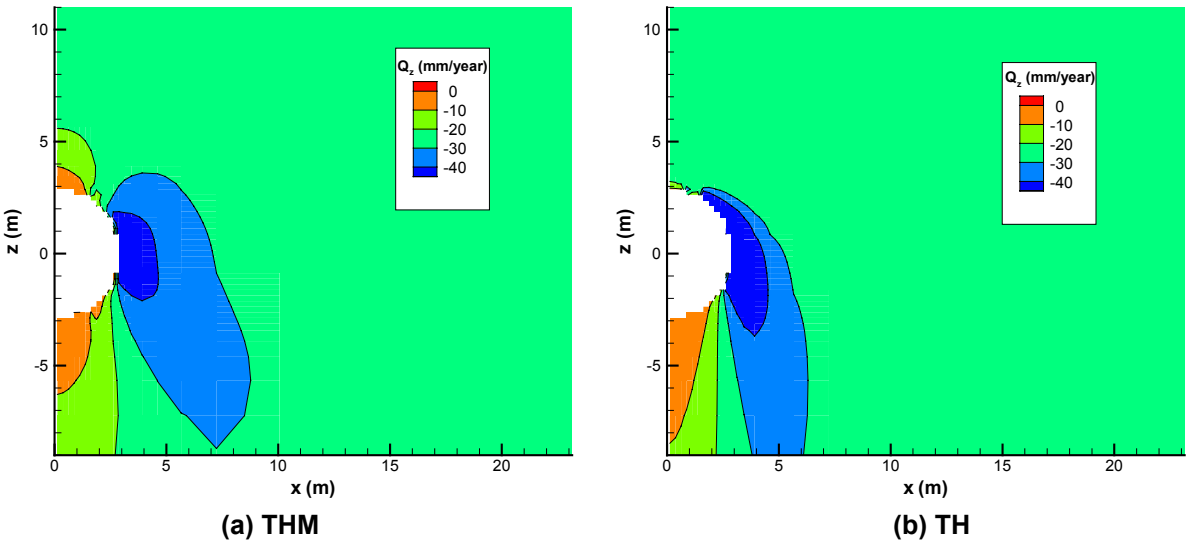

Output - DTN: LB0306DRSCLTHM.002

Figure 6.5.5-5. Comparison of the Distribution of Vertical Percolation Flux (Q_z) in Fractures at 10,000 Years for a Fully Coupled THM Simulation and TH Simulation (Tptpmn Model Domain)

6.6 SIMULATION RESULTS FOR THE TPTPLL MODEL DOMAIN

This subsection of the Model Report presents modeling results for a representative drift located in the Tptpll unit. Modeling results of temperature and thermal-stress evolution for the Tptpll model domain are similar to those for the Tptpmn model domain and will therefore not be repeated. This section focuses on the difference between the impact of THM processes in the Tptpmn unit and the Tptpll unit, and the reasons for these differences. Their impact on the evolution of hydraulic properties and vertical percolation flux are presented below in Section 6.6.1 and 6.6.2.

6.6.1 Evolution of Hydraulic Properties

Figure 6.6.1-1 presents the permeability changes induced by the excavation of the emplacement drift in the Tptpll unit. The permeability correction factor is about 8 for the horizontal permeability and about 1.3 for vertical permeability. These changes can be compared with corresponding results for a repository located in the Tptpmn unit, which are presented in Figure 6.5.1-1. The maximum correction factor in the Tptpll repository unit (about 8 in Figure 6.6.1-1a) is roughly half of the maximum correction factor in the Tptpmn repository unit (about 19 in Figure 6.5.1-1a). This is explained by the fact that a higher initial permeability, and hence a larger initial fracture aperture in the Tptpll unit, leads to a relatively smaller change in permeability upon excavation. This is also consistent with the general trend of smaller changes in permeability for initially higher permeability values observed at the niche experiments (BSC 2001 [158463], Figures 6.1.2-11 to 6.1.2-15).

The evolution of permeability changes in the Tptpll model domain is presented in Figures 6.6.1-2 and 6.6.1-3. A comparison of these results with corresponding results of permeability correction factors for the Tptpmn model domain in Figures 6.5.5-1 and 2 shows that the general pattern of permeability changes are similar with early-time permeability changes occurring around the drift

and then gradually spreading away from the drift with time, However, the magnitudes are slightly smaller in the Tptpll model domain than in the Tptpmn model domain. For example, the blue area ($F_{kz} < 0.5$) extends up to 290 m in the Tptpmn model domain (z = -110 to z = +100 in Figure 6.5.4-1, 1,000 years), but only to about 180 m in the Tptpll model domain (z = +30 to z = +210 in Figure 6.6.1-1). Furthermore, the minimum permeability correction factor is less than 0.1 in the Tptpmn model domain, whereas in the Tptpll model domain, it is between 0.3 and 0.5. The reason for the relatively smaller changes in permeability in the Tptpll model domain is that the overburden stress is larger, because of the additional geological layers (tcw11-12 and PTn units) on top of the vertical column. The additional geological layers provide an additional 100 m of overburden, which in turn results in an increased *in situ* stress at the depth of corresponding geological units. For example, in the Tptpmn model domain, the Tptpmn unit is located at a depth of about 200 m, whereas in the Tptpll model domain, the Tptpmn unit is located at a depth of about 280 m. A higher initial stress implies that fractures are more closed, with a higher normal stiffness, and closer to their residual permeability values. All these factors contribute to a relatively smaller change in permeability during the heating of the rock mass.

Figures 6.6.1-4 and 6.6.1-5 present calculated permeability correction factors near a repository located in the Tptpll unit at 10 and 1,000 years. The corresponding results for a repository in the Tptpmn unit are presented in Figures 6.5.4-3 and 6.5.4-5. Again, the general pattern of permeability changes is similar, but the magnitude is very different. In the Tptpmn model domain, the permeability decreases to as low as 3% of its original value, while in the Tptpll model domain, the permeability stays above 50% of its original value.

Figure 6.6.1-6 shows the correction factor for capillary pressure at 10 and 1,000 years. Compared to corresponding results for a repository in the Tptpmn unit (Figure 6.5.4-6a and c), the stress-induced changes in capillary pressure are much smaller in the Tptpll unit. However, in both cases, capillary pressure strength decreases adjacent to the wall of the drift. This reduction results from the general unloading and opening of fractures oriented parallel to the drift wall.

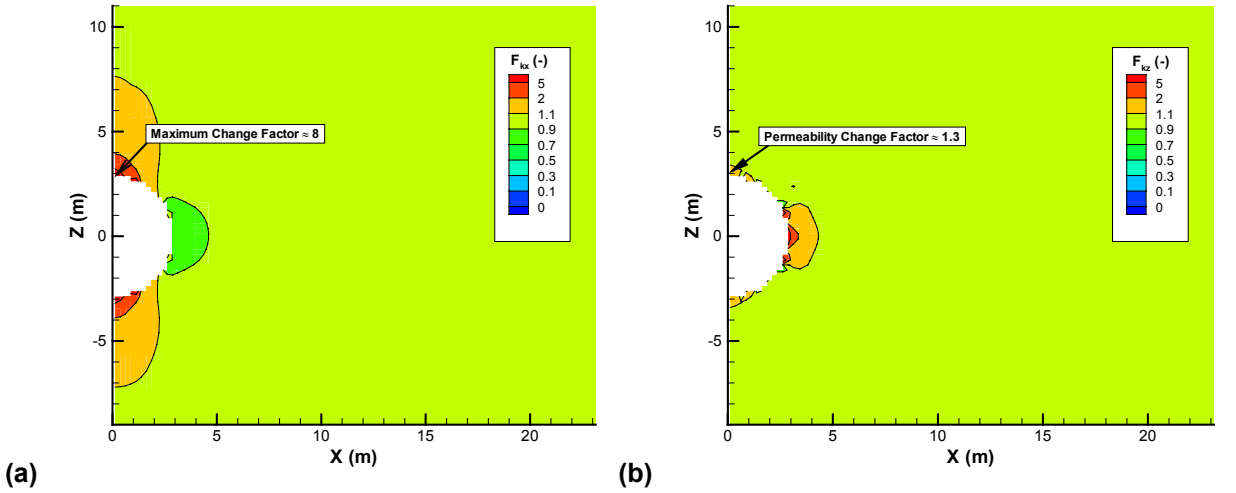

Output - DTN: LB0306DRSCLTHM.002

Figure 6.6.1-1. Permeability Correction Factor Caused by Stress Redistribution during Excavation of the Emplacement Drift: (a) Correction Factor ($F_{kx} = k_x/k_i$) for Horizontal Permeability, (b) Correction Factor ($F_{kz} = k_z/k_i$) for Vertical Permeability (Tptpll Model Domain)

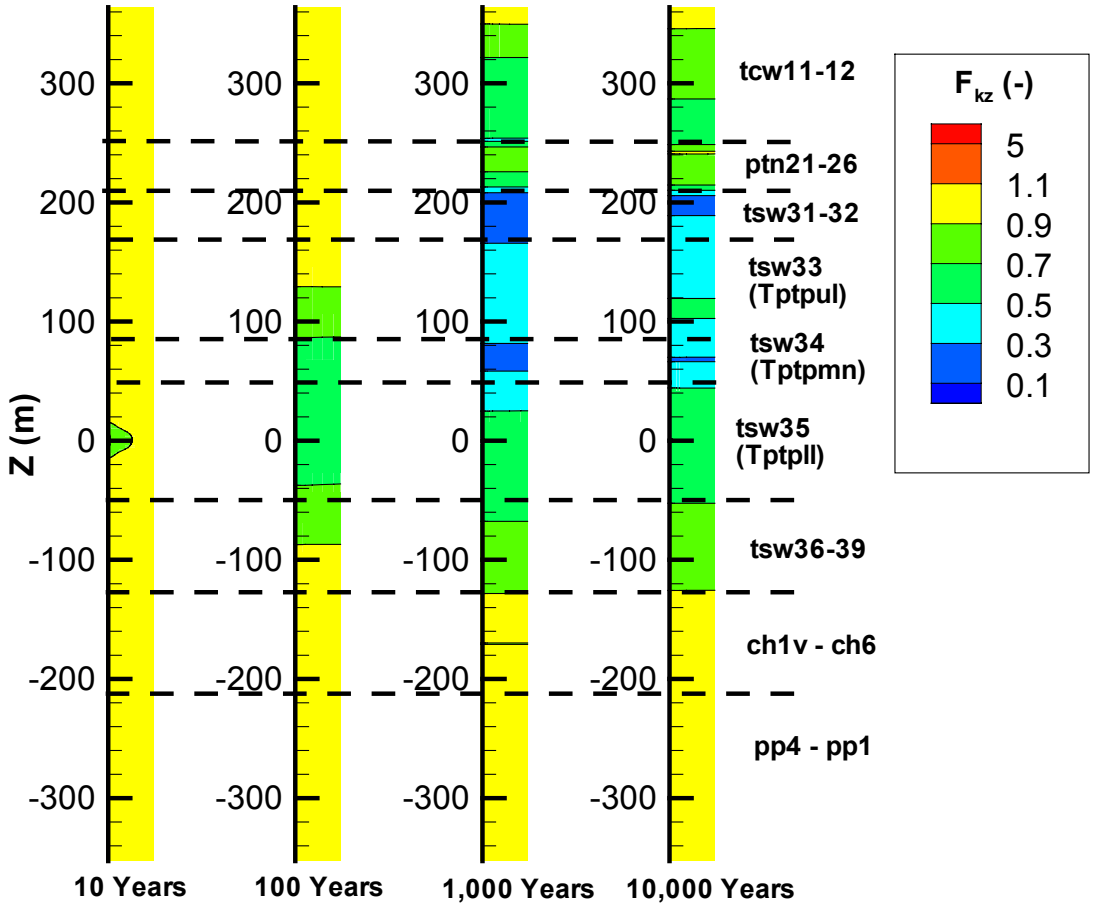

Output - DTN: LB0306DRSCLTHM.002

NOTE: The width of each column is 40.5 meters. The top is the ground surface and the bottom is the water table.

Figure 6.6.1-2. Evolution of Vertical Permeability Correction Factor ($F_{kz} = k_z/k_i$) in the Tptpll Model Domain

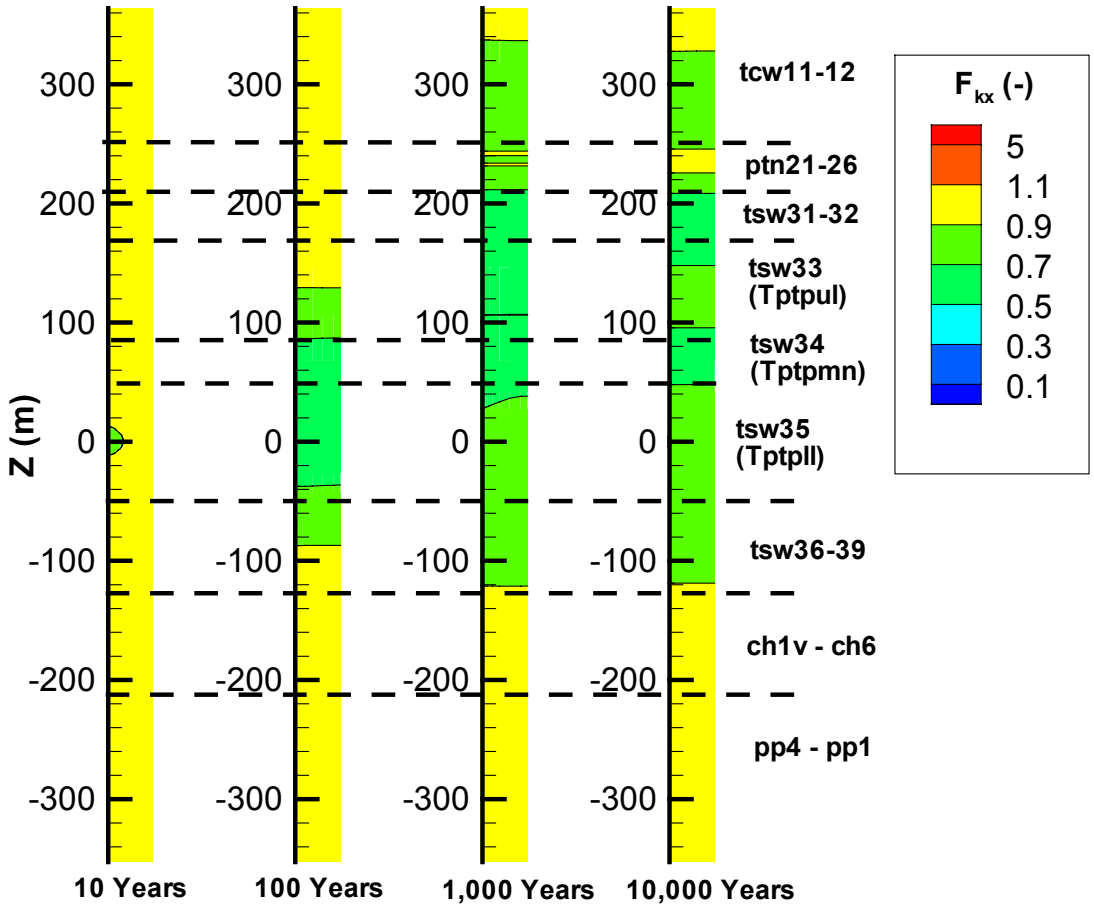

Output - DTN: LB0306DRSCLTHM.002

NOTE: The width of each column is 40.5 meters. The top is the ground surface and the bottom is the water table.

Figure 6.6.1-3. Evolution of Horizontal Permeability Correction Factor ($F_{kx} = k_x/k_l$) in the Tptpll Model Domain

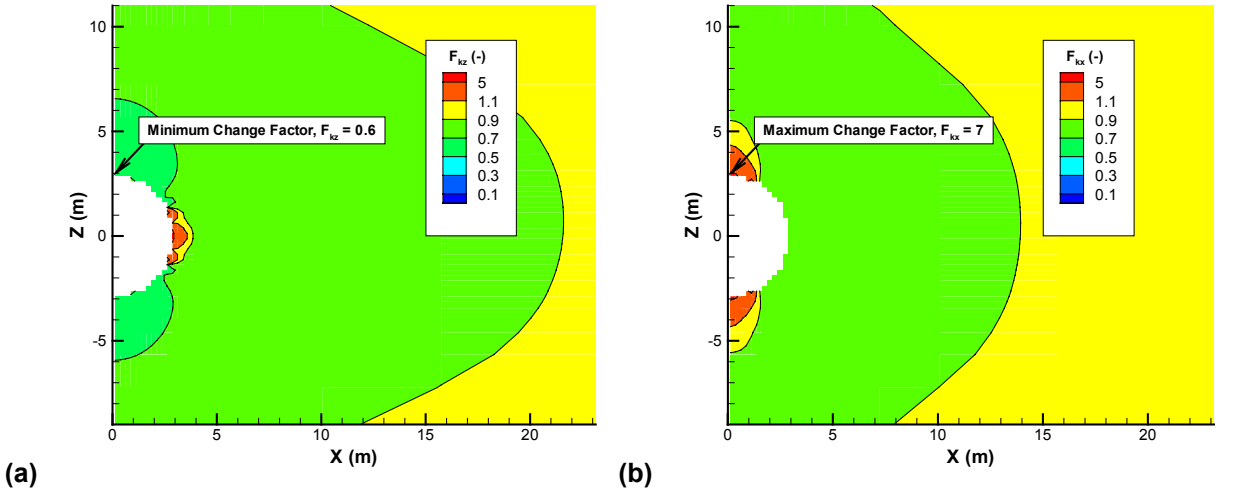

Output - DTN: LB0306DRSCLTHM.002

Figure 6.6.1-4. Distribution of (a) Vertical Permeability Correction Factor ($F_{kz} = k_z/k_i$) and (b) Horizontal Permeability Correction Factor ($F_{kx} = k_x/k_i$) around an Emplacement Drift in the Tptpll Unit at 10 years

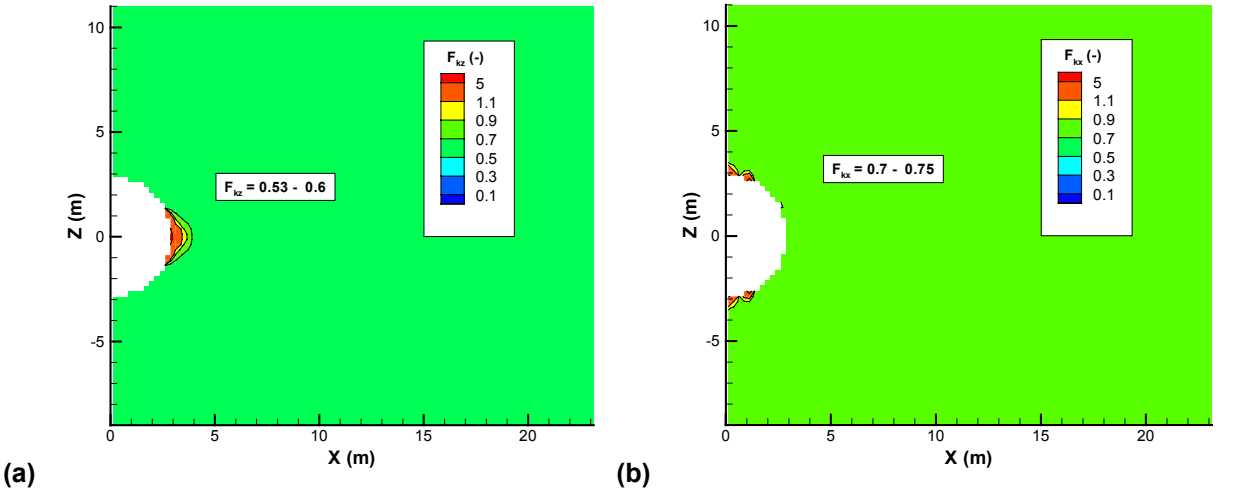

Output - DTN: LB0306DRSCLTHM.002

Figure 6.6.1-5. Distribution of (a) Vertical Permeability Correction Factor ($F_{kz} = k_z/k_i$) and (b) Horizontal Permeability Correction Factor ($F_{kx} = k_x/k_i$) around an Emplacement Drift in the Tptpll Unit at 1,000 Years

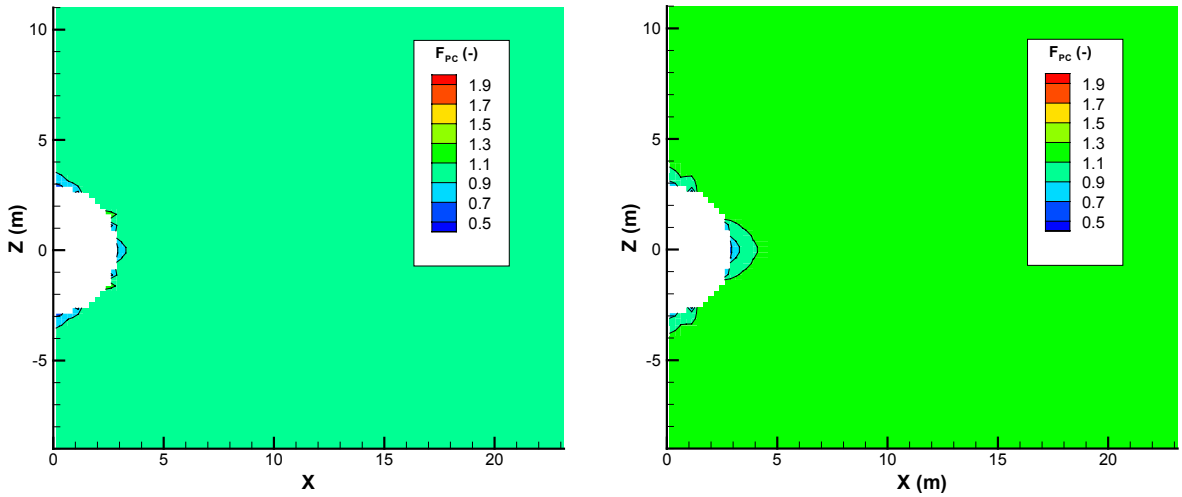

Output - DTN: LB0306DRSCLTHM.002

Figure 6.6.1-6. Evolution of Stress-Induced Capillary-Pressure Correction Factor ($F_{PC} = P_c/P_{ci}$) around an Emplacement Drift in the Tptpll Unit

6.6.2 Impact on the Fluid Flow Field

Figures 6.6.2-1 to 6.6.2-3 present calculated vertical percolation flux for a fully coupled THM analysis and a partially coupled TH analysis. The results are qualitatively similar to the results for a repository in the Tptpmn unit, with the formation of a dryout zone and a condensation zone above the drift, subsequent rewetting of the dryout zone and with a slightly contracted dryout zone in the case of THM analysis. Figures 6.6.2-1 to 6.6.2-3 also show that the impact of THM processes is minimal for a repository in the Tptpll unit, with only a slight change in the flow pattern. As explained in Section 6.5.5, the impact of THM processes on the percolation flux is small, because a reduction in fracture intrinsic permeability can be compensated by a larger relative permeability, leading to an unchanged flow mobility. The impact of THM processes is relatively smaller in the Tptpll unit than in the Tptpmn unit because the permeability changes less in the Tptpll unit than in the Tptpmn unit (for reasons explained in Section 6.6.1). However, while the analysis indicates that the impact of THM processes is going to be smaller in the Tptpll unit, the prediction of THM changes in Tptpll units is more uncertain because of the lack of field experiments in the Tptpll unit. Moreover, the recent *Drift Degradation Analysis* BSC (2003 [164285]) indicates that for sections of poor rock quality in the Tptpll unit, extensive inelastic behavior would occur near the drift, which could potentially lead to an increased permeability near the drift wall. These uncertainties are further discussed in Section 6.8.

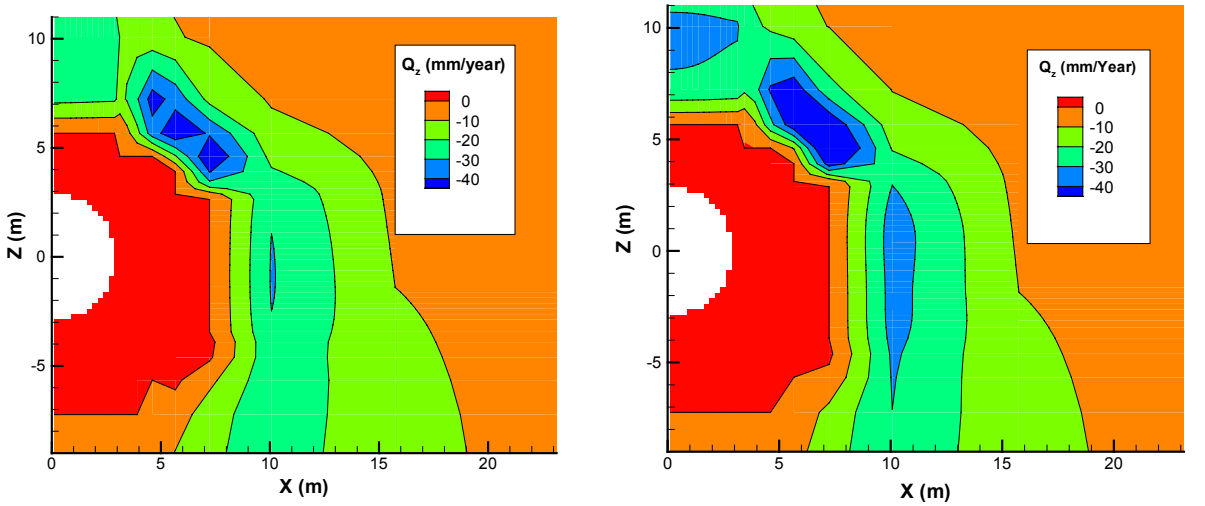

Output - DTN: LB0306DRSCLTHM.002

Figure 6.6.2-1. Comparison of the Vertical Percolation Flux (Q_z) at 100 Years for a Fully Coupled THM Simulation and TH Simulation (Tptpll Model Domain)

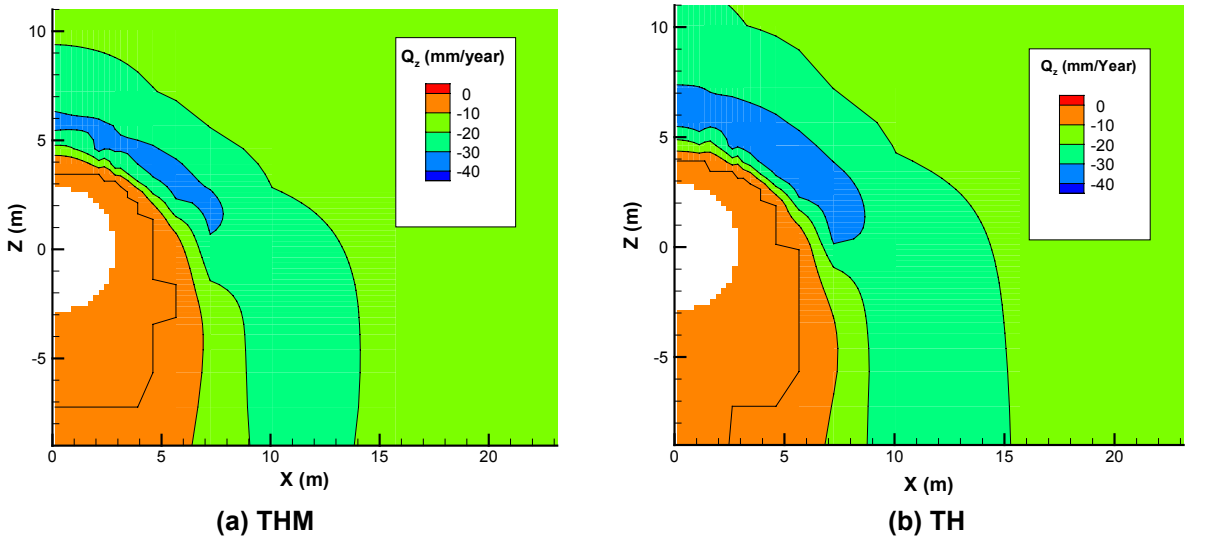

Output - DTN: LB0306DRSCLTHM.002

Figure 6.6.2-2. Comparison of the Vertical Percolation Flux (Q_z) at 1,000 Years for a Fully Coupled THM Simulation and TH Simulation (Tptpll Model Domain)

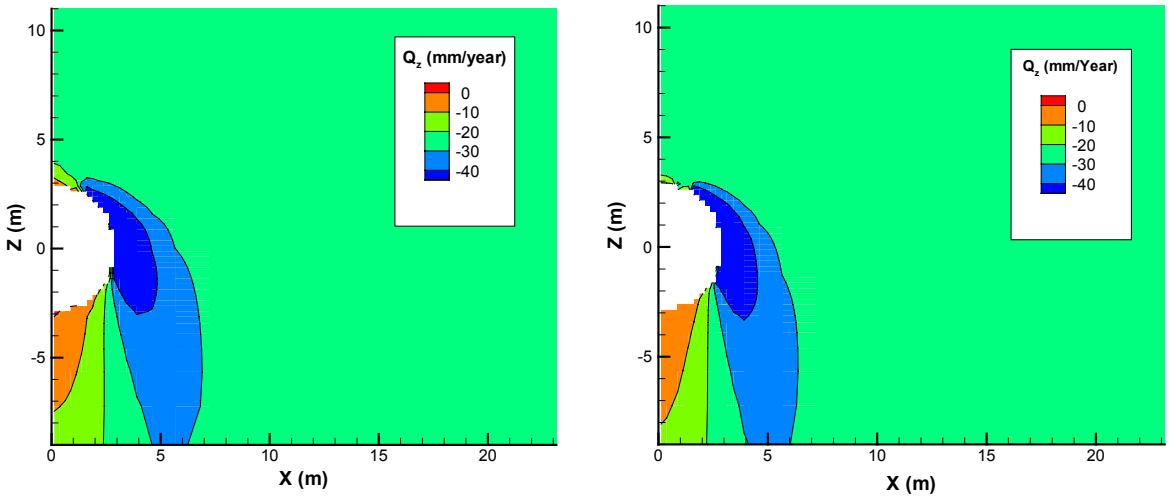

Output - DTN: LB0306DRSCLTHM.002

Figure 6.6.2-3. Comparison of the Vertical Percolation Flux (Q_z) at 10,000 Years for a Fully Coupled THM Simulation and TH Simulation (Tptpll Model Domain)

6.7 SUMMARY OF RESULTS AND DISCUSSION ON THE IMPACT OF PREDICTED THM EFFECTS ON DRIFT-SCALE PERFORMANCE

The results of the coupled Drift-Scale THM model presented in Sections 6.5 (Tptpmn model domain) and 6.6 (Tptpll model domain) shows that the impact of THM processes will last for well over 10,000 years, but these processes have a small or moderate impact on the drift scale TH behavior, including a negligible impact on the temperature evolution and small impact on the percolation flux. These model results were obtained for a conservative estimate of input THM properties (thermal expansion coefficient and stress versus permeability function), which is sufficient for bounding the possible impact of the THM processes on permeability and percolation flux.

Away from the emplacement drift, increased horizontal thermal stresses tend to tighten vertical fractures toward their residual aperture values. As a result, the vertical intrinsic permeability will decrease in a zone extending more than one hundred meters both above and below the repository (Figures 6.5.4-1). Using a conservative (more sensitive) stress-permeability relationship, the vertical permeability in the Tptpmn unit will decrease at most to a factor of 0.03 of its original permeability. In the Tptpll unit, vertical permeability is estimated to decrease to a factor of 0.5 of its original value.

At the drift crown, within one drift radius, horizontal fractures tend to stay open because they are oriented parallel to the stress-free open drift. Consequently, at the drift crown, the vertical permeability will decrease at the same time horizontal permeability tends to increase, leading to a pronounced anisotropy in the permeability field. As an example, Figure 6.5.4-3d and Figure 6.5.4-4d show that at the drift crown, the horizontal permeability has increased at the most by a factor of 19 at the same time the vertical permeability is decreased by a factor of 0.05.

The impact of these THM-induced changes in hydraulic properties was evaluated by a comparison of the liquid percolation flux for a partially coupled TH simulation and a fully coupled THM simulation. The comparison shows that away from the emplacement drift, where changes in permeability and capillaries are uniformly distributed horizontally, THM processes have no significant impact on the vertical liquid flow field. Any water that is infiltrated on top has to be accommodated by the system, keeping the downward percolation flux unchanged. In this case, the unsaturated hydrological system adjusts to accommodate the infiltrated water by compensating for the stress-induced reduction in vertical permeability with an increased relative permeability. Thus, the stress-induced permeability changes are canceled out by increased relative permeability, and the vertical liquid flow rate remains unchanged.

Close to the drift, where changes are not uniform over the horizontal plane, some redistribution of the flow field can be observed. Another impact of the THM processes is that the dryout zone around the emplacement drift becomes smaller and contracts faster towards the drift wall. A smaller dryout zone in the THM case may be related to changes in capillary pressure or to smaller air permeability, resulting in less effective heat convection in the boiling zone. As a result, the time period that the dryout zone is present is slightly shorter for the THM case. A shorter dryout period could have an impact on the possibility for seepage of water into the drift. However, the small impact on the dryout time and the overall results of this analysis indicate that THM processes do not have a major impact on drift-scale repository performance including seepage of ground water into the drift and its chemical composition. Moreover, the THM-induced changes in hydrological properties calculated in this model report are used for evaluation of the impact of THM processes on drift seepage in the Model Report, entitled *Seepage Model for PA Including Drift Collapse* (BSC 2003 [163226], Section 6.7). That analysis shows a slight reduction in drift seepage when THM coupling is considered.

6.8 DISCUSSION OF UNCERTAINTIES

The model predictions in this analysis critically depend on a sufficiently accurate representation of TM-induced changes in hydraulic properties, and in particular changes in fracture permeability. In this context, a number of potential sources for uncertainties deserve further attention: (1) simplified conceptualization of the fracture network geometry, (2) drift-wall inelastic behavior, (3) possible fracture-shear-induced permeability enhancement, (4) fracture stress versus permeability relationship, (5) effects of heterogeneous rock properties, and (6) mechanical properties of the Tptpll unit. In general, there are additional uncertainties associated with the prediction of coupled THM behavior in the Tptpll unit, basically caused by a lack of coupled THM experiments in that unit. These uncertainties are discussed in the remainder of this section in light of the previous analysis conducted in BSC (2001 [155957]).

6.8.1 Simplified Conceptualization of the Fracture Network

For correction of hydraulic properties, three orthogonal sets, two vertical and one horizontal, are assumed. These fracture sets reflects the three main fractures sets observed in the TSw2 TM unit (CRWMS M&O 1998 [102679], Section 7.4.5):

1. One prominent vertical, southeast trending
2. One less prominent vertical, southwest trending

3. One less prominent subhorizontal

In the field, there are also fractures labeled as randomly oriented that account for a smaller portion of all fractures measured in the ESF (Exploratory Studies Facility) (CRWMS M&O 1998 [102679], p. 37). These randomly oriented fractures could impact the calculated changes in permeability in certain regions of the drift wall. For example, the calculated permeability correction factor presented in Figure 6.5.1-1 indicates that the fracture permeability increases preferably on top of the drift (red contour in Figure 6.5.1-1a) and at the spring line (red contour in Figure 6.5.1-1b). These increases in permeability are caused by the unloading of fractures with strikes that parallel the drift opening, which are fractures that are either horizontal or vertical. Figure 6.5.1-1 also shows that there are zones at the drift wall that show little or no increase in permeability. These zones are located at the drift wall at an orientation about 45° above and below the horizontal. The fracture permeability increases less in this zone because no fractures dip 45° in the stress-permeability model; hence, no fractures are oriented parallel to the drift in this area. If, on the other hand, randomly oriented fractures would be considered in the model, the permeability may also increase in this area, giving a more uniform increase in permeability around the drift wall. Furthermore, the three fracture sets discussed above are probably better represented in the Tptpmn stratigraphic unit than in the Tptpll stratigraphic unit, which both belong to the TSw2 TM unit. In the Tptpll unit, a rock matrix containing dense vertical fractures connects lithophysal cavities. Thus, the adopted conceptualization of the fracture network is likely to be more accurate in the Tptpmn unit, for which the model has been extensively validated against field experiments. Moreover, for drift seepage, the simplified fracture network used in this Model Report provides a conservative case, since the zone of increased permeability, combined with no increased permeability at the above-mentioned 45° location, can act as a bottleneck, preventing fluid flowing around the drift.

6.8.2 Drift-Wall Inelastic Behavior

After ventilation, a steep temperature rise (above 100°C) will induce mechanical deformations near the drift wall, with associated fracture responses and permeability changes. A general increase in compressive stresses around the emplacement drift will tend to tighten fractures, resulting in a reduction of permeability. However, at the drift wall, high thermal stresses could induce inelastic behavior in the form of shear slip along pre-existing fractures or rock spalling due to development of tensile fractures, which could lead to increased permeability.

The possibility of rock failure at the drift wall of an emplacement drift can be assessed by a comparison to conditions and new observations of inelastic drift wall behavior in the DST (BSC 2002 [160771], Section 6.3.3.7). At the DST, a limited scaling of rock at the drift crown has been observed, first as small rock chips falling on the floor of the test drift after about 2 years of heating, then as larger pieces of loose rock appearing after 3 to 3.5 years of heating. A simulation of the DST is conducted in Section 7.4 for validation of the Drift-Scale THM Model. From this analysis, Figure 6.8.2-1 presents calculated evolution of horizontal stress (maximum principal compressive stress) at the point of the DST drift crown, where limited scaling has been observed. The figure shows that the calculated compressive stress is about 61 and 68 MPa at 2 and 3 years, respectively, which indicates that limited failure at a drift wall could occur when the maximum compressive stress reaches about 60 MPa. This stress value is about one-third of the uniaxial

compressive strength of laboratory-scale intact rock (CRWMS M&O 1997 [103564], Table 2-9, p. 2-23).

The results of the Tptpmn model simulation indicate that the maximum principal compressive stress at the drift crown does not exceed 31 MPa (see Figure 6.5.3-3). Thus, the expected maximum principal stress at the wall of the emplacement drift is roughly half the magnitude at which limited rock scaling was observed in the DST. It is reasonable that the thermal stress is much higher at the DST because of an aggressive heating that is 6 to 12 time larger than the areal thermal loading for the current repository design (BSC 2002 [160771], Section 6.3.3.7). Moreover, the uneven drift wall exacerbated the scaling at the DST, whereas repository drifts will be excavated with a tunnel boring machine, leading to smoother walls that may further prevent scaling. The results of calculated thermal stress at the drift crown, as well as the estimated *in situ* rock compressive strength at the DST, is consistent with the results of the *Drift Degradation Analysis* (BSC 2003 [164285], Section 6.2 and Section 7.7.5.3). On the other hand, for a highly fractured zone in the Tptpmn unit, the *Drift Degradation Analysis* (BSC 2003 [164285], Section 6.3.2) indicated that rock failure is likely during ground motion caused by an earthquake. Overall, both the analysis conducted in this Model Report and the Drift Degradation Analysis show that inelastic drift wall behavior is not likely in the Tptpmn unit, except in intensively fractured zones during ground motion.

The analysis in this Model Report also indicates that inelastic behavior would not occur for a repository located in the Tptpll unit. However, recent slot tests conducted in the Tptpll unit indicate that the rock-mass strength and deformability is less than previous estimates (SN0301F4102102.006 [161876]), and therefore inelastic behavior at the rock wall is possible in the Tptpll unit (as illustrated in Figure 6.2-2a). The potential impact of these new properties is discussed in Section 6.8.6.

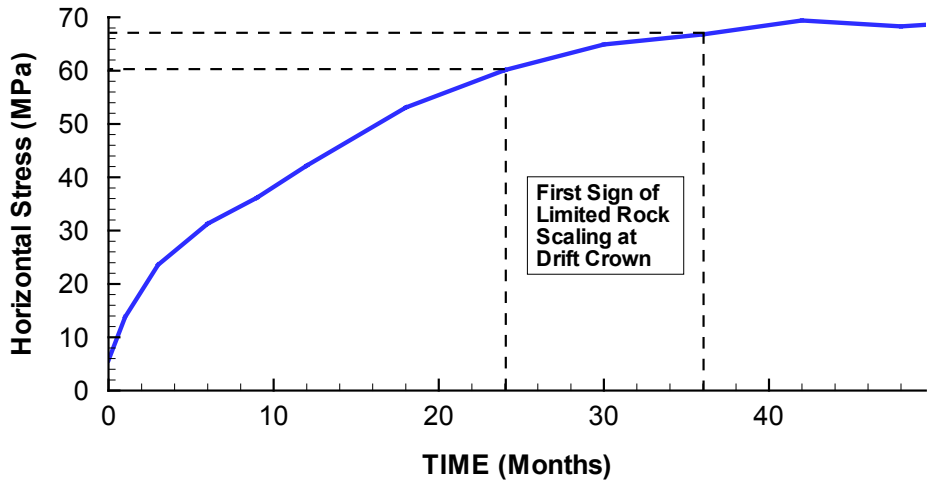

Output - DTN: LB0306DSTTHMVL.002

Figure 6.8.2-1. Calculated Evolution of Maximum Principal Compressive Stress (Horizontal Stress) at the Crown of the Heated Drift from the Analysis of the DST Presented in Section 7.4 of This Model Report

6.8.3 Possible Fracture-Shear-Induced Permeability Enhancement

During heating of the rock mass, the horizontal stresses in the repository unit (away from the drift wall) increase with time, reaching a maximum at about 800 years when the average temperature at the repository level peaks (Figures 6.6.2-1 and 6.5.3-4), while the vertical stresses remain almost constant. This will lead to high differential stress, which might trigger shear slip along unfavorably oriented fractures and faults. Fracture shear slip would likely first occur near the drift wall, where the differential stresses are highest but could also occur in the rock mass away from the drift. The stress analysis presented in Figures 6.5.3-1 and 6.5.3-2 indicate that except for the drift vicinity, the highest difference between vertical and horizontal stress would occur above the repository and toward the ground surface. For example, at z = 40 m, the horizontal stresses increase to about 13 MPa at 1,000 years, whereas the vertical stress is about 4 MPa. Using a Mohr-Coloumb failure criteria, it can be shown that if such a slip occurred, it would preferably take place along subhorizontal fractures, or fractures oriented at an angle of about 30° to the horizontal (maximum principal) stress. Vertical fractures, on the other hand, are not likely to slip during the thermal period because heating will increase the stress normal to these fractures, and hence increase their shear strength. Furthermore, a potential fracture shear-induced enhancement of permeability along subvertical fractures is likely to be counteracted by the high compressive horizontal stresses that would tend to keep the fractures closed at a low permeability. This indicates that the vertical permeability is not likely to be enhanced by shear slip.

Furthermore, observations at the SHT and the ongoing DST show very little evidence of inelastic rock-mass behavior (Sobolik et al. 1998 [162049]; Sobolik et al. 1999 [163202], p. 735) or shear-induced permeability enhancement, and during heating, the permeability generally decreases (Section 7.9). Although these tests span up to at most several years of heating and may therefore not fully represent long-term behavior, the heating is generally more aggressive (resulting in larger differential stress). However, as discussed in Section 6.8.2, fracture shear slip could possibly occur very close to the drift wall: loose blocks could slip because of a lack of mechanical confinement near the drift wall. Such loosening of blocks and rock fall, which is studied in *Drift Degradation Analysis* (BSC 2003 [164285]), changes the shape of the drift and will most likely lead to an additional increase in permeability in the zone of loose blocks. The permeability in the loose-block zone is likely to increase because of shear dilation. An upper bound for such shear-induced permeability can be estimated from the maximum increase in permeability for a fully dilated fracture. Laboratory shear tests have shown that permeability can increase by 1 to 2 orders of magnitude during shear (Rutqvist and Stephansson 2003 [162583]).

6.8.4 Fracture Stress versus Permeability Relationship

The model predictions in this analysis are critically dependent on a sufficiently accurate relationship between stress and fracture permeability. An upper bound of maximum permeability correction factor and a lower bound of minimum permeability correction factor bound the predicted changes in fracture permeability. The upper bound is important for the prediction of possible permeability increase caused by unloading in the excavation disturbed zone of an emplacement drift. The lower limit is important for the prediction of the maximum possible reduction in permeability caused by thermal stresses.

Near the drift wall, the analysis shows that permeability can increase about one order of magnitude in a direction parallel to the drift wall (Figure 6.5.1-1). This magnitude of change is dictated by the upper bound of the fracture normal stress versus permeability function, which have been calibrated against *in situ* tests in both the Tptpmn and Tptpll unit (Figure 6.4-2). The fact that mean permeability increases about one order of magnitude near the drift in the Tptpmn unit and less than one order of magnitude in the Tptpll unit is well established from observed permeability changes at excavated niches. BSC (2001 [158463], Table 6.1.2-1) shows that the geometric mean of the post/pre ratio varies between 9.42 to 25.38 for three niches in the Tptpmn unit, whereas Table 6.1-2-2 shows that the geometric mean of post/pre ratio is 2.37 for one niche in the Tptpll unit). Thus, the upper bound of the fracture stress-permeability function is established from these field data.

In the longer term, at 1,000 to 10,000 years, the analysis in this Model Report shows that permeability decreases significantly in an area extending hundreds of meters above and below the drift (Figure 6.4.4-1). The model simulation shows that the permeability decreases most in the vertical direction, by closure of vertical fractures. Such closure of vertical fractures has also been confirmed in calculations by BSC (2001 [155957], Section 7, bullet 2), using the alternative distinct-element model. In BSC (2001 [155957], Section 6.3.3) permeability decreases of up to 6 orders of magnitude were calculated. This was a model artifact of having no residual fracture aperture that could limit the amount of fracture closure. Our calculated lower limit of permeability decrease—a factor of 0.03 in the Tptpmn unit (Figure 6.5.4-3c) and 0.6 in the Tptpll unit (Figure 6.6.1-5a)—is strongly dependent on the residual fracture permeability. This residual permeability is a parameter constrained by the maximum observed decrease in permeability at the DST and SHT. The fact that the parameter is constrained from the maximum observable change at DST and SHT implies that predicted change in permeability provides a bounding worst case of THM-induced permeability changes at a future repository.

There are currently no *in situ* tests available to estimate residual permeability within the Tptpll unit. However, considering the trend of relatively smaller changes in permeability for initially larger permeability values observed at the niche excavation experiments (BSC 2001 [158463], Section 6.1.2.3), the impact of THM processes on fluid flow is likely to be smaller in the Tptpll unit than in the Tptpmn unit. This trend is also captured in the modeling results presented in Section 6.5 and 6.6, which show a relatively smaller change in permeability for the Tptpmn unit than the Tptpll unit. Nevertheless, further *in situ* testing in the Tptpll unit is desirable for constraining a residual permeability, considering the fact that 70 to 80% of the repository drifts are proposed to be located in the Tptpll unit.

6.8.5 Effects of Heterogeneous Rock Properties

The analysis in this Model Report was conducted with initially homogeneous rock properties for each stratigraphic unit, based on calibrated mean hydrological properties and a conservative fracture normal stress versus permeability relationship. An initially heterogeneous permeability field would result in heterogeneous changes in permeability, with the largest changes occurring in a zone with an initially lower permeability (see also results of niche experiments in Figure 7.5.1). A trend of larger changes in zones with initially lower permeability could lead to a redistribution of the flow field, which in turn could lead to increased flow focusing to high permeability zones around the repository drift. However, the overall results from the above-

mentioned niche experiments show that while the changes in mean permeability are about 1 order of magnitude, the standard deviation of the heterogeneous permeability field changes much less (BSC 2001 [158463], Table 6.1.2-1). This indicates that the main impact of THM is a change in the mean permeability, even for an initially heterogeneous permeability field. Therefore, it is appropriate to apply the mean permeability changes calculated in this Model Report to a seepage analysis that considers either the homogenous or heterogeneous permeability field.

6.8.6 Mechanical Properties of the Tptpll Unit

The analysis conducted in this Model Report uses the qualified mechanical properties for the TSw2 TM unit, which covers the stratigraphic units Tptpul, Tptpmn, and Tptpll. Thus the same modulus of elasticity is used for the Tptpmn and Tptpll units. This is in contrast to recent slot tests conducted in the Tptpll unit, which indicate that the rock-mass deformability and strength for the Tptpll unit are less than previous estimates (DTN: SN0301F4102102.006 [161876]). A low rock strength in the Tptpll units could lead to more extensive inelastic behavior near the drift wall that could ultimately result in rock fall and drift collapse, which essentially changes the shape of the drift. These are long-term effects that are part of the *Drift Degradation Analysis* (BSC 2003 [164285]). For the rock outside the inelastic zone, the changes in permeability would still be bounded by upper and lower limits provided by the stress permeability function. Furthermore, a lower rock-mass deformability applied to the THM analysis of this Model Report would result in a smaller thermal stress and hence a smaller increase in horizontal compressive stresses during the thermal period. This implies that the TM-induced permeability reduction in vertical fractures would be smaller for the Tptpll unit than the ones calculated in this Model Report. In addition, as discussed in Section 6.8.2, lower strength properties could lead to inelastic behavior near the drift wall, which would tend to relieve stresses near the drift wall and even unlock blocks of rocks, leading to fracture opening beyond the elastic regime. As discussed in Section 6.8.3, the permeability in a potential loose-block zone is likely to increase because shear dilation.

6.9 DISCUSSION OF AN ALTERNATIVE CONCEPTUAL MODEL

As mentioned in Section 6.2, a continuum model was selected for the analysis in this Model Report for the following reasons:

1. It is consistent with the continuum approaches used in all other UZ models, including the Drift Scale TH and THC Models, which all have been extensively validated for TH processes (e.g. BSC 2001 [157330], Section 6).

2. A consistent conceptual model with the TH analysis facilitates a more conclusive evaluation of the impact of THM processes, and hence the possible impact of neglecting the full THM coupling in the current partially coupled TH approach.

3. Previous analyses of TM processes at Single Heater Test and DST have indicated that a continuum approach with a linear elastic or nonlinear elastic material model is sufficient to capture observed displacements (Sobolik et al. 1998 [162049]; Sobolik et al. 1999 [163202], p. 735).

4. Previous comparison of a continuum conceptualization with an alternative discrete-fracture conceptualization for TM analysis has shown minor differences in the calculated rock-mass deformations (BSC 2001 [155957], p. 125).

An alternative discrete-fracture approach could be used to obtain essentially the same results as with the continuum model approach used in this Model Report. The results would be similar, provided that a similar stress-aperture function is used in both modeling approaches. This would include a similar residual fracture aperture and fracture normal deformability that provides the upper and lower limits of possible changes in fracture permeability. Thus, a correctly calibrated stress-aperture function should limit the permeability changes to about one order of magnitude for both a continuum and an alternative discrete-fracture approach. However, a discrete-fracture approach (such as in a distinct-element model) requires much more effort in model development, simulations, and output data processing. A continuum approach is preferable because it adequately captures all the relevant THM processes at various *in situ* tests at Yucca Mountain (Section 7) and is sufficient for performing bounding predictions of THM-induced changes in permeability and its impact on the flow field. The exception may be the case for which a zone of loose blocks forms around a failing drift, in which the separation of blocks and associated permeability changes might be difficult to capture in a continuum model.

7. MODEL VALIDATION

The Drift-Scale Thermal-Hydrological-Mechanical (THM) Model is first tested by a coupled THM simulation of the Yucca Mountain Drift Scale Test (DST) and a coupled hydrological-mechanical (HM) simulation of the Yucca Mountain niche experiments. This is a model validation that aims to test the underlying conceptual model for representing the fractured rock and to demonstrate that the Drift-Scale THM Model appropriately captures all THM processes relevant to the performance of the repository at Yucca Mountain. Additional validation is conducted by corroboration with results of an alternative conceptual model and through publication in peer-review format. Multiple lines of evidence are provided from natural analogues in the geothermal field and from other heater tests.

7.1 SPECIFICS OF THE DRIFT-SCALE THM MODEL VALIDATION

The most important part of the validation of the Drift-Scale THM Model is simulation of the DST, with comparison of calculated results to measurements. A basic requirement is that the Drift-Scale THM Model should be able to capture the general and most relevant THM responses in the field. It needs to be assured that any disparity between measurements and simulations is not widespread, but merely a local and isolated event that does not distract from the overall agreement of calculated and measured THM responses.

The Drift-Scale THM Model is a continuum model consistent with the overlapping-continuum (matrix and fracture continuum) approach applied in the Drift-Scale Coupled Processes (DST and TH seepage) Models Report (BSC 2003 [161530], Section 6.2.1). The validity of the conceptual model for simulating TH processes at the Yucca Mountain site has been demonstrated through model validations against various *in situ* tests (BSC 2003 [161530], Section 7). Hence, it remains for the Drift-Scale THM Model to validate the conceptual model for thermal-mechanical (TM) and HM processes. Special emphasis is placed on the validation for HM processes, which are key processes for the Drift-Scale THM Model, and which is a new development in this Model Report.

The validation of the Drift-Scale THM Model against the DST is conducted in the following steps:

1. Check that the simulated temperature field is in reasonable agreement with the observed temperature field to ensure that the THM model is properly implemented in terms of thermal behavior.

2. Check that simulated rock-mass displacements capture the general trends and average magnitudes of observed displacements (validation of TM processes).

3. Check that the simulated changes in air permeability capture the general trends and magnitudes observed in the field (validation of THM processes).

The validation criteria for validation of TM and THM processes against measurements at the DST are given in *Technical Work Plan for: Performance Assessment Unsaturated Zone* (BSC 2002 [160819], Section I-3-3-1, p. 45). For TM processes, the average magnitudes of relative

displacement and the trends of displacement evolution should be captured in the numerical model. During heating, the average magnitudes of relative displacement measured between two points essentially depended on the average thermal expansion coefficient for the rock mass in between the two measurement points. The average thermal expansion coefficient is also important for prediction of the thermal stresses during heating. A representation of the average thermal expansion coefficient as ±50% of *in situ* values is deemed sufficient and achievable. This implies that the average displacements, for the rock mass as a whole, taken over the entire heating sequence, should be within 50%. Moreover, as will be shown in Section 7.4.2, the measured displacements at the DST generally span over ±50% for various but equivalently located monitoring points. For THM processes, the validation criterion is to find the general, qualitative agreement with air-permeability measurements and trends during the heating phase. The predicted changes in air permeability are in the correct direction and correct within an order of magnitude; that is, log (k/k_i) simulated and measured differ by less than 1. Observed trends (e.g., k/k_i decreases followed by increases, or the reverse) are matched by model predictions.

The validation of the Drift-Scale THM Model against the DST is complemented with validation against the niche tests to check that the conceptual model for stress-versus-permeability coupling is appropriate over a larger permeability range. Further support for the Drift-Scale THM model is provided by evidence from other heater tests, from comparison to an alternative conceptual model, and publication in peer-reviewed journals.

7.2 THE DRIFT SCALE TEST

7.2.1 Design and Geometry

The DST is a large-scale, long-term thermal test designed to investigate coupled thermal-mechanical-hydrological-chemical behavior in a fractured, welded tuff rock mass (CRWMS M&O 1998 [111115]). The test block is located in one of the alcoves of the Exploratory Studies Facility (ESF) in the Tptpmn unit. Figure 7.2.1-1 gives a plan view of the test block, and Figure 7.2.1-2 shows a 3-D perspective of the DST, showing electrical heaters and many of the approximately 150 instrumented boreholes for measuring thermal, hydrological, mechanical, and chemical processes. The DST test block centers around the Heated Drift, which is 47.5 m long. Heating is provided by nine floor canister heaters within the Heated Drift, as well as 50 rod heaters, referred to as "wing heaters," placed into horizontal boreholes emanating from the Heated Drift. Each wing heater is composed of two equal-length segments (4.44 m) separated by a 0.66 m gap. The distance between the Heated Drift wall and the tip of the first heater segments is 1.66 m. Dimensions of the Heated Drift and canister heaters are similar to the current design of waste emplacement drifts. The heaters of the DST were activated on December 3, 1997. The heating phase continued for approximately four years, till January 14, 2002. Currently, the DST is in the midst of a planned four-year period of monitoring the natural cooling process.

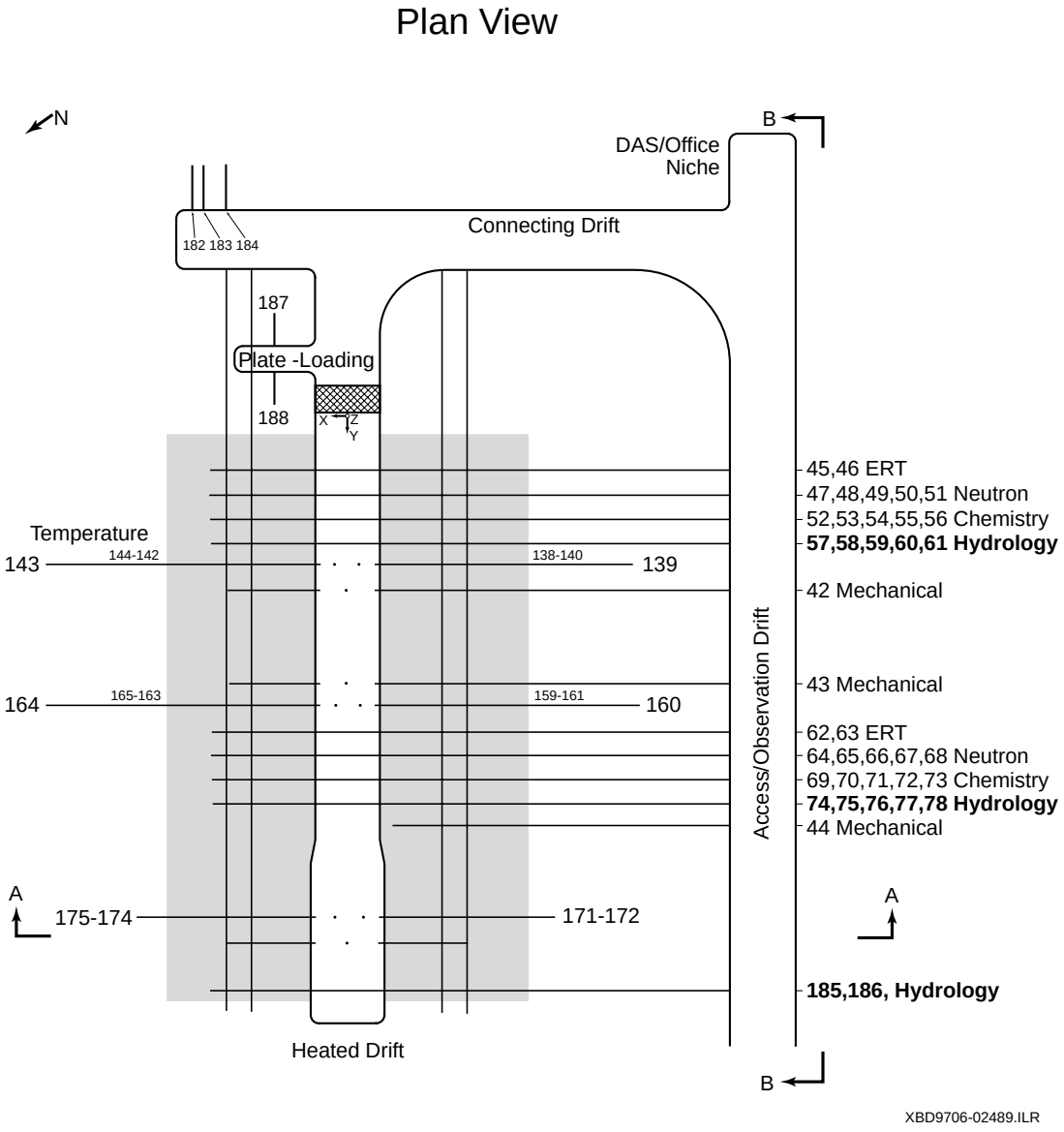

Source: Birkholzer and Tsang (1997 [100597], Figure 3.1-1).

Figure 7.2.1-1. Plan View of DST Block

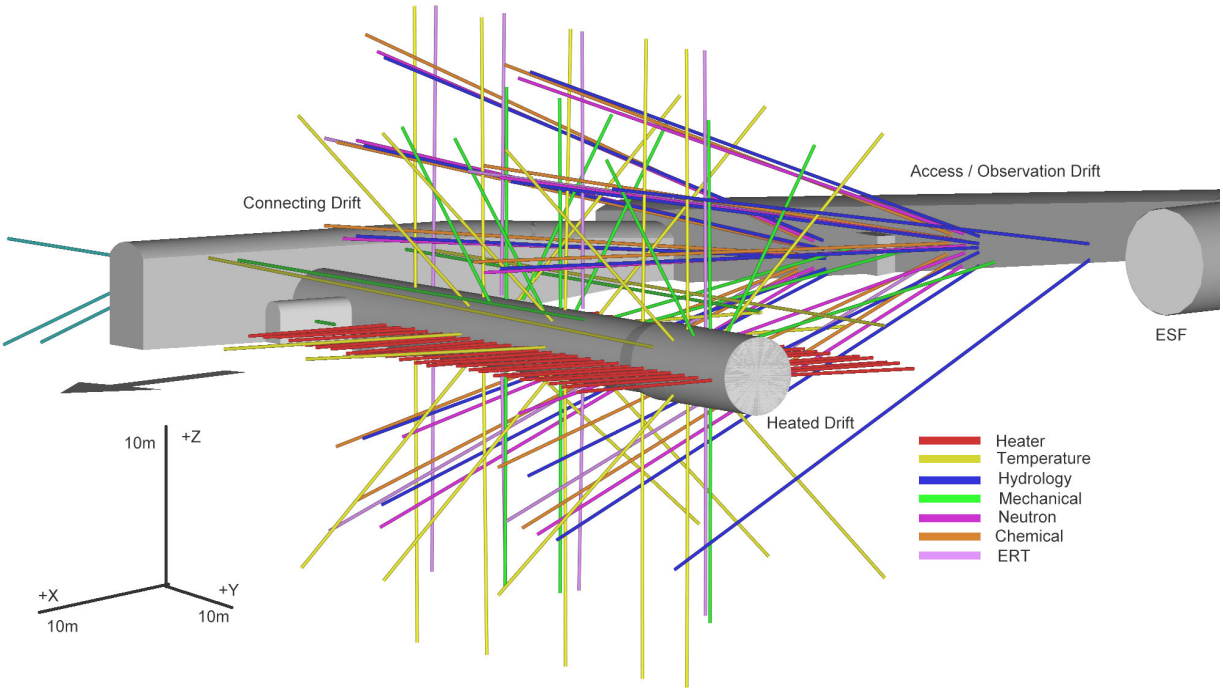

Source: BSC 2002 [160771], Figure 6.3-2.

Figure 7.2.1-2. Three-Dimensional Perspective of the As-Built Borehole Configuration of the DST

7.2.2 Measurements to Probe the Coupled THM Processes

Measurements in the DST include laboratory and field characterization of the test block prior to the activation of heaters, passive monitoring and active testing during the heating and subsequent cooling phase, and planned postcooling laboratory and field characterization activities similar to those conducted prior to activation of heaters. Preheat laboratory characterization included measurements of thermal properties, hydrological properties, mechanical properties, mineral-petrology studies, and pore-water chemical and isotopic analysis from rock cores. Preheat field characterization of the thermal test block involved rock-mass classification, fracture mapping, video logging of the boreholes, geophysical measurements, and air-permeability testing.

Measurements during the heating and cooling phases of the DST are divided into two categories: the continuous passive monitoring data and the active testing data, which are taken periodically. The DST test block has been instrumented with thousands of sensors to monitor the thermal, mechanical, hydrological, and chemical processes on at least an hourly basis. In Figure 7.2.1-2, the instrumented boreholes are color-coded according to their functions. For the purposes of this Model Report, the focus is on boreholes designed to measure thermal (yellow), hydrological (blue), and mechanical (green) behavior, as extracted from Figures 7.2.2-1 to 7.2.2-3. Radial arrays of 20 m long boreholes emanating from the Heated Drift monitor the temperature evolution, as do longitudinal boreholes parallel to and extending over most of the length of the

Heated Drift. Temperature sensors in each borehole are installed at approximately 30 cm intervals. Most boreholes labeled as "hydrological" originate from the Observation Drift. These are clusters of 40 m long boreholes forming vertical fans that bracket the Heated Drift and the wing heaters. These boreholes are used for periodic active testing of air-permeability changes to track the time evolution and spatial distribution of drying and condensation zones in the test block. Deformation of the rock mass is being monitored with an array of multiple-point borehole extensometer (MPBX) systems. In the radial MPBX boreholes, there are four anchors attached to the borehole wall at a distance of about 1, 2, 4, and 15 m from the drift wall. The displacements of each anchor, relative to the drift wall, are continuously monitored.

The DST design and geometry are described in the following reports: *Drift Scale Test Design and Forecast Results* (CRWMS M&O 1997 [146917]) and *Drift Scale Test As-Built Report* (CRWMS M&O 1998 [111115]). The results of preheat characterization of the test block are contained in the report *Ambient Characterization of the Drift Scale Test Block* (CRWMS M&O 1997 [101539]). A comprehensive documentation of DST measurements for the four-year heating period is given in the *Thermal Testing Measurements Report* (BSC 2002 [160771]). This report elaborates on the testing methods, gives representative results, and discusses measurement uncertainties. The comparison of simulated and measured DST results below primarily uses data described in this report.

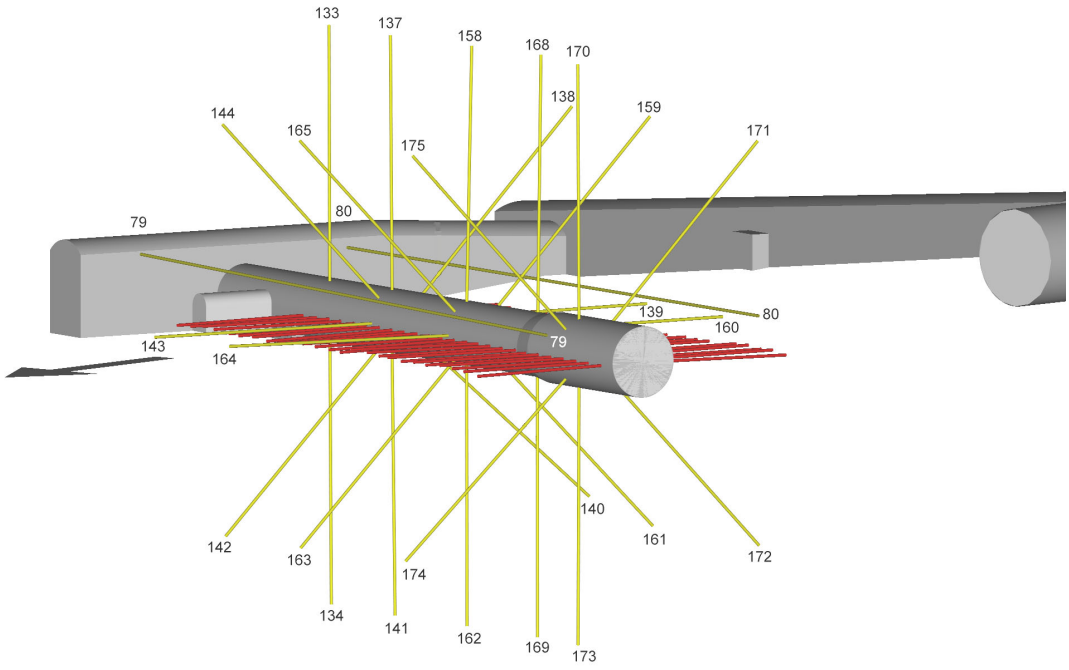

Source: BSC 2002 [160771], Figure 6.3-3.

Figure 7.2.2-1. Three-Dimensional Perspective of Wing Heaters and Temperature Boreholes in the DST

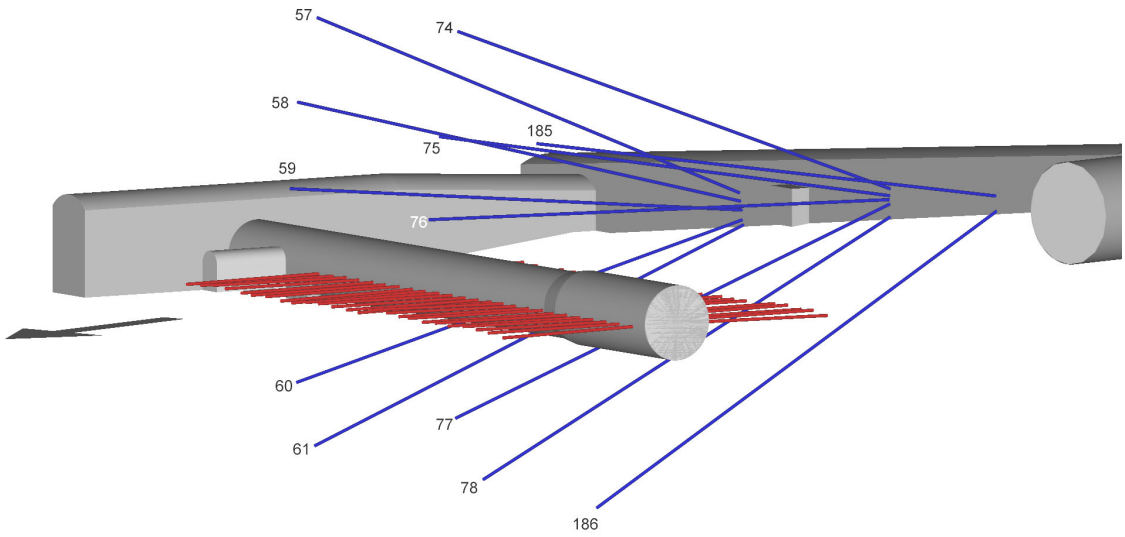

Source: BSC 2002 [160771], Figure 6.3-4.

Figure 7.2.2-2. Three-Dimensional Perspective of Wing Heaters and Hydrology Boreholes in the DST

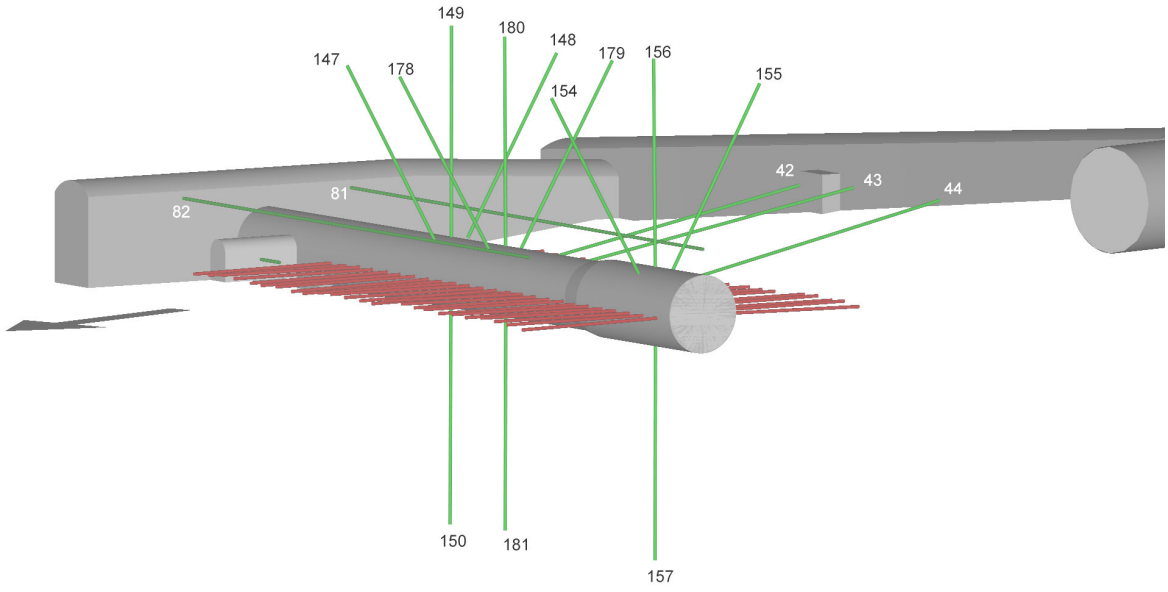

Source: BSC 2002 [160771], Figure 6.3-5.

Figure 7.2.2-3. Three-Dimensional Perspective of Wing Heaters and Boreholes for Mechanical Measurements in the DST

7.3 DST MODEL DOMAIN

The DST model domain is a two-dimensional representation of the DST in a section crossing the heated drift perpendicular to its axis (Figure 7.3-1a). The two-dimensional model is half-symmetric with a vertical symmetry plane along the center axis of the Heated Drift. The model domain extends vertically 250 m from the top of the Tptpul stratigraphic unit (z = 100) down to the bottom of the Tptpll stratigraphic unit (z = -150 m) (The stratigraphy of the geological units is extracted from the nearby borehole USW SD-9.) The lateral model boundary is placed at a distance of 100 m from the center of the Heated Drift. Model components include the three geological units (Tptpul, Tptpmn, and Tptpll), the Heated Drift, the concrete invert, and wing heaters. The Heated Drift is represented by a gridblock that is assigned a large permeability and heat conductivity to allow for advective, conductive, and radiative transport of heat. An extra grid element is added to simulate loss of heat and vapor through the bulk head at the end of the Heated Drift.

The mechanical, hydraulic, and thermal boundary conditions (as well as initial conditions) are presented in Figure 7.3-1b–d. The initial vertical stress is estimated using an average density of 2,200 kg/m^3 for the overlying rock units, leading to a vertical stress of about 5.8 MPa at the depth of the Heated Drift (267.5 m). The average value of the rock bulk density was calculated for the overlying rock mass using values of saturated rock densities given in 1999 TBV-332/TBD 325 Resolution Analysis: Geotechnical Rock Properties, Table 9 (DTN: MO9911SEPGRP34.000 [148524]). The magnitude of maximum and minimum principal compressive horizontal stresses are a factor of 0.6 and 0.5 of the vertical stress, with the maximum stress oriented normal to the drift axis (CRWMS M&O 1997 [103564], Table 3-2, pp. 3–23). The stress normal to the top boundary (representing the stress produced from the overlying rock mass) and the left lateral boundary (representing the remote maximum principal compressive stress) are fixed throughout the simulation. The top and bottom model boundary conditions are identical to the ones used in the *Thermal Tests Thermal-Hydrological Analyses/Model Report* (BSC 2001 [157330], Section 6.1.2). The fixed hydraulic and thermal boundary conditions on the top and bottom of the model were obtained from an independent TH simulation of a one-dimensional model domain extending from the ground surface to the water table (BSC 2001 [157330], Section 6.1.2).

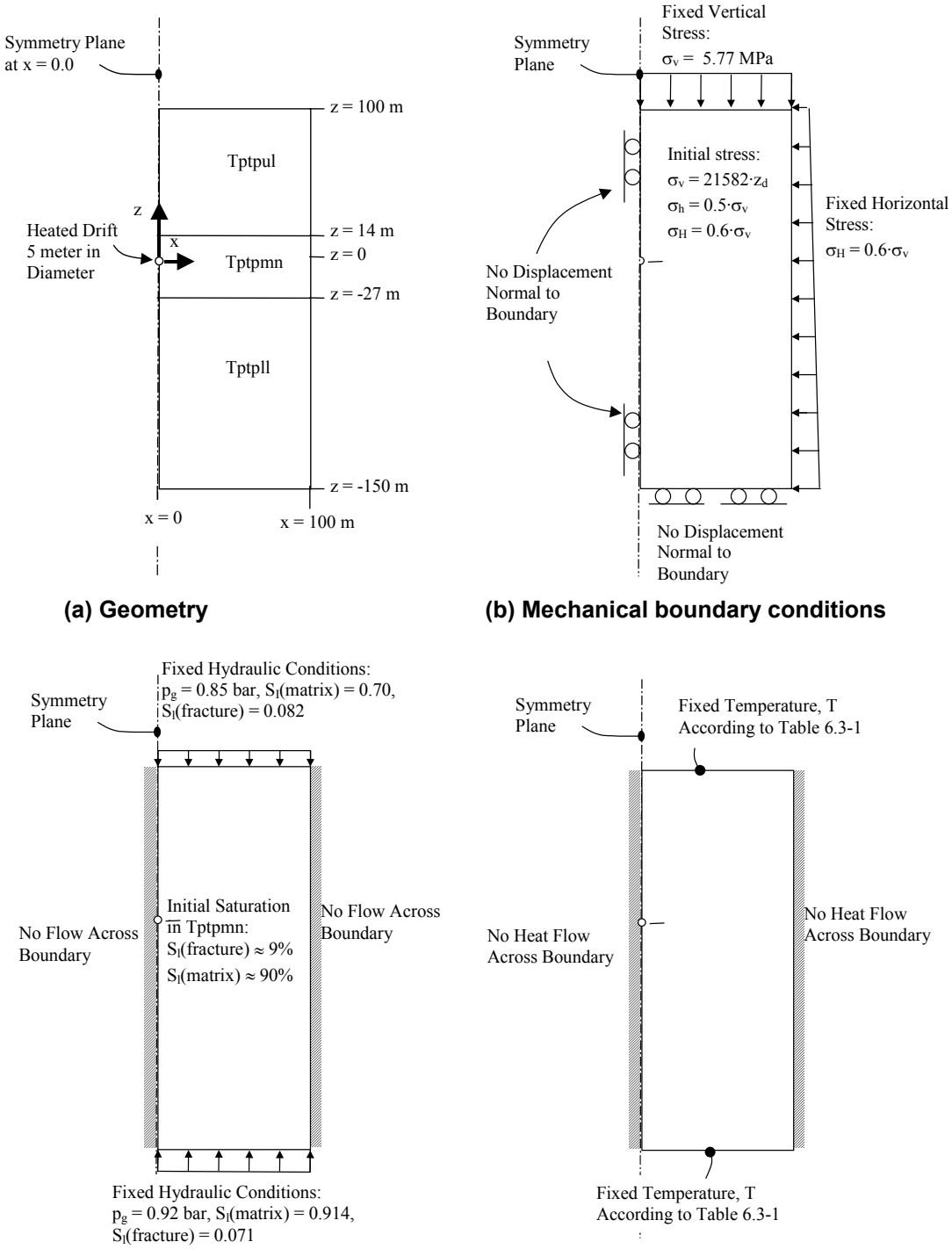

NOTES: P_g = gas pressure, S_l = liquid saturation, z_d = depth below ground surface

Figure 7.3-1. Two-Dimensional Representation of the DST in a Section Crossing the Heated Drift Perpendicular to Its Axis Presented with (a) Geometry; (b) Mechanical; (c) Hydrological; and (d) Thermal Boundary Conditions

The total heating power applied to the DST model domain reflects average values of the actual heating power. Average values were calculated for various time periods in BSC 2003 ([161530], Table 7.3.4-1). The periods of identical average power output, as applied to the model, are given in Table 7.3-1 separately for the drift heaters and the wing heaters. The heat power for the two-dimensional model was calculated from the total heat power in Table 7.3-1, divided by 47.5 m (the length of the heat source along the Heated Drift). In addition, the heat power for the drift heater in the half-symmetric model is divided by two, and the power of the wing heaters are distributed with 43.1% to the inner wing heaters and 56.9% to the outer wing heaters. This is in accordance with a ratio of heat power between the outer and inner wing heaters of 1.3188, as given in DTN: MO9912SEPDOIHP.000 [129272].

Table 7.3-1. Total Average Heater Power at Various Times of Heating in the DST

Time	Drift Heaters (kW)	Wing Heaters (kW)
12/03/1997-05/31/1999	52.1	132.1
06/01/1999-03/02/2000	50.0	125.1
03/02/2000-05/02/2000	47.9	120.4
05/02/2000-08/15/2000	45.8	114.6
08/15/2000-03/31/2001	43.3	106.4
04/01/2001-05/02/2001	43.4	106.7
05/02/2001-08/22/2001	41.4	101.6
08/22/2001-09/30/2001	39.4	96.3
10/01/2001-01/14/2002	39.4	96.8

Source: BSC 2003 [161530] Table 7.3.4-1

The properties utilized in the DST model domain are summarized in Table 4.1.4. TH properties are taken from the site-specific rock-property set DKM-TT99, which is also used in the DST TH Model in the *Drift-Scale Coupled Processes (DST and TH Seepage) Models* Report (BSC 2003 [161530], Table 4.1.2). The rock-mass mechanical properties (Young's Modulus and Poisson's Ratio) are extracted from the qualified data set in the 1999 TBV-332/TBD 325 Resolution Analysis: Geotechnical Rock Properties (MO9911SEPGRP34.000 [148524], Tables 10 and 11 for 40% cumulative frequency). These elastic parameters, which represent the bulk rock mass (including the effect of fractures), have been estimated using an empirical method based on the Geological Strength Index (GSI). The adopted rock-mass Young's modulus is about 50% lower than the Young's modulus of intact rock determined on core samples from the site.

The TM and HM properties of the rock mass were developed in Section 6.4 of this model report. The parameters for these properties are given in Table 7.3-2. In Figure 7.3-2, the function for a temperature-dependent thermal expansion coefficient is compared to measured thermal expansion coefficients on intact rock samples from the DST block. The adopted thermal expansion coefficient is close to the site-specific values of the intact-rock thermal expansion coefficient (Figure 7.3-2) for a temperature up to 200°C. Values close to the intact-rock thermal expansion coefficient were adopted in Section 6.4 based on TM simulation results by Sobolik et al. (1999 [163202], p. 741) and BSC (2001 [155957], pp. 21 and 115–125), which showed that measured TM responses are well predicted by assigning the rock mass an intact-rock thermal expansion coefficient.

Table 7.3-2. Summary of TM and HM Parameters and Properties of the Rock Mass Developed in This Model Report for the DST Model Domain

	Geol. Unit >	*Tptpul (tsw33)*	*Tptpmn (tsw34)*	*Tptpll (tsw35)*	Source
Initial Hydraulic Aperture	b_i (μm)	167	52	153	Calculated using Equation (6.4-1) and frequency and permeability given in Table 4.1-5
Parameters b_{max} and α for the Stress-Aperture Function	b_{max} (μm) α (1/MPa)	200 0.52	200 0.52	200 0.52	Developed in Section 6.4 of this Model Report
Thermal Expansion Coefficient	α_T (10^{-6}/°C)	5.0+0.0583×T	5.0+0.0583×T	5.0+0.0583×T	Derived from intact rock thermal expansion coefficient in Section 6.4 of this Model Report

NOTE: T = Temperature in °C

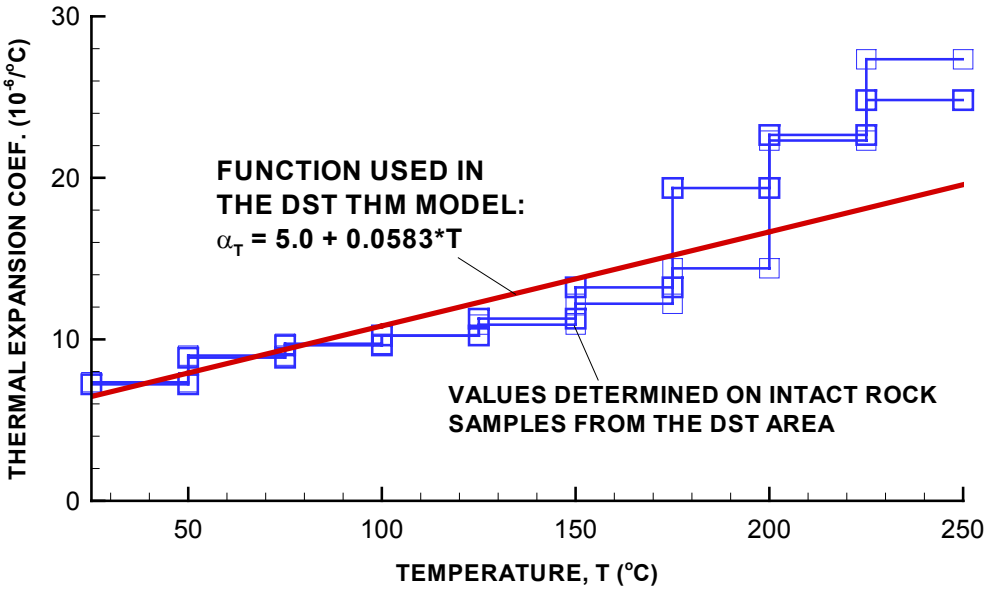

DTN: MO0004RIB00035.001 [153848], Tables 9 and 11

NOTE: Laboratory values were determined on core samples from the DST block during two cycles of heat-up.

Figure 7.3-2. Temperature-Dependent Thermal Expansion Coefficient Used in the DST Model Domain and Comparison to Laboratory-Determined Values on Intact Rock

7.4 DST VALIDATION RESULTS

The Drift-Scale THM Model is validated for measurements taken during the 49.5-month heating phase of the DST. The results are presented by comparing the calculated THM responses to measurements, which have been grouped into equivalent categories based on their location relative to the Heated Drift. Such grouping of the field data is conducted to display typical trends of the field data and their variability.

7.4.1 Modeling of Temperature Field

For the purpose of validating the Drift-Scale THM Model for TM and HM processes, the calculated temperature field must be in reasonable agreement with measured temperature. This is essential because the temperature field is the driving force behind both TM and THM processes. In modeling the DST, an accurate agreement between the calculated and measured temperature was obtained if heat loss through the bulkhead was simulated. A bulk-head heat-loss coefficient of 0.4375 W/ºK was determined by calibrating the model for a drift-wall temperature of 150°C at 12 months (Wang 2003 [162654], SN-LBNL-SCI-204-V2, p. 60). Without considering the heat loss through the bulkhead, the temperature at the drift wall would be overestimated, and consequently, TM forces and displacements would also be overestimated.

Figure 7.4.1-1 shows calculated temperature after 12 months of heating and the location of thermal boreholes used for validation of the temperature calculation. Figures 7.4.1-2 and 7.4.1-3 show the comparison of measured and simulated temperature profiles. The measured temperature includes data from four borehole arrays located at y ≈ 12, 23, 32 and 39 m along the Heated Drift. These borehole arrays are located well inside the axial extensions of the Heated Drift and wing heaters. In Figures 7.4.1-2 and 7.4.1-3, the calculated temperatures are well within the range of measured values. Furthermore, it can be concluded from Figures 7.4.1-2 to 7.4.1-3 that the two-dimensional and half-symmetric model approximation is justified and accurate for predicting temperatures in boreholes located well within the extension of the Heated Drift.

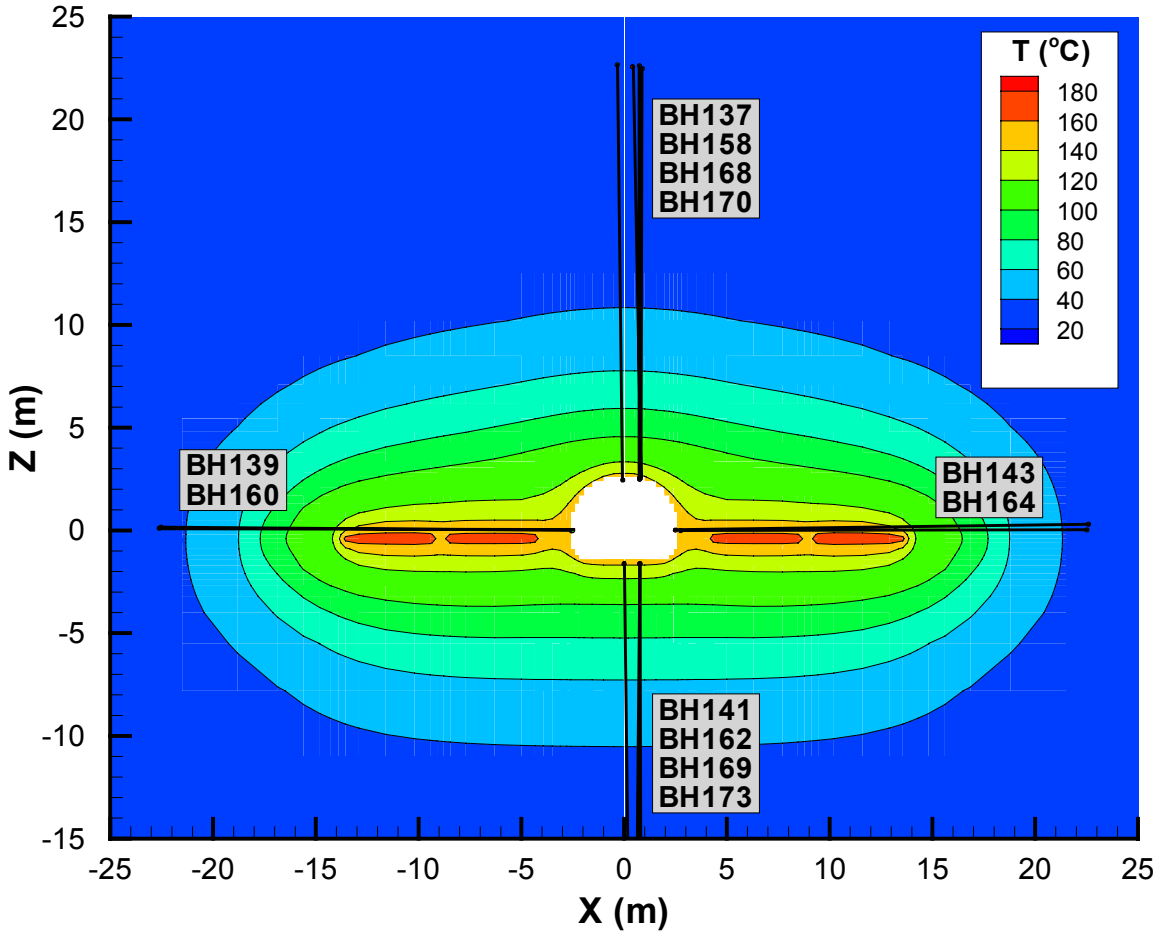

DTN (borehole locations): MO0002ABBLSLDS.000 [147304]

Output – DTN (simulated contour): LB0306DSTTHMVL.002

Figure 7.4.1-1. Calculated Temperature Distribution after 12 Months of Heating and Location of Thermal Boreholes for Comparison of Simulated and Measured Temperature Profiles

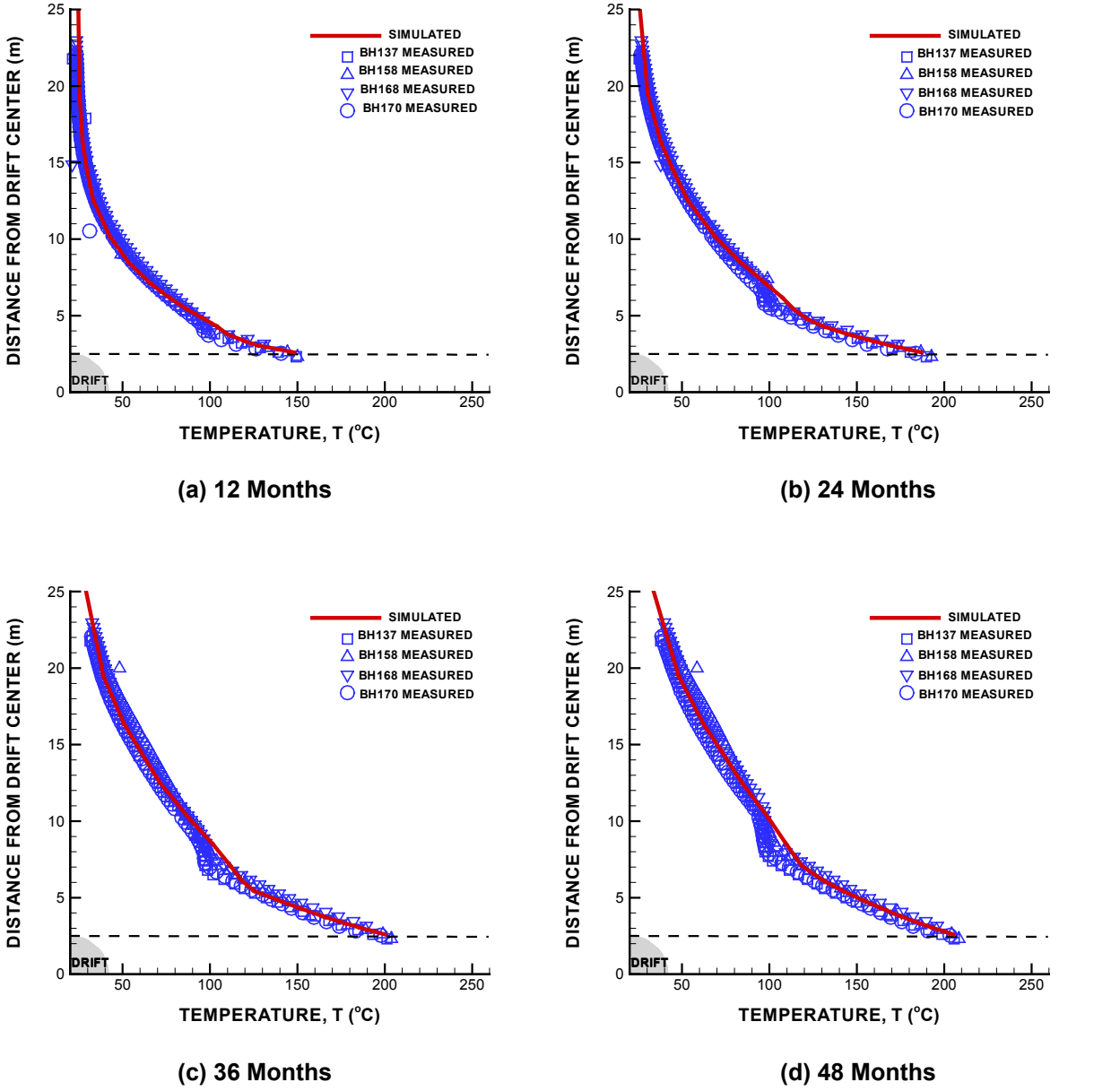

DTN (measured): MO0208RESTRDST.002 [161129]
Output – DTN (simulated): LB0306DSTTHMVL.002

Figure 7.4.1-2. Measured and Simulated Temperature Profiles along Vertically-Up Boreholes at the Drift Crown

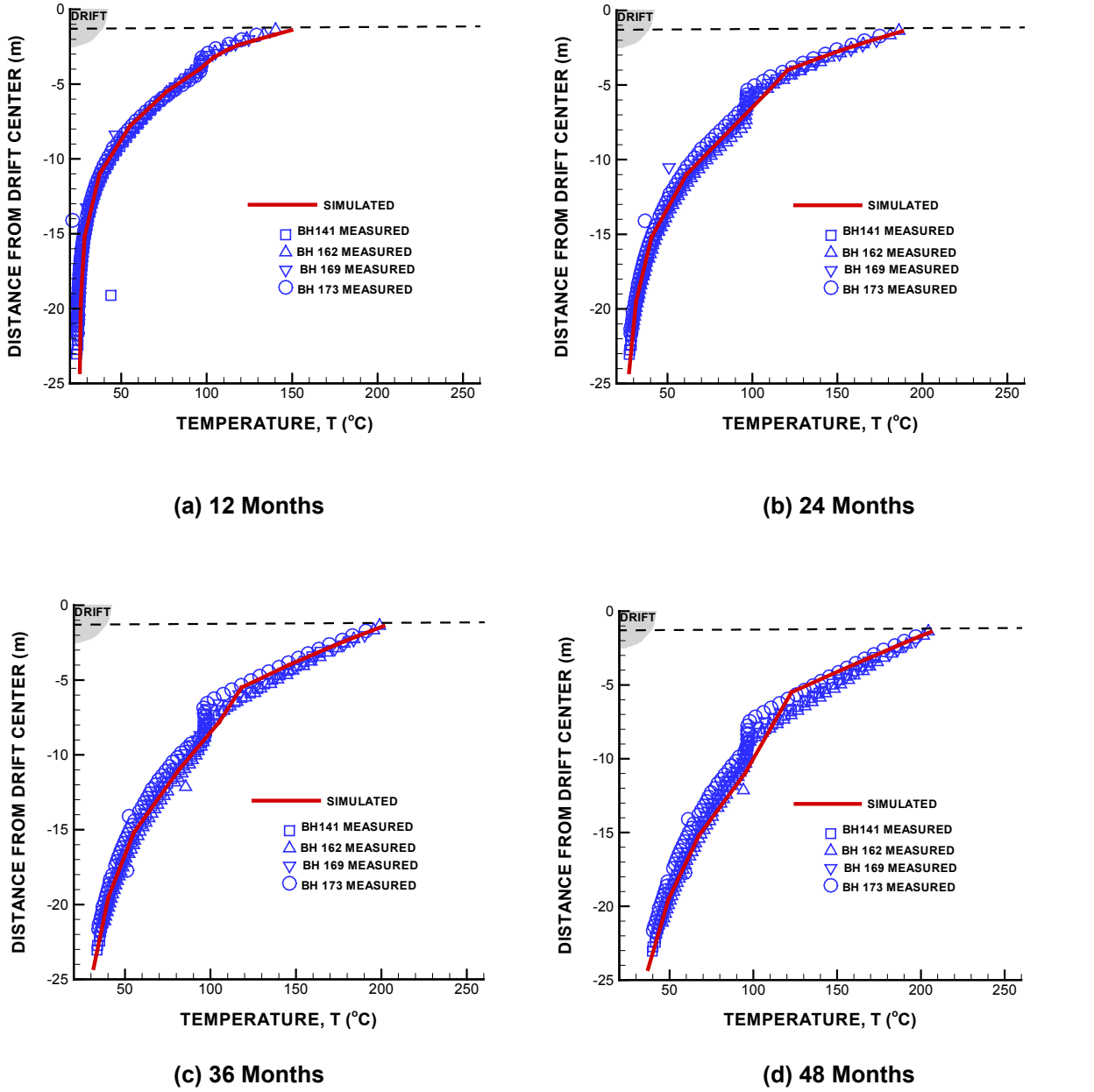

DTN (measured): MO0208RESTRDST.002 [161129]
Output – DTN (simulated): LB0306DSTTHMVL.002

Figure 7.4.1-3. Measured and Simulated Temperature Profiles along Vertically-Down Boreholes Extending Downward from the Drift Floor

7.4.2 Validation for TM Processes

The TM part of the Drift-Scale THM Model is validated by comparing calculated and measured displacements in radial MPBX boreholes. Such comparison essentially validates the Drift-Scale THM Model for the thermal expansion process, as well as for the values of the thermal expansion coefficient.

Figure 7.4.2-1 shows calculated displacements relative to the drift axis and the locations of radial MPBX boreholes and their anchors, which are used for validation of the calculated thermal expansion. Measured data includes displacements from MPBX borehole arrays located at y ≈ 41.1, 21.0, and 13.7. All these arrays are within the axial extensions of the Heated Drift, with the one at y ≈ 41.1 being farthest out, located about 4.6 m from the edge of the heated area. In general, the measured displacements show a larger spread than temperature measurements. This reflects the fact that mechanical displacements are more sensitive to local heterogeneities in the rock mass, such as fractures. In addition, there are a few anchors in which the measured data are erratic, unreasonable or missing, and therefore excluded from this analysis. The quality of displacement measured in the various anchors is documented in the *Thermal Testing Measurements Report* (BSC 2002 [160771], Section 6.3.3.1.1).

The measured displacements at various points in the rock mass are grouped according to their radial distances from the drift wall. That is, measurements taken at Anchors 1, 2, 3, and 4, respectively located at 1, 2, 4, and 15 m from the drift wall, are compiled into four groups regardless of their angular direction and axial location along the Heated Drift. The measured and simulated displacements for each group are compared in Figure 7.4.2-2. With the exception of the very early time, the simulated displacements are within the range of measured displacement. It appears that the agreement is best for Anchors 2 and 3, whereas the calculated displacement in Anchor 1 is a lower-bound prediction. In Anchor 4, the displacement is slightly underpredicted during the first half the heating period, whereas good agreement is obtained at the end of the heating period.

A quantitative evaluation of model predictions are provided by statistical measures according to Wagner et al. (2001 [163532]). Three statistical measures were considered in the quantitative evaluations: root-mean-square-difference (RMSD), mean-difference (MD) and normalized-absolute-mean difference (NAMD). The three statistical measures are a function of simulated ($V_{sim,\ i}$) and measured ($V_{meas,\ i}$) variables that in this case are the simulated and measured displacements.

The root-mean-square-difference (RMSD), which for a specific time is described as:

$$RMSD = \left[\frac{\sum_{i=1}^{N} \left(V_{sim,i} - V_{meas,i} \right)^2}{N} \right]^{1/2} \qquad \text{(Eq. 7.4.2-1)}$$

RMSD is a classic statistical measure that has a bias towards larger differences between measured and simulated responses. The smaller the RMSD, the better agreement between simulated and measured responses. N is the number of measurements for a specific time.

The mean difference (MD), which for a specific time is described as:

$$MD = \frac{\sum_{i=1}^{N} \left[V_{sim,i} - V_{meas,i} \right]}{N} \qquad \text{(Eq. 7.4.2-2)}$$

A positive MD indicates a general overestimation of the measured variable, whereas the converse applies for a negative MD.

The normalized absolute mean difference (NAMD) for a specific time is described as:

$$NAMD = \sum_{i=1}^{N} \left| \frac{V_{sim,i} - V_{meas,i}}{V^{0}_{meas,i}} \right| \cdot \frac{1}{N} \qquad \text{(Eq. 7.4.2-3)}$$

where $V^{0}_{meas,i}$ in this case is measured displacement. NAMD provides a percentage of the absolute difference between measured and simulated variables relative to the measured variable.

Figure 7.4.2-3 presents the RMSD, MD, and NAMD for all simulated and measured displacements shown in Figure 7.4.2-2. The curves in Figure 7.4.2-3 were calculated using an MS Excel spreadsheet as described in detail in Attachment II. In Figure 7.4.2-3a, the RMSD increases from about 1 mm at 6 months to about 2 mm at the end of the heating. The increasing RMSD with time reflects the increasing variability in measured displacement. The MD shows that the overall displacement field during the first 30 months is underestimated by about 1 mm, a number that is reduced to about 0.5 mm at the end of the heating period (Figure 7.4.2-3b). The NAMD is about 45% at 6 months, but gradually reduces to less than 25% after 24 months of heating. Thus, as a whole, the displacements are well predicted at the DST and clearly within the validation criterion of ±50% discussed in Section 7.1.

The general agreement in the magnitude of displacement over the entire heating period confirms the findings by Sobolik et al. (1999 [163202], p. 741) and BSC (2001 [155957], pp. 21 and 115–125), suggesting that the intact-rock thermal expansion coefficient is an appropriate representation of the *in situ* thermal expansion coefficient at the DST. Also, the SHT was simulated using the intact-rock thermal expansion coefficient and showed generally good agreement with measured results (CRWMS M&O 1999 [129261], pp. 9–10).

The finding that the intact rock thermal expansion coefficient is appropriate seems to contradict results from separate determinations of what is described as a "rock-mass thermal expansion coefficient" at the SHT and DST (CRWMS M&O 1999 [129261], p. 9-11 and BSC 2002 [160771], p. 6.3-35). In that case, the *in situ* thermal expansion coefficient was back-calculated directly from measured deformations and temperature changes along certain extensometers at the SHT and DST. It was found that the *in situ* thermal expansion coefficient determined by this method is about 50% lower than intact-rock thermal expansion coefficient. The 50% lowering of the *in situ* thermal expansion coefficients were attributed to some of the displacements being accommodated by closure of fractures. The apparent contradiction between the results of numerical modeling (which generally shows that the intact-rock thermal expansion coefficient is appropriate) and the direct back-calculated *in situ* thermal expansion (which indicates that a 50% lower thermal expansion coefficient would be appropriate) can have two contributing causes:

1) The *in situ* back-analyzed thermal expansion coefficients at SHT and DST were determined from measurements in horizontal boreholes, whereas the comparison of measured and simulated displacements in this Model Report was conducted for vertical or subvertical boreholes. The *in situ* thermal expansion coefficient along

horizontal boreholes may lower because vertical fractures are most abundant at the site.

2) The *in situ* back-analyzed thermal expansion coefficient at the SHT and DST is impacted by simultaneous increases in temperature and thermal stress and may therefore be different from the basic thermal expansion coefficient that is part of the input to a numerical model. The basic thermal expansion coefficient is a measure of the expansion of the rock for a temperature increase under constant stress. If the thermal expansion coefficient is determined under an increasing thermal stress, some of the rock expansion will be prevented, and thereby the basic thermal expansion coefficient would be underestimated.

Nevertheless, the *in situ* back-analyzed thermal expansion is expected to provide a lower bound for the basic *in situ* thermal expansion coefficient, whereas the intact-rock thermal expansion coefficient is expected to provide an upper bound. In this study, it was shown that in the vertical direction at the DST, the intact-rock thermal expansion coefficient is appropriate.

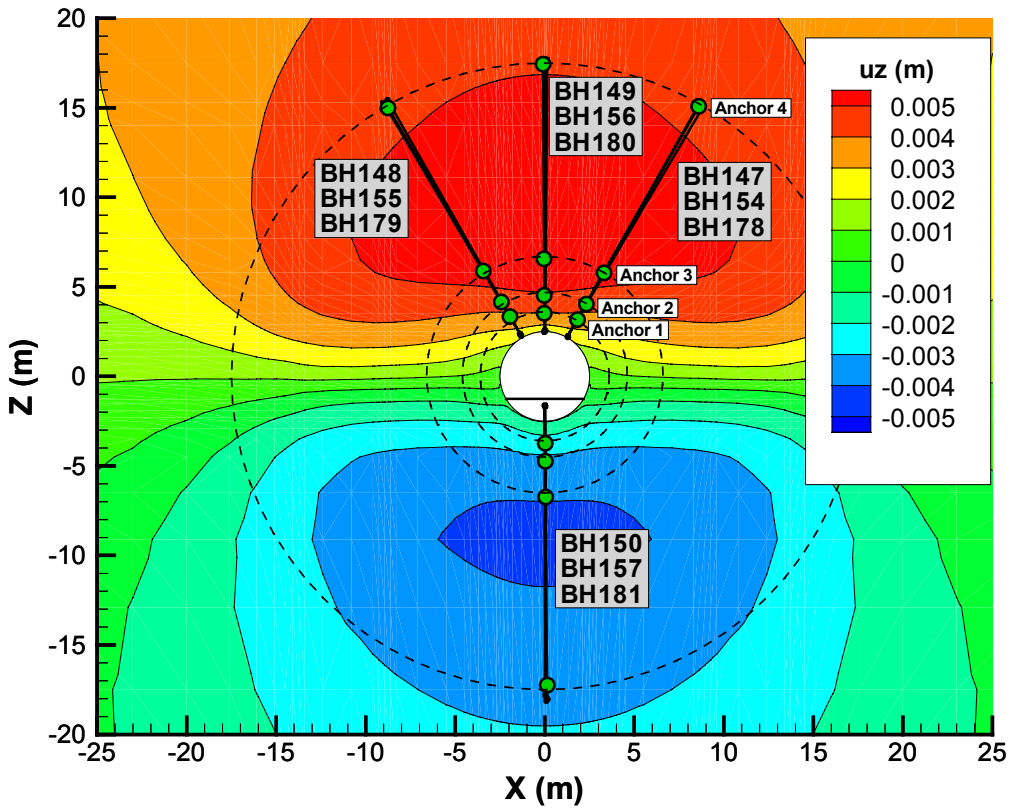

DTN (borehole locations): MO0002ABBLSLDS.000 [147304]

Output – DTN: LB0306DSTTHMVL.002

Figure 7.4.2-1. Simulated Vertical Displacement (UZ) after 12 Months of Heating and Location of Mechanical MPBX Boreholes for Comparison with Measured Displacement

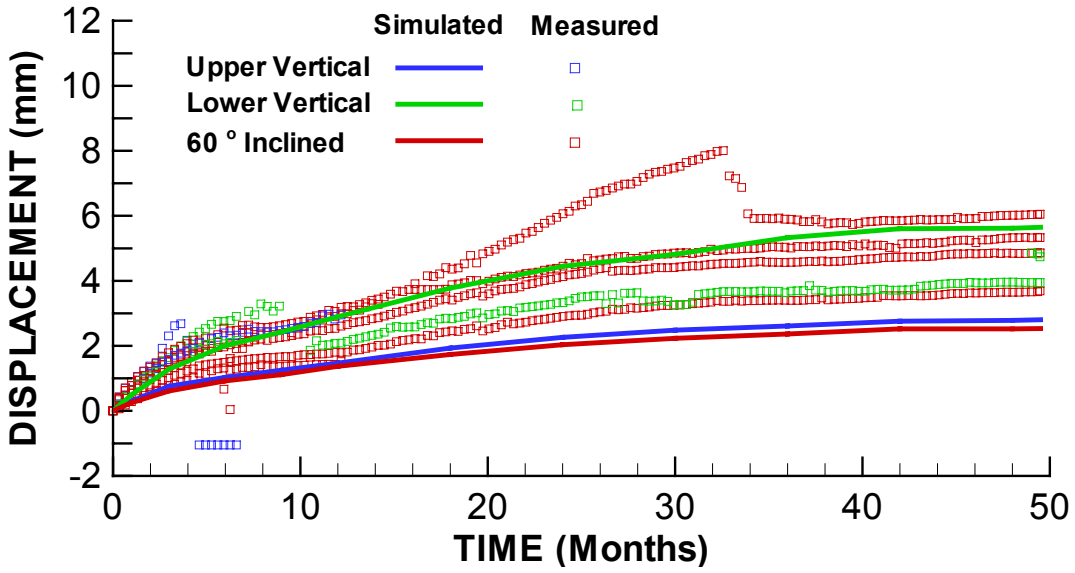

(a) Anchor 1

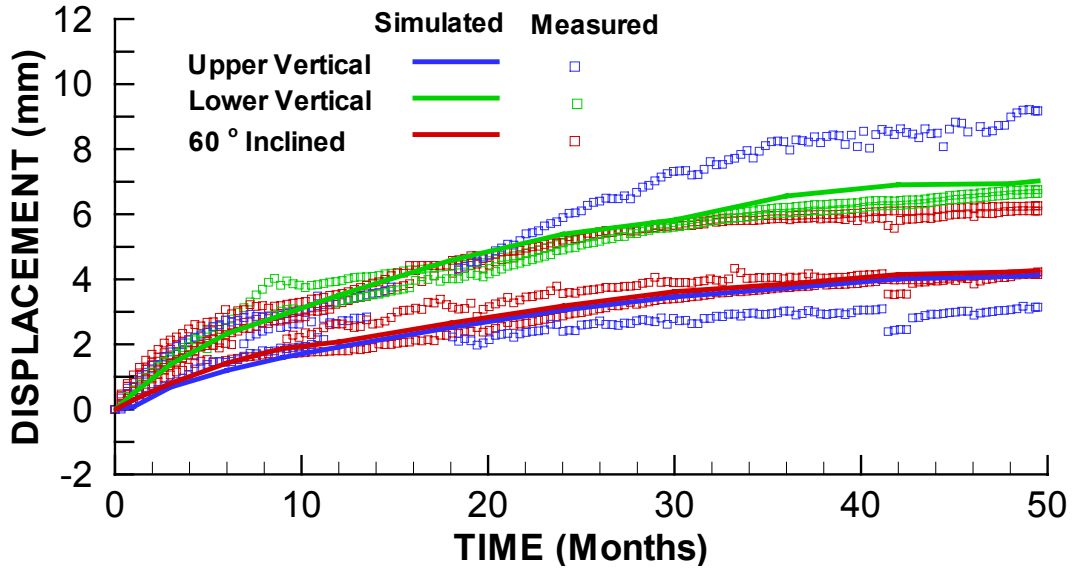

(b) Anchor 2

DTN (measured): SN0207F3912298.037 [162046]
Output – DTN (simulated): LB0306DSTTHMVL.002

NOTE: Measured values are from borehole numbers shown in Figure 7.4.2-1.

Figure 7.4.2-2. Measured and Simulated Evolution of Displacement in MPBX Boreholes

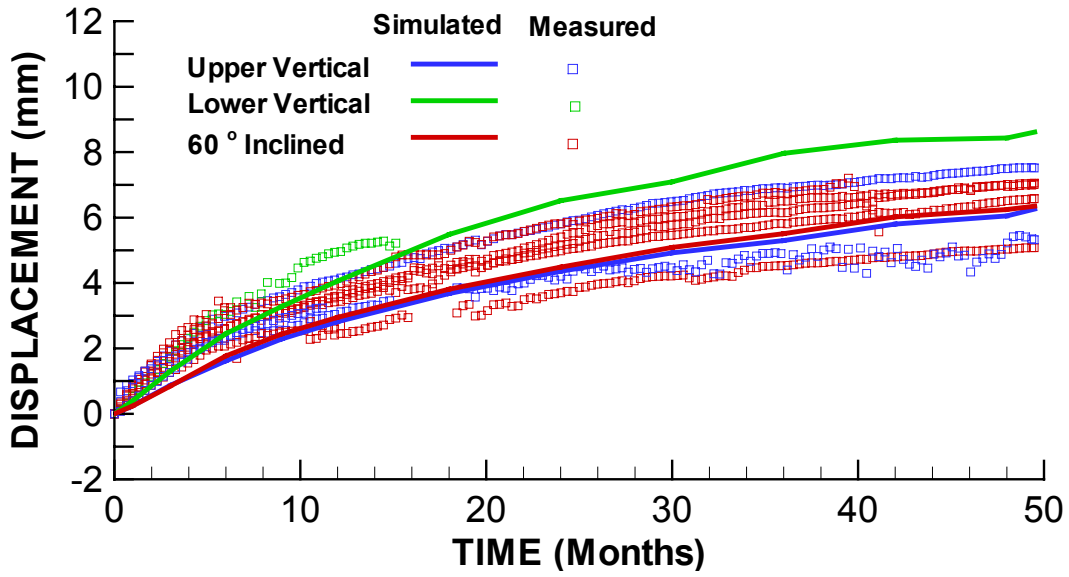

(c) Anchor 3

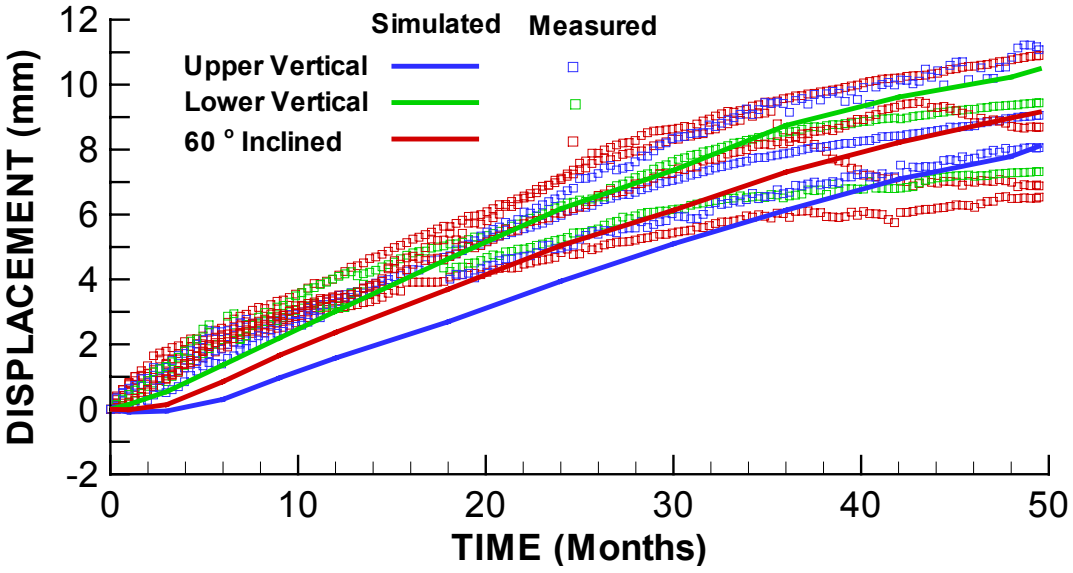

(d) Anchor 4

DTN (measured): SN0207F3912298.037 [162046]
Output – DTN (simulated): LB0306DSTTHMVL.002

NOTE: Measured values are from borehole numbers shown in Figure 7.4.2-1.

Figure 7.4.2-2. (Continued) Measured and Simulated Evolution of Displacement in MPBX Boreholes

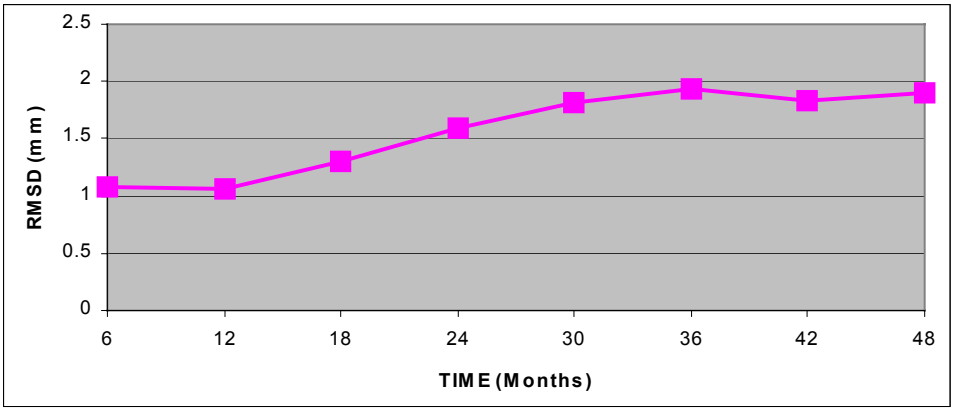

(a) Root-mean-square-difference (RMSD)

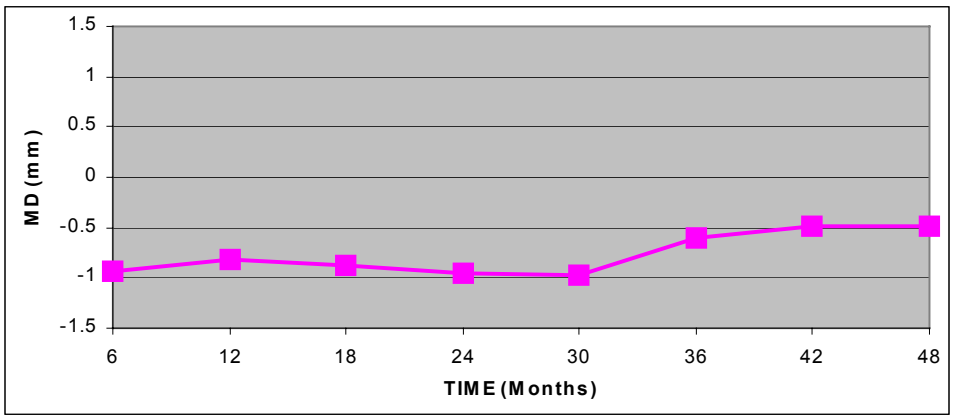

(b) Mean-difference (MD)

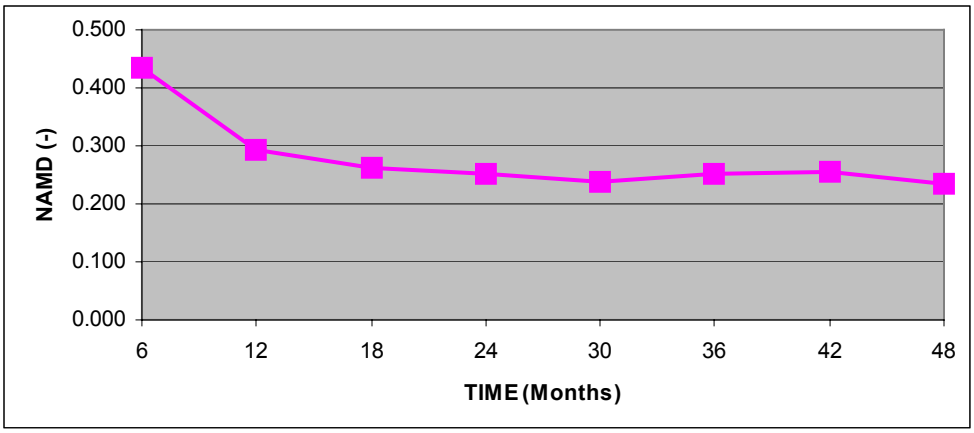

(c) Normalized-absolute-mean-difference (NAMD)

NOTE: Statistical analyses leading to the curves presented in this figure are described in Attachment II.

Output – DTN (Statistical analysis): LB0306DSTTHMVL.002

Figure 7.4.2-3. Statistical measures for displacement comparative analysis

7.4.3 Validation for THM Processes

The Drift-Scale THM Model is validated for THM processes by comparing calculated against measured changes in absolute air permeability. The measured change in air permeability reflects two simultaneous processes: TM-induced changes in intrinsic permeability and TH-induced changes in relative permeability for air flow. TM-induced changes in intrinsic permeability result from thermal stresses associated with the heating of the rock mass. Thermal stresses act upon existing fractures, changing their aperture, which in turn may either increase or decrease the intrinsic fracture permeability. TH-induced changes are associated with thermally driven changes of moisture content in fractures. Wetting and drying in fractures (in other words, increase and decrease of liquid saturation) gives rise to changes in relative permeability for air flow.

Figure 7.4.3-1 presents the simulated liquid fracture saturation after 12 months of heating and the location of boreholes for air-permeability measurement. The figure shows that a dryout zone has formed around the Heated Drift and wing heaters. Just outside the dryout zone, a zone of higher-than-ambient saturation forms because the produced vapor condenses in cooler areas. The dryout zone and the condensation zone progressively move away from the heated drift over time. This movement is controlled by the flow of vapor away from the heat source along the thermal gradient and a reversed liquid flow along the pressure gradient toward the inner, dryer regions. In addition, there is a gravity-driven liquid flow that tends to drain the condensation zone above the heated drift. Air-permeability measurements performed in the condensate zone should exhibit a decrease in air permeability. Corresponding moisture-induced changes in relative permeability caused by the wetting and drying of fractures are shown in Figure 7.4.3-2a. This figure shows that the increased fracture liquid saturation in the condensate zone causes a reduction in relative permeability to about 30% of its original value. In the dryout zone, the relative permeability has increased slightly from its original value, because fractures in this zone are completely dry.

Figure 7.4.3-2b shows the total permeability changes, combining TH-induced relative permeability changes with TM-induced changes in intrinsic permeability. The figure shows that TM effects cause the permeability to decrease around the drift and wing heaters, including the inner dryout zone and the outer condensate zone. In the condensate zone, the permeability has now decreased to about 10% of its original value. In Figure 7.4.3-2b, a zone of increased permeability appears above the Heated Drift at about z = 20 m. This zone of increased permeability is caused entirely by TM effects, which is caused by open vertical fractures. Vertical fractures open in this area because of a reduction in horizontal stresses. This reduction causes the redistribution of horizontal stresses towards the Heated Drift to balance high thermal stresses near the heat source.

The calculated permeability changes are compared to air-permeability measurements in Figure 7.4.3-3. The comparisons between calculated and measured responses are made at three locations about 6, 12, and 18 m above the center of the drift. At z = 6 m, four boreholes sections—76:3, 76:4, 59:3, and 59:4—are located symmetrically around x = 0 (see Figure 7.4.3-1). In these sections, the air permeability first decreases with time to reach a minimum at about 24 months. Thereafter, the permeability increases slightly in three of four boreholes sections and dramatically in the fourth (Figure 7.4.3-3a). The figure compares measured changes in air permeability at the four borehole sections with calculated changes in permeability. The solid line indicates the calculated changes in air permeability, which are the product of the intrinsic

permeability (TM effect) and gas relative permeability (TH effect). The figure shows that the solid line representing the combined TH and TM effects matches three of four measurements best. In the fourth section, 59:3, the measured changes appear to match a pure TH response the best.

At about z = 12, three borehole sections—75:3, 75:4, and 58:3—are located symmetrically around x = 0 and between z =10 and 14 m. Measured responses in these three boreholes are very consistent, with an initial increase in air permeability during the first 9 months, followed by a gradual decrease with time until the end of heating. The decrease in permeability can be interpreted either as a change in intrinsic permeability (TM), or as a change in relative permeability (TH), or a combination of the two (THM). However, the initial increase during the first 9 months can only be explained as a TM response.

For the measurements located farthest away from the drift—74:4 and 57:4 at z ≈ 18 m— there is an increase in air permeability caused solely by TM-induced changes in intrinsic permeability (TM in Figure 7.4.3-3c). At this location, far away from the Heated Drift, no effect from TH-induced changes appears until about 36 months, when a slight wetting starts to take place.

The results in Figure 7.4.3-3 are calculated with the parameters b_{max} = 200 μm and α = 0.52 MPa^{-1} as developed in Section 6.4 of this Model Report. The overall simulated changes in air permeability using those parameters are in agreement with the measured change, and the validation criterion discussed in Section 7.1 is met. That is, the predicted changes in air permeability are in the correct direction and correct within an order of magnitude: log (k/k_i) simulated and measured differ by less than 1. Observed trends (e.g., k/k_i decreases followed by increases, or the reverse) are matched by model predictions. The predicted THM responses are on average stronger than the measured ones, and hence the stress-aperture function defined by the parameter b_{max} = 200 μm and α = 0.52 MPa^{-1} can be considered conservative. As a sensitivity case, a second simulation is conducted with a more moderate stress-aperture function defined by b_{max} = 150 μm and α = 0.6 MPa^{-1}. The results of this simulation show a better agreement with the "average" observed HM behavior at the DST (Figure 7.4.3-4).

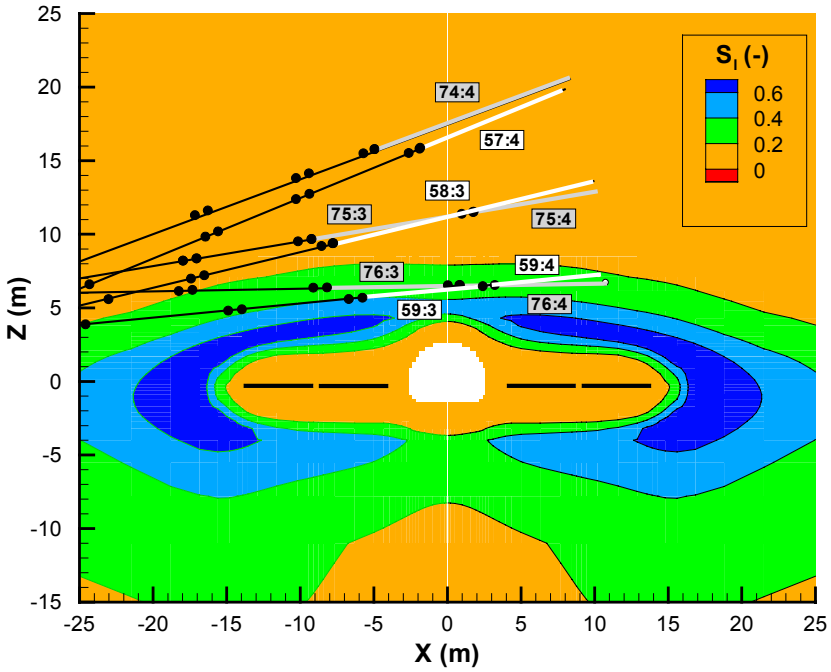

DTN (borehole locations and sensors): MO0002ABBLSLDS.000 [147304]
Output – DTN: LB0306DSTTHMVL.002

NOTE: Initial fracture liquid saturation is approximately 0.09.

Figure 7.4.3-1. Simulated Distribution of Fracture Liquid Saturation (S_l) after 12 Months of Heating and Location of Borehole Sections Where Simulated and Measured Air Permeability is Compared

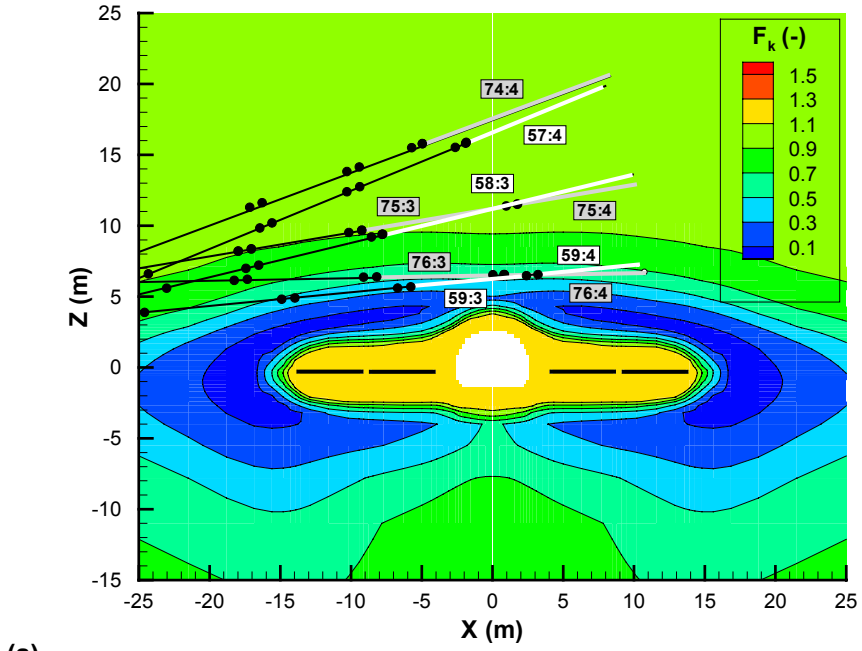

(a)

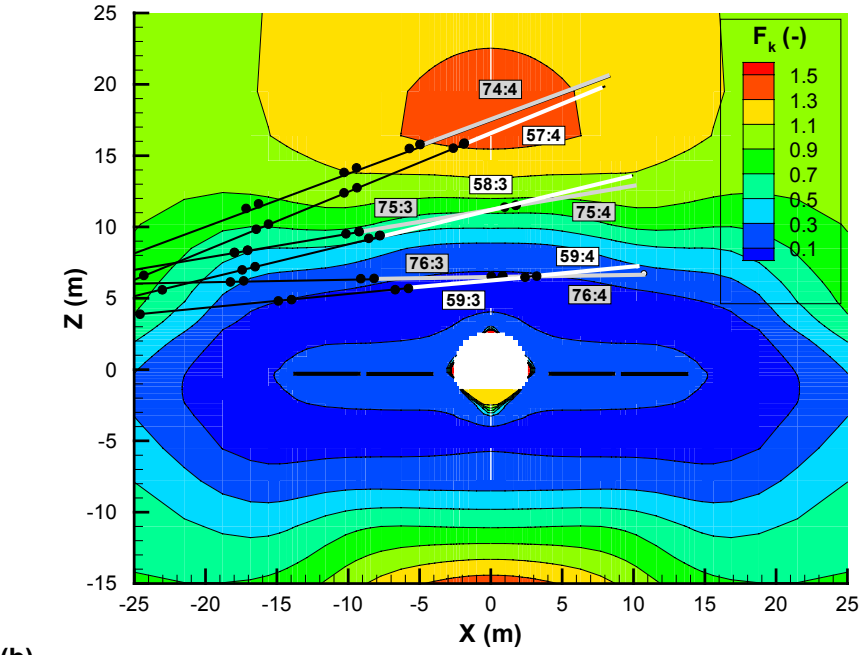

(b)

DTN (borehole locations and sensors): MO0002ABBLSLDS.000 [147304]
Output – DTN: LB0306DSTTHMVL.002

NOTE: (a) Changes in relative air permeability caused by TH-induced moisture redistribution.
(b) Change in absolute air permeability caused by the combined effect of moisture redistribution and stress-induced changes in intrinsic permeability.

Figure 7.4.3-2. Simulated Changes in Air Permeability at the Drift Scale Test after 12 Months of Heating Expressed in Terms of Permeability Correction Factor ($F_k = k/k_i$) Relative to Preheating Permeability (k_i)

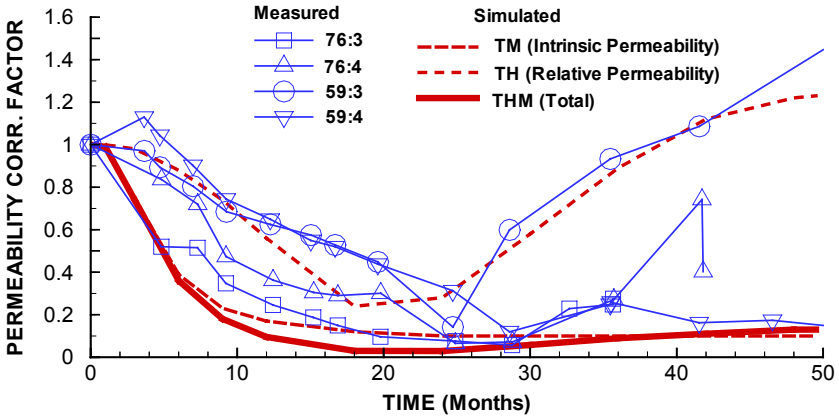

(a) Group located at z ≈ 6 m

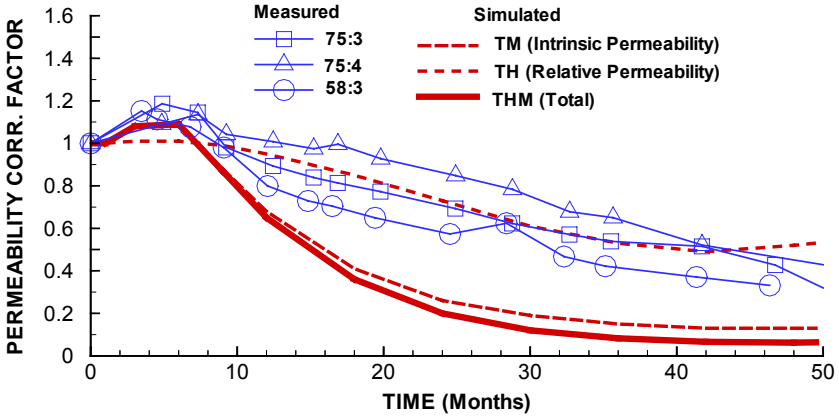

(b) Group located at z ≈12 m

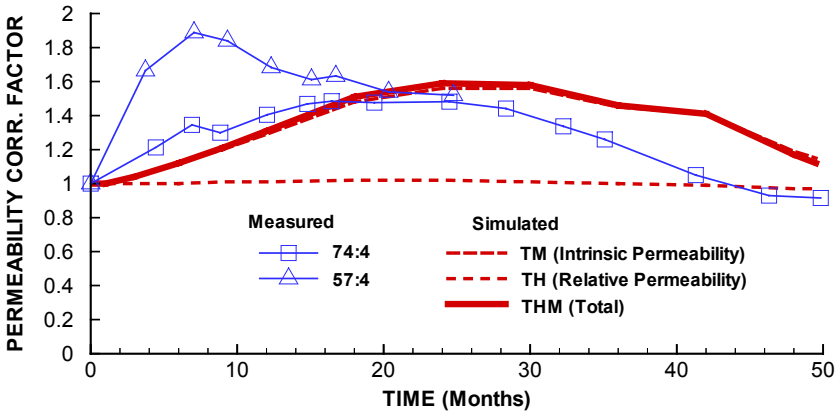

(c) Group located at z ≈18 m

DTN (measured): LB0208AIRKDSTH.001 [160897]
Output – DTN (simulated): LB0306DSTTHMVL.002

Figure 7.4.3-3. Measured and Simulated Evolution of Permeability Correction Factors ($F_k = k/k_i$) for Three Groups Located at Various Distances above the Heated Drift. b_{max} = 200 μm, α = 0.52 MPa^{-1}

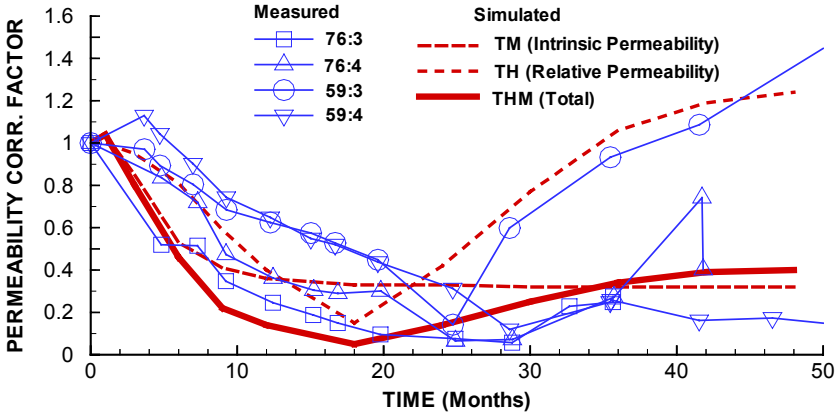

(a) Group located at z ≈ 6

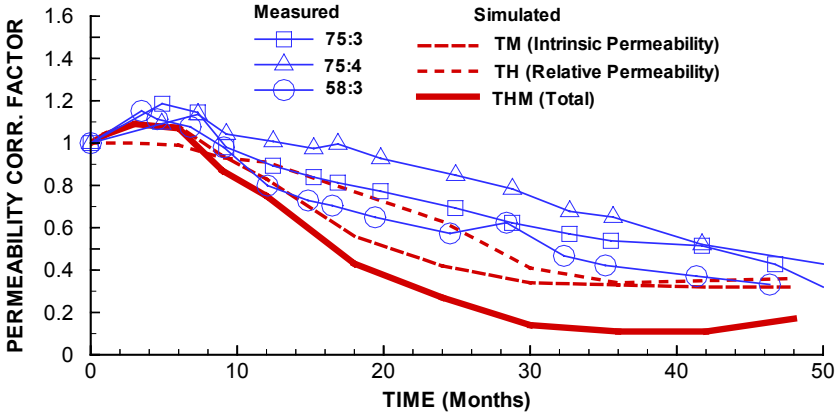

(b) Group located at z ≈12 m

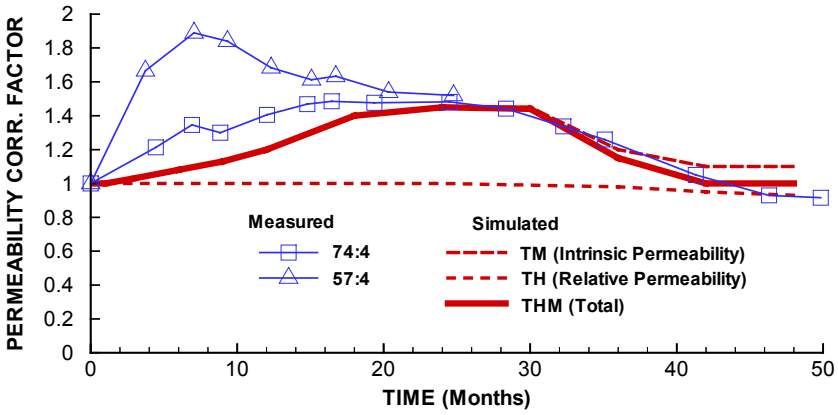

(c) Group located at z ≈ 18 m

DTN (measured): LB0208AIRKDSTH.001 [160897]
Output – DTN (simulated): LB0306DSTTHMVL.002

Figure 7.4.3-4. Measured and Simulated Evolution of Permeability Correction Factors ($F_k = k/k_i$) for Three Groups Located at Various Distances above the Heated Drift. b_{max} = 150 μm, α = 0.6 MPa^{-1}

7.5 VALIDATION AGAINST NICHE TESTS

An additional validation of the Drift-Scale THM Model is conducted against air-permeability measurements conducted at three excavated niches located in the Tptpmn unit and one excavated niche located in the Tptpll unit. These tests were conducted to study permeability changes near a drift wall caused by excavation effects (i.e., mechanical unloading of the rock mass near the drift wall, causing fracture opening and consequent permeability increase). In the Tptpmn unit, the air permeability was measured before and after excavation in 0.3 m packer-isolated sections along three boreholes located about 0.65 m above the niches (BSC 2001 [158463], Section 6.1). The boreholes located at about 0.65 m above the drift are denoted UM (Upper Middle), UL (Upper Left) and UR (Upper Right). All these boreholes are located at the same elevation (about 0.65 m above the drift), with UM located above the centerline of the drift and UR and UL located about 1 meter to the right and left of the centerline, respectively. Section 6.4 of this Model Report, one data point of the permeability-change ratio was extracted from this data set to determine the parameters b_{max} and α. The validation performed in this section aims to investigate the validity of the stress-permeability model and the stress-aperture function over a range of initial permeability values. The calculated changes in permeability presented in this section were derived using an MS Excel spreadsheet as described in Attachment III.

In this study, the niche excavations were modeled using the FLAC3D V2.0 (LBNL 2001 [154783])code to calculate changes in the stress field. A model of the niches is described in Rutqvist (2002 [162047], p. 14). Based on the calculated stress field, new fracture apertures for each fracture set can be calculated from Equation (6.2-9). The new apertures are then inserted into Equation (6.2-5) to calculate the excavation permeability correction factors F_{kxe}, F_{kye}, F_{kze} in the x, y, and z direction. Finally, the geometric mean of the excavation permeability correction factors is calculated from Equation (6.4-3). This calculation is repeated for different initial permeability values to cover a range k = 1e-15 m^2 to k = 1e-9 m^2 (see Attachment III for details). Figure 7.5-1 compares calculated and measured pre- to post-excavation ratios for the four niches. The calculated values are within the scatter of the measurements, and the calculation appears to represent an ”average” HM behavior at the niches. Furthermore, the calculation correctly captures the observed trend that in general, permeability generally changes more in initially lower-permeability sections. A scatter of the measured data in Figure 7.5-1 of orders of magnitude is not surprising, considering that a very short packer spacing of 0.3 was used. The drift-scale hydraulic properties are derived from the mean values of such packer tests, and therefore the validation of the numerical model should be toward the mean permeability changes.

The variability in pre- to post-excavation ratios at a fixed initial permeability can be explained by mechanical responses in fractures belonging to different fracture sets (Figure 7.5-2a). The largest permeability increases can occur as a result of opening of fractures in Set 3, which is a horizontal fracture set. Such large permeability increases could occur for the extreme case of a borehole interval connected only to horizontal fractures. Another extreme is the case in which the borehole is connected to a fracture of Set 2, in which the fractures are vertical, striking along the drift. Theoretically, this could give a significant reduction in permeability. However, the network at the Tptpmn and Tptpll units are highly fractured, and therefore a strong reduction in permeability caused by fracture closure in one fracture set only is unlikely. Although fractures in Set 2 would be close to their residual value, it is likely that they are connected to vertical fractures that are kept open. Fracture Set 1 is oriented perpendicular to the borehole axis and is

therefore the most likely to intersect the borehole. Figure 7.5-2b illustrates the calculated permeability changes in different directions (x, y, and z). The figure shows that permeability increases in all directions, with most changes occurring in the horizontal permeability.

In summary, the good agreement between calculated mean value and trends in both the Tptpmn unit (Figure 7.5-1a–c) and Tptpll unit (Figure 7.5-1d) shows that the stress-permeability model of the Drift-Scale THM model is applicable for both Tptpmn and Tptpll units over their entire range of initial permeability values. The model is also able to explain the local variability of permeability-change factors as the impact of fracture orientation for fractures intersecting the borehole (Figure 7.5-2). For the air-permeability test conducted in the Tptpll unit, some extreme permeability changes occur (even at high initial permeability) that cannot be captured in the model. The presence of lithophysals may have impacted the measurements. In general, the measurements conducted at one-foot borehole length are difficult in the Tptpll unit, since it contains lithophysal cavities that can be larger than one foot in diameter.

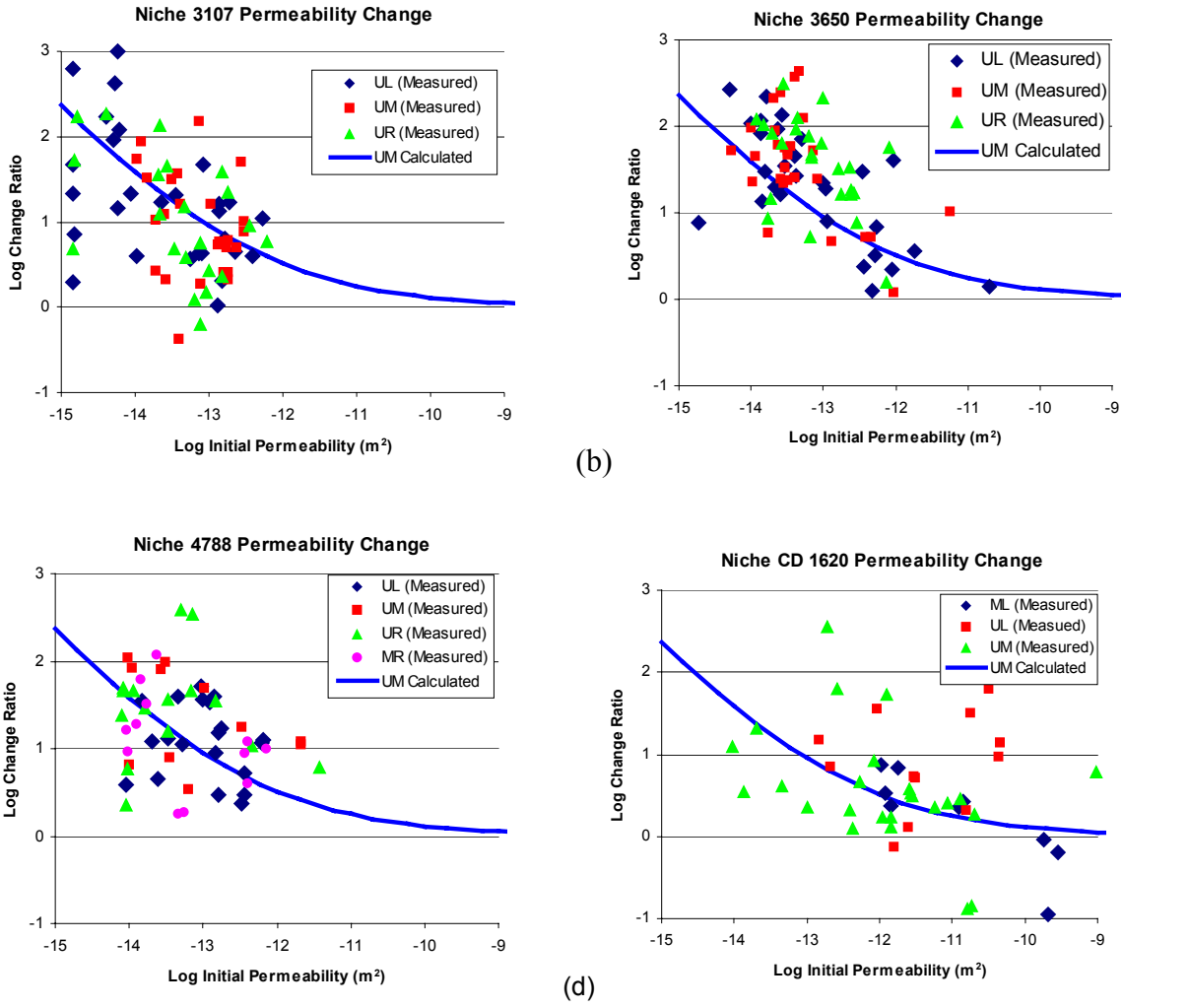

DTN (measured): LB0110AIRK0015.001 [162179]
Output – DTN (calculated): LB0306DSTTHMVL.002

NOTE: UM is located directly above the drift along the centerline of the drift, whereas UL and UR are located at the same elevation but about 1 meter to the left and right of the centerline respectively. Calculation is conducted with b_{max} = 200 μm and α = 0.52 MPa^{-1}, and calculated results represent the mean permeability change factor F_k defined in Equation (6.2-7). The calculation of the lines for UM calculated is described in Attachment III. In DTN: LB0110AIRK0015.001 [162179] the measured Log Change Ratio for Niche 3107, 3560, 4788, and 1620 is found in filename "Plots of pre and post holes N2 N3 N4 N5 N5AK-reformated N4 corrected reviewed.xls." In this file data for Niche 3107, 3560, 4788, and 1620 is found under sheets denoted N3, N2, N4 and N5, respectively.

Figure 7.5-1. Measured and Calculated Permeability Change Ratio at Niche 3107, 3560, and 4788 in the Tptpmn Unit and Niche 1620 in the Tptpll Unit

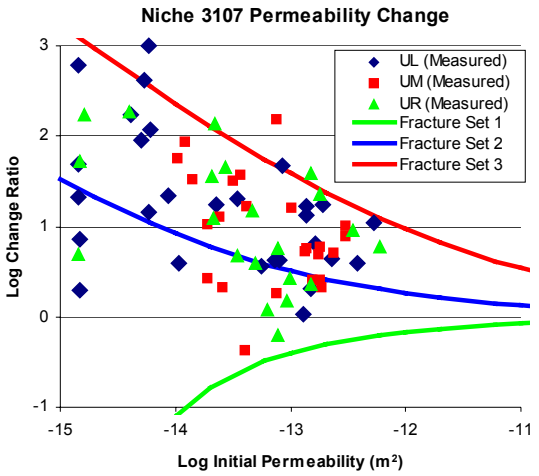

(a)

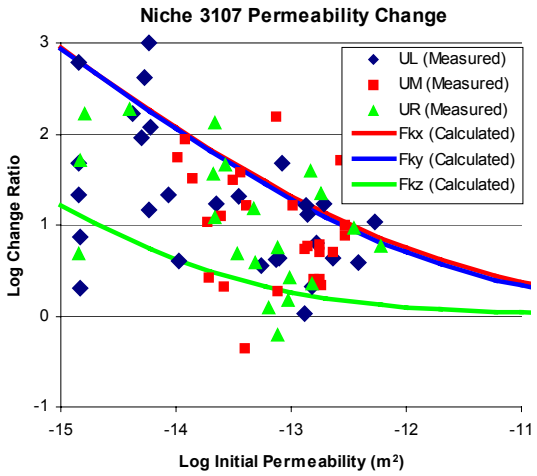

(b)

DTN: LB0110AIRK0015.001 [162179]
Output – DTN: (calculated) LB0306DSTTHMVL.002

NOTE: Calculation is conducted with b_{max} = 200 μm and α = 0.52 MPa^{-1}. The calculations resulting in the three lines (blue, red and green) in (a) and (b) are described in Attachment III.

Figure 7.5-2. Measured and Simulated Permeability-Change Ratio at Niche 3107: (a) Comparison to Simulated Permeability-Change Ratio in the Three Fracture Sets; (b) Comparison to Permeability Correction Factors in x, y, and z Direction

7.6 COMPARISON TO AN ALTERNATIVE CONCEPTUAL MODEL

An additional validation of the Drift-Scale THM Model is conducted by comparing this model to the results of a previous analysis of the DST by BSC (2001 [155957], Section 6.4.2). In BSC (2001 [155957], Section 6.4.2), the first 18 months of the DST was simulated by two separate three-dimensional analyses, one using a continuum-based model and one using a discrete-fracture model (see Section 1 for a brief description of the alternative discrete-fracture model). In both simulations, the thermal expansion coefficient was set to 9.73°C^{-1}. In Figure 7.6-1, the simulated results of BSC (2001 [155957], Section 6.4.2) are compared to a separate simulation using the Drift-Scale THM Model for displacement at Anchor 4 in borehole 148. In this analysis, the Drift-Scale THM Model was applied using an equivalent value of the thermal expansion coefficient (9.73°C^{-1}). It can be concluded that the three separate models analyzing DST—the two continuum-based (one Drift-Scale THM, one BSC) and one discrete-element model—all provided similar results in magnitude and trend, even taking into account differences in model discretization and temperature handling. The good agreement between Drift-Scale THM Model and the alternative discrete-fracture approach shown in Figure 7.6-1 is typical for comparisons made at several anchors around the DST. The good agreement between the independent numerical models provides great confidence for the validation of the TM part of the Drift-Scale THM Model. Moreover, the results in Figure 7.6-1 supports a continuum approach being sufficient to model the thermal expansion of the rock mass.

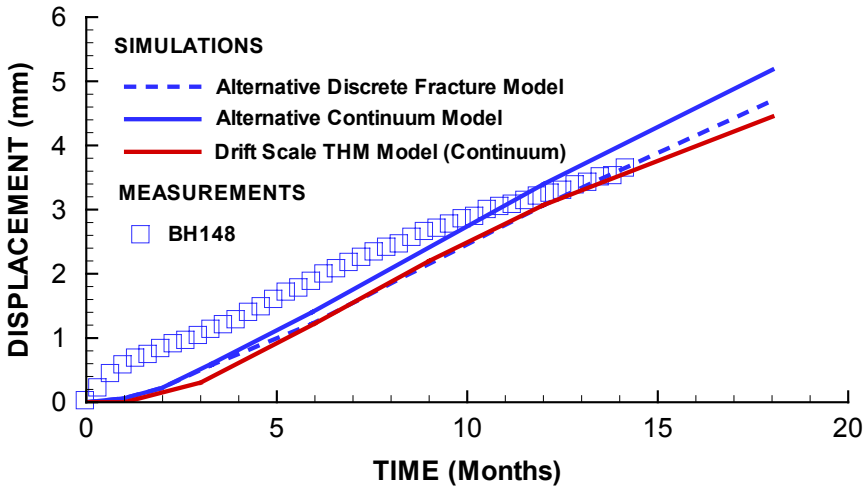

Output – DTN: LB0306DSTTHMVL.002

NOTE: The simulation results of alternative discrete fracture model and alternative continuum model have been extracted from BSC (2001 [155957], Figure 6.4.2-12, p. 121). Simulation results using the Drift-Scale THM Model are compared to the simulation results of BSC (2001 [155957]). The measured values were extracted from DTN: SN0207F3912298.037 [162046].

Figure 7.6-1. Simulated and Measured Evolution of Displacements at Anchor 4 in MPBX Borehole 148

7.7 MULTIPLE LINES OF EVIDENCE

The impact of THM processes (such as excavation and heating) on the performance of the potential repository at Yucca Mountain have been assessed through field studies at a variety of underground sites. These studies indicate that the effects of excavation on rock stability tend to be highly site-specific, depending on rock physical properties, the presence and orientation of faults and fractures, and the local stress regime. Excavation often leads to localized increases in permeability. Heating generally results in an increase in stress and a reduction in permeability due to thermal expansion. The results of THM experiments conducted at the Nevada Test Site and the Stripa underground laboratory in Sweden are summarized below.

7.7.1 Nevada Test Site Thermal-Hydrological-Mechanical Experiments

Four TM/THM experiments relating to high-level nuclear waste research were conducted at the G-tunnel in Rainier Mesa. These tests included a single borehole heater test, a small-diameter heater test, a heated block test, and a prototype engineered-barrier-system field test. One objective of the heated block test was to measure rock-mass mechanical and TM properties of ash-flow tuff under controlled thermal- and stress-loading conditions. The block was subjected to maximum temperatures ranging from 76° to 130°C and equal biaxial stresses with magnitudes up to 10.6 MPa (Zimmerman et al. 1986 [145625]). The effective modulus of deformation ranged from 0.4 to 0.83 times the intact rock measurements, depending on the number of joints included and their apertures. A slight dependence of modulus on stress was indicated, but no significant temperature effects on modulus were identified.

A second objective of the heated block test was to determine the effects of excavation, stress, and temperature changes on the permeability of a single joint. The permeability of a single near-vertical fracture was measured using three vertical boreholes in a linear array. The largest changes in permeability were associated with excavation of the block, when the apparent permeability increased from 76 to 758 microdarcies. Subsequent compressive loading decreased the permeability but did not completely reverse the unloading conditions, and the apparent permeability ranged from 252 to 332 microdarcies over a stress range of 3.1 to 10.6 MPa (Hardin and Chesnut 1997 [100534], pp. 4–6). Increased temperature under biaxial confinement decreased the fracture aperture, lowering the apparent permeability from 234 to 89 microdarcies during heating caused by rock thermal expansion. These observations are consistent (i.e., of the same order of magnitude) with the Yucca Mountain THM modeling and field studies described earlier. That is, fracture permeability increases about one order of magnitude as a result of unloading during excavation and decreases by less than one order of magnitude during heating.

7.7.2 Underground Testing at Stripa

A time-scaled heater test was performed at Stripa to investigate the long-term TM response to thermal loading (Chan et al. 1980 [154672]). Analysis showed that, in the full-scale and time-scale heater tests, heat flow conformed to linear conduction theory and was not affected by fractures or other discontinuities. Thermoelastic deformation of the rock mass was nonlinear and less than expected. Early in the tests, measured displacements were much less than predicted by linear thermoelasticity. Later, the displacements increased uniformly, but in fixed proportions to predicted levels. This was likely a result of the closing of fractures in response to thermal expansion. Fracture closure was confirmed by observation of diminished water inflow to the heater and instrument boreholes (Nelson et al. 1981 [150092], p. xi) and by increased compressional wave velocity during heating (Paulsson et al. 1980 [154570], p. 4). The closing of fractures (and resulting changes in fracture permeability due to thermal input) is consistent with the results of the Yucca Mountain studies described in this report.

7.7.3 DECOVALEX Findings at Fanay-Augeré and Kamaishi Mine Heater Tests

The results in this Model Report can also be compared to findings in the international cooperative project DECOVALEX (DEvelopment of COupled Models and their VALidation against EXperiments in nuclear waste isolation). Model validation against *in situ* tests such as Fanay-Augeré (Rejeb 1996 [162589]) and Kamaishi Mine (Rutqvist et al. 2001 [162586]) demonstrates that the temperature field can be predicted with confidence because it is mainly governed by heat conduction through rock masses, with little influence from discrete fractures. Rock-mass deformation measured along extensometers between anchors placed several meters apart can also be predicted reasonably well in trends and magnitudes. This is because the bulk thermal expansion of the rock is dominated by the thermal expansion of the matrix rock, while fractures have a secondary effect that appears as a reduction of the rock-mass thermal expansion coefficient. It can also be concluded from these two heater tests that the general thermal expansion of the rock mass is essentially elastic for measurements conducted over several meters of fractured rock. However, although the bulk thermal expansion of the rock mass is essentially elastic and reversible, the displacement and aperture changes measured over individual fractures are generally irreversible. That is, there is a remaining change in fracture aperture after the rock mass has cooled down to ambient conditions. Furthermore, it is generally much more difficult to

predict the responses of individual fractures than to predict the overall rock-mass thermal expansion. This might be important for predicting changes in hydraulic permeability, which critically depend on the aperture changes of fractures.

7.7.4 Geothermal Reservoir Temperature-Permeability Correlation

In addition to field studies of coupled THM processes that provide direct evidence of how a potential repository at Yucca Mountain would perform, corroborative results for coupled THM effects may be found in the geothermal literature. A survey of geothermal reservoir properties worldwide (Björnsson and Bodvarsson 1990 [154606], pp. 19–21) showed a correlation between permeability and temperature for various geothermal systems (Figure 7.7.4-1). The values are scattered, but they indicate a trend toward decreasing permeability with increasing temperatures. The low permeability at temperatures around 300°C and above is more likely caused by geochemical effects. THM effects may be present at lower temperatures.

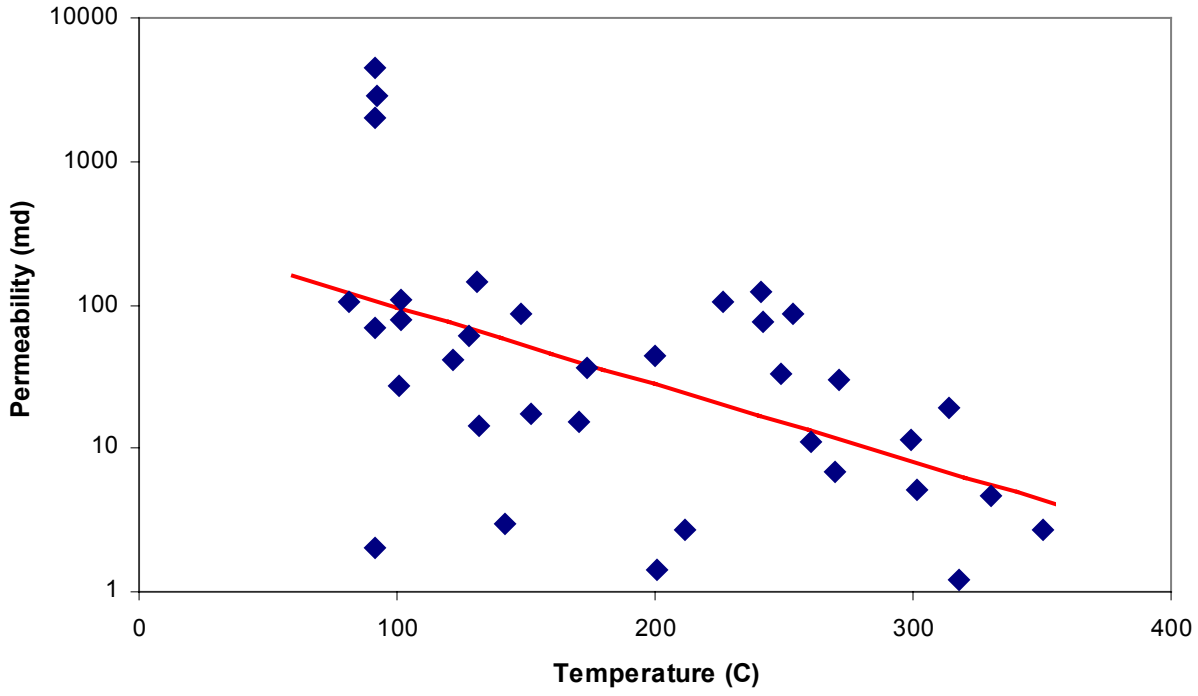

NOTE: Based on Figure 1 of Björnsson and Bodvarsson 1990 [154606].

Figure 7.7.4-1. Correlation between Permeability and Temperature for Geothermal Reservoirs Worldwide

7.7.5 Coupled THM Analyses of the Yucca Mountain Drift Scale Test within DECOVALEX III

The TM and THM responses of the Yucca Mountain Drift Scale Test are independently analyzed by the participants of the DECOVALEX III project, which is an international research project "to develop coupled models and their validation against experiments." The outcome of the analyses by the DECOVALEX participants, generally corroborative of the contents of this model report, are to be presented in the GeoProc2003 conference to be held in Stockholm, Sweden, in October 2003 and will be published in a special issue of the *International Journal of Rock Mechanics*.

7.8 PUBLICATION IN PEER-REVIEWED JOURNALS

The TOUGH2-FLAC3D simulator was presented in the International Journal of Rock Mechanics & Mining Sciences in 2002 (Rutqvist et al. 2002 [162048]). This paper includes the fundamental theories and underlying conceptual models for the TOUGH2 code, the FLAC3D code, and the coupling functions between the two codes. An application of the simulator for a drift-scale THM analysis of the repository at Yucca Mountain has been reviewed and accepted for publication in an upcoming issue of *Journal of Contaminant Hydrology* (Rutqvist and Tsang 2003 [162584]). This published analysis is similar to the one conducted in this model report, but does not include the recent extensive validation against the DST. The result and the general conclusions of the published analysis are consistent with the results presented in this Model Report. An application of the TOUGH2-FLAC3D code to problems related to HM processes in the geological sequestration of greenhouse gases has been published (Rutqvist and Tsang 2002 [162587]).

7.9 DISCUSSION OF VALIDATION ACTIVITIES

The comparison of the coupled THM model results against DST heating-phase data supports the contention that all relevant processes are well represented by the model. In general, calculated responses are within the range of measurements. Only a few minor aspects of the model validation could be improved. One of those is the calculated displacement during the first few months of heating, which disagrees slightly with measurement results. More precise matching of calculated and measured air-permeability changes might be possible. However, the present analysis of the DST heating phase shows that the Drift-Scale THM Model is valid for the analysis of coupled THM processes, and that the underlying conceptual model is sound.

Furthermore, the analysis shows that the conceptual model for HM coupling is valid. This validation indicates that fracture opening and closing caused by changes in normal stress is the dominant mode of permeability changes. Mechanical responses in the DST indicates that no significant shear slip occurs, except possibly in isolated instances such as the event in Anchor 1 of borehole 154 (discussed above). The measured change in air permeability at the DST does not show any widespread increase. Although a few increases in permeability have been observed, they appear to be isolated to one packed-off section, while no such increase can be noticed in neighboring sections. This observation provides further evidence that shear-induced permeability enhancement is not significant, and that fracture opening or closure by changes in normal stress is the dominant mode of permeability changes.

The air-permeability measurement during the natural cooling phase of the DST will be extremely helpful for confirming the stress-aperture function and for observing potential irreversible (permanent) permeability changes. For an elastic rock mass, mechanical deformations and permeability changes would be fully reversible, meaning that after the temperature declined to ambient, MPBX displacements and air permeability would go back to their original values (see Figure 7.9-1a). However, irreversible changes will almost certainly occur in permeability and displacement after the temperature has declined to ambient (Figure 7.9-1b). Although rock-mass behavior is essentially elastic, small irreversible inelastic changes are still expected. The question is, how large will these irreversible changes be? Trends in displacement and permeability changes at the DST so far indicate that the irreversible changes in permeability will be small, most certainly not larger than one order of magnitude.

The findings here in Section 7 of this Model Report are generally supported by studies of similar heater tests such as Stripa Mine, Fanay-Augéres, and Kamaishi Mine (Section 7.7). In particular, the temperature field and the bulk thermal expansion of the rock can be predicted with confidence using a simple thermoelastic model. Analyses of Fanay-Augéres and Kamaishi Mine experiments indicate that predicting the magnitude displacements at individual points of the rock mass and over individual fractures can be difficult (Section 7.7). However, the rock-mass characteristics at Yucca Mountain differ from those at these other heater tests: The rock mass of the repository units at Yucca Mountain is heavily fractured volcanic tuff, while the above-mentioned experiments have been conducted in sparsely fractured granitic rock. In relation to other fractured rock sites, the rock mass at Yucca Mountain is relatively homogenous (ubiquitously fractured), with much less spatial variability in rock-mass mechanical and hydrological properties. This is especially evident for hydraulic permeability, which at sparsely fracture sites generally ranges over six orders of magnitude, whereas the permeability at each rock unit at Yucca Mountain generally spans less than three orders of magnitude. The conceptual model in Figure 6.2-2, combined with a continuum model approach, is shown to be appropriate for the analysis of THM processes, because the rock mass at Yucca Mountain is ubiquitously fractured, forming a dense, well-connected fracture network for fluid flow. This is the main reason why the Drift-Scale THM Model consistently captures all relevant THM responses at Yucca Mountain.

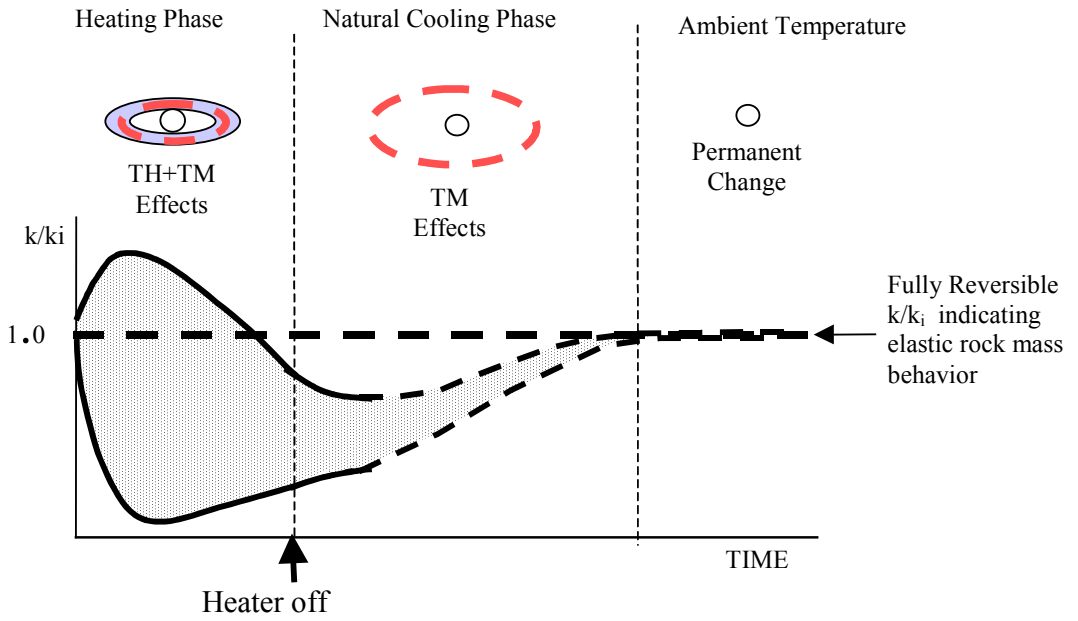

(a) Fully reversible elastic rock mass behavior

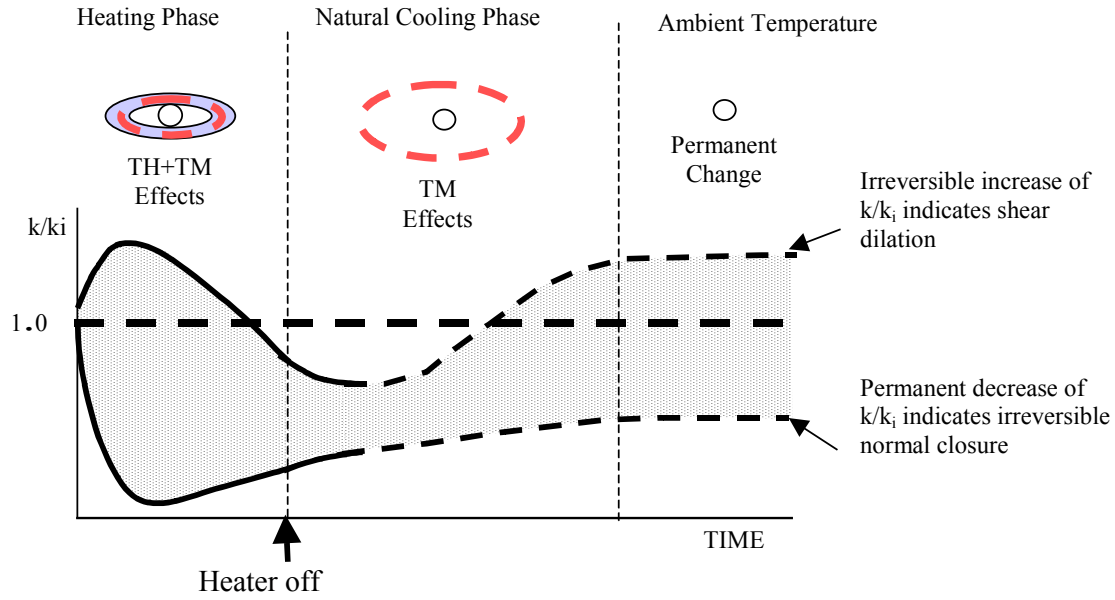

(b) Irreversible inelastic rock mass behavior

NOTE: These are not simulation results, nor an exact representation of the field data.

Figure 7.9-1. Concepts of Possible Evolution of Air Permeability at the Drift Scale Test Showing the Expected Responses for the Case of (a) Elastic Fully Reversible Rock-Mass Behavior and (b) Inelastic Irreversible Rock-Mass Behavior

7.10 EXTENSION TO MOUNTAIN-SCALE THM PROCESSES

The prediction of mountain-scale THM processes will be documented in the upcoming revision of the *Mountain-Scale Coupled Processes* Model Report (CRWMS M&O 2000 [144454]). The validation for THM processes on the drift scale presented in this Model Report can be extended to that of the mountain scale by considering scale dependency of mechanical and hydraulic properties. Mechanical and thermal properties are not expected to be significantly different at the mountain scale than at the drift scale. Indeed, the mechanical displacements along MPBX boreholes in Figure 7.4.2-3 of this Model Report is well captured from the one-meter scale (Anchor 1) to the 15-meter scale (Anchor 4). This lack of scale dependency in TM properties from 1 to 15 meters, not to mention the general lack of scale dependency, suggests that the drift-scale TM and mechanical properties are valid at mountain scale. A lack of scale dependency in thermal and mechanical properties from meter scale and up can be attributed to a relatively dense fracturing resulting in a relatively homogeneous rock mass. Hydraulic properties, on the other hand, have been shown to be dependent on the measurement scale (BSC 2003 [161773], Section 6.1.1.1). At Yucca Mountain, mountain-scale calibrated fracture permeability is generally one to two orders of magnitude larger than drift-scale calibrated fracture permeability (BSC 2003 [160240], Sections 6.3.2 and 6.3.3). However, the result in Figure 7.5-1 indicates that the conceptual model for stress-induced permeability changes are valid over a wide range of initial permeability values. The larger permeability at the mountain scale, and the observed reduction in permeability-change ratio with permeability (shown in Figure 7.5-1), suggests that permeability changes will be smaller at the mountain scale than at the drift scale. This is in agreement with observations from other fractured rock sites, which indicate that permeable, highly conductive fracture zones are generally less sensitive to stress then zones of more competent rock (Rutqvist and Stephansson 2003 [162583]).

The issue of upscaling THM properties and their impact on the performance assessment of nuclear waste repositories is also part of an ongoing effort in the international cooperative project DECOVALEX. In the DECOVALEX project, the TOUGH2-FLAC3D simulator is applied in a benchmark test to the upscaling of THM properties at Sellafield, UK. The rock at Sellafield consists largely of welded tuff, a similar type of rock to the repository units at Yucca Mountain. The TOUGH2-FLAC3D code are being applied in the DECOVALEX project using the same conceptual model for HM coupling as applied in this Model Report. Moreover, a methodology for upscaling of HM properties is being developed by the LBNL research team. The status of the work is reported in a progress report titled *Understanding the Impact of Upscaling THM Processes on Performance Assessment (DECOVALEX III BMT2*) by Liu et al. 2003 (Boyle 2001 [163533]). The outcome of the analyses by all the DECOVALEX participants is to be presented in the GeoProc2003 conference to be held in Stockholm, Sweden, October 2003, and will be published in a special issue of the *International Journal of Rock Mechanics*.

INTENTIONALLY LEFT BLANK

8. CONCLUSIONS

8.1 SUMMARY AND CONCLUSIONS

This Model Report documents the results obtained from numerical simulation of the coupled thermal-hydrological-mechanical (THM) processes in the vicinity of a waste emplacement drift at the proposed nuclear waste repository at Yucca Mountain. One of the main objectives for the drift-scale coupled simulations (TH, THC, and THM) is to investigate the impact of coupled processes on the potential for water entering a repository drift (seepage). Coupled THM processes can impact the potential for seepage in several ways, because the heat generated by the decay of radioactive waste results in rock temperature elevated from ambient for thousands of years after emplacement. Heating of rock water to above-boiling conditions causes strong vapor movement along the thermal gradient, with the effect of creating a dryout zone around the emplacement drift. This dryout zone is an effective barrier, preventing moisture from entering the repository drift for thousands of years. At the same time, heating of the rock will cause thermal expansion of the rock, which in turn will change the stress field around the emplacement drift. Thermally induced changes in the stress field will act upon pre-existing fractures, which generally tend to tighten to smaller apertures, with the result of changing the hydrological properties of the rock mass. The aim of this Model Report is to assess the magnitude of stress-induced changes in hydrological properties and the impact such changes might have on the flow field around the vicinity of a repository drift.

The Drift-Scale THM Model developed in this Model Report is capable of assessing the magnitude and distribution of changes in hydrological properties and of analyzing the impact of such changes on the percolation flux in the rock mass around a repository drift. The model was applied to analyze the impact of coupled THM processes in the case of a repository located either in the Tptpmn unit (Tptpmn model domain) or in the Tptpll unit (Tptpll model domain). Results from the Drift-Scale THM Model are presented in Sections 6.5 (Tptpmn model domain) and 6.6 (Tptpll model domain), and have been submitted to the Technical Data Management System (TDMS) as output under DTNs listed in Section 9.4. A brief summary and discussion of the results are given in Section 6.7. The following main conclusions are drawn from Section 6 of this Model Report:

- The maximum THM effects will occur around 100 to 1,000 years after emplacement of the waste, when the temperature in the rock mass at the repository level reaches its maximum. The primary THM effects are thermally-induced and excavation-induced changes in the stress field that will act on pre-existing fractures, thereby causing fracture closure or opening with accompanying changes in fracture permeability and capillary pressure. These effects will last well over 10,000 years, because the temperature over that time is still significantly over ambient.

- Thermal stresses in the horizontal direction will increase significantly, whereas the vertical stresses will remain almost unchanged through the thermal period. The analysis indicates that horizontal stresses will increase by more than 10 MPa at the repository level (Figure 6.5.3-1). As a result, the vertical intrinsic permeability will decrease in a zone extending several hundred meters above and below the repository (Figures 6.5.4-

1). Using a conservative (more sensitive) stress-permeability relationship, the vertical permeability in the Tptpmn unit will decrease at most to a factor of 0.03 of its original permeability. In the Tptpll unit, vertical permeability is estimated to decrease to a factor of 0.6 of its original value.

- The maximum principal compressive stress will occur at the drift crown at around 100 to 500 years after the emplacement and is expected to be about 31 MPa (Figure 6.5.3-4). An analysis of the observed rock scaling at the crown of the DST shows that a maximum principal stress of about 60 MPa would be required to initiate limited rock scaling. Thus, the Drift-Scale THM Model shows that thermal stress is not likely to induce failure at a repository located in the Tptpmn unit.

- The analysis indicates that the impact of stress-induced changes in hydrological properties on the flow field is small to moderate, with the strongest impact occurring for a repository located in the Tptpmn model domain. While the liquid vertical flux distribution in the fracture continuum is slightly affected, the main impact appears to be on the dryout zone near the repository drift. When stress-induced changes in hydrological properties are considered, the extent of the dryout zone is slightly smaller, and consequently the liquid water will reach the drift wall in a shorter time (Figure 6.5.5-4). In the longer term, at around 10,000 years, vertical permeability is still significantly decreased, especially just above the repository drift. The impact of this reduction in permeability is small, but tends to prevent vertical flux from reaching the drift wall at the drift crown (Figure 6.5.5-5).

- The impact of stress-induced changes in hydraulic properties on the flow field around a repository in the Tptpll unit is similar to those for a repository in the Tptpmn unit, but the magnitude of impact is much smaller. The reason for a smaller impact in the Tptpll unit is that both the initial stresses and initial fracture permeability are higher in the Tptpll unit than in the Tptpmn unit. Higher initial stresses imply that fractures are initially already compressed to a higher stiffness and closer to their residual aperture value, which prevents further closure during the thermal period. Higher initial fracture permeability results in a larger residual fracture aperture, and therefore the possible relative reduction in permeability is smaller.

8.2 MODEL VALIDATION AND UNCERTAINTIES

The Drift-Scale THM Model, which is used to derive the above conclusions, is validated against the DST and niche excavation experiment, as described in Section 7 of this Model Report. The analysis of the DST heating phase shows that the Drift-Scale THM Model can capture all relevant THM processes and that the underlying conceptual model is sound. In particular, analysis of the DST shows that the conceptual model for stress-versus-permeability coupling is valid and capable of capturing the observed changes in permeability. Based on the simulations and observations at the DST and niches, the following conclusion can be drawn regarding fundamental rock-mass THM behavior:

- The dominant mode of stress-induced permeability changes is elastic fracture opening or closing caused by changes in stress normal to the fractures. This conclusion is supported

by the good agreement between measured and simulated air-permeability changes in the DST (Section 7.4.3) and the ability of the model to capture mean permeability changes at niche experiments. Furthermore, no sign of extraordinary permeability enhancement by shear slip has been observed at the DST. Therefore, it is expected that THM-induced irreversible (permanent) changes in fracture permeability will be less than one order of magnitude. Further analysis of the shear slip at the DST and in particular for the natural cooling phase of the DST can help to confirm this conclusion.

The fracture normal stress versus permeability relationship is the most important aspect of this analysis. The relationship (discussed in Section 6.8.4) is the key for an accurate assessment of the possible stress-induced changes in hydraulic properties at the repository. The relationship provides limits for how much permeability can decrease or increase from the impact of stresses. Other aspects, or sources of uncertainties, such as conceptualization of the fracture network (Section 6.8.1) or possible inelastic mechanical responses near the drift wall (Section 6.8.2) and even possible shear slip (Section 6.8.3), are of minor importance compared to the limits of the stress-versus-permeability relationship. If these limits are correctly determined, then an accurate prediction of the main coupled THM processes is expected. If, on the other hand, the upper and lower limits for permeability changes are incorrect, then predicted changes in permeability would be incorrect. In this study, the upper and lower limits of the normal stress-versus-permeability function were determined and validated against field experiments at a relevant drift scale. The stress-permeability function adopted for the predictive analysis with the Drift-Scale THM Model is a conservative one in the sense that it tends to result in larger permeability changes, and hence, a larger impact on the percolation flux.

Because of the limited number of field experiments in the Tptpll unit, there are larger uncertainties regarding predicted THM behavior in this unit. Furthermore, as discussed in Section 6.8.6, recent slot tests indicate that deformability and strength in the Tptpll unit is lower than the previous estimates that were used in this Model Report. A low rock strength in the Tptpll units could lead to more extensive inelastic behavior near the drift wall, which could ultimately result in rock fall and drift collapse and essentially change the shape of the drift (BSC 2003 [164285]). On the other hand, a lower rock-mass deformability applied to the Drift-Scale THM Model would result in a smaller thermal stress in the Tptpll unit. Furthermore, the lower strength properties could lead to inelastic behavior near the drift wall, which would tend to relieve stresses near the drift wall. A smaller thermal stress and a relieved stress caused by inelastic behavior near the emplacement drift would lead to an overall smaller thermal impact on permeability, as discussed in Section 6.8.6. Thus, for the rock mass outside a potentially collapsed drift in the Tptpll unit, the impact of THM effects on permeability is likely to be smaller than for the results presented in this Model Report. Thus, stress-induced permeability changes are likely to be bounded within one order of magnitude for both the Tptpmn and Tptpll units. Because these bounds were obtained for a conservative estimate of input THM properties (thermal expansion coefficient and stress versus permeability function), the possible impact of the THM processes on percolation flux is adequately bounded in concurrence with YMPR acceptance criteria as discussed in Section 4.2.

8.3 OUTPUT DTNS

All the simulation cases presented in this model report have, without exception, been submitted to the Technical Data Management System (TDMS). For all simulation cases, all computer files needed to reproduce the model results using the qualified software have been submitted. The input and output files for each simulation case and the developed data are presented in separate DTNs as presented below:

Drift-Scale THM Model Predictions: Simulations: LB0306DRSCLTHM.001

Summary plots: LB0306DRSCLTHM.002

DST and Niche THM Model Validation: Simulations: LB0306DSTTHMVL.001

Summary plots: LB0306DSTTHMVL.002

Reproducibility by a qualified individual is possible by consulting the Model Report and the pertinent Scientific Notebook pages listed in Table 6-1.

9. INPUTS AND REFERENCES

The following is a list of the references cited in this document. Column 1 represents the unique six-digit numerical identifier (the Document Input Reference System [DIRS] number), which is placed in the text following the reference callout (e.g., BSC 2002 [160819]). The purpose of these numbers is to assist the reader in locating a specific reference. Within the reference list, multiple sources by the same author (e.g., BSC 2002) are sorted alphabetically by title.

9.1 DOCUMENTS CITED

100597 Birkholzer, J.T. and Tsang, Y.W. 1997. *Pretest Analysis of the Thermal-Hydrological Conditions of the ESF Drift Scale Test*. Milestone SP9322M4. Berkeley, California: Lawrence Berkeley National Laboratory. ACC: MOL.19971201.0810.

154606 Bjornsson, G. and Bodvarsson, G. 1990. "A Survey of Geothermal Reservoir Properties." *Geothermics, 19*, (1), 17-27. [New York, New York]: Pergamon Press. TIC: 249741.

163533 Boyle, W. 2001. "New BMT Revision." E-mail from W. Boyle to R. Datta, December 7, 2000, with attachment. ACC: MOL.20010125.0434.

100653 Brodsky, N.S.; Riggins, M.; Connolly, J.; and Ricci, P. 1997. *Thermal Expansion, Thermal Conductivity, and Heat Capacity Measurements for Boreholes UE25 NRG-4, UE25 NRG-5, USW NRG-6, and USW NRG-7/7A*. SAND95-1955. Albuquerque, New Mexico: Sandia National Laboratories. ACC: MOL.19980311.0316.

155957 BSC (Bechtel SAIC Company) 2001. *Coupled Thermal-Hydrologic-Mechanical Effects on Permeability Analysis and Models Report*. ANL-NBS-HS-000037 REV 00. Las Vegas, Nevada: Bechtel SAIC Company. ACC: MOL.20010822.0092.

156304 BSC (Bechtel SAIC Company) 2001. *Drift Degradation Analysis*. ANL-EBS-MD-000027 REV 01 ICN 01. Las Vegas, Nevada: Bechtel SAIC Company. ACC: MOL.20011029.0311.

158463 BSC (Bechtel SAIC Company) 2001. *In Situ Field Testing of Processes*. ANL-NBS-HS-000005 REV 01. Las Vegas, Nevada: Bechtel SAIC Company. ACC: MOL.20020108.0351.

158204 BSC (Bechtel SAIC Company) 2001. *Multiscale Thermohydrologic Model*. ANL-EBS-MD-000049 REV 00 ICN 02. Las Vegas, Nevada: Bechtel SAIC Company. ACC: MOL.20020123.0279.

157330 BSC (Bechtel SAIC Company) 2001. *Thermal Tests Thermal-Hydrological Analyses/Model Repor*t. ANL-NBS-TH-000001 REV 00 ICN 02. Las Vegas, Nevada: Bechtel SAIC Company. ACC: MOL.20011116.0025.

158726 BSC (Bechtel SAIC Company) 2001. *UZ Flow Models and Submodels*. MDL-NBS-HS-000006 REV 00 ICN 01. Las Vegas, Nevada: Bechtel SAIC Company. ACC: MOL.20020417.0382.

158375 BSC (Bechtel SAIC Company) 2002. *Drift-Scale Coupled Processes (DST and THC Seepage) Models*. MDL-NBS-HS-000001 REV 01 ICN 02. Las Vegas, Nevada: Bechtel SAIC Company. ACC: MOL.20020312.0156.

159124 BSC (Bechtel SAIC Company) 2002. *Geologic Framework Model (GFM2000)*. MDL-NBS-GS-000002 REV 01. Las Vegas, Nevada: Bechtel SAIC Company. ACC: MOL.20020530.0078.

160798 BSC (Bechtel SAIC Company) 2002. *Repository Design Project, Repository/PA IED Emplacement Drift Configuration*. 800-IED-EBS0-00200-000-00A. Las Vegas, Nevada: Bechtel SAIC Company. ACC: MOL.20021031.0104.

159527 BSC (Bechtel SAIC Company) 2002. *Repository Design, Repository/PA IED Subsurface Facilities Plan Sht. 1 of 5, Sht. 2 of 5, Sht. 3 of 5, Sht. 4 of 5, and Sht. 5 of 5*. DWG-MGR-MD-000003 REV A. Las Vegas, Nevada: Bechtel SAIC Company. ACC: MOL.20020601.0194.

160819 BSC (Bechtel SAIC Company) 2002. *Technical Work Plan for: Performance Assessment Unsaturated Zone*. TWP-NBS-HS-000003 REV 02. Las Vegas, Nevada: Bechtel SAIC Company. ACC: MOL.20030102.0108.

160771 BSC (Bechtel SAIC Company) 2002. *Thermal Testing Measurements Report*. ANL-NBS-HS-000041 REV 00. Las Vegas, Nevada: Bechtel SAIC Company. ACC: MOL.20021004.0314.

160146 BSC (Bechtel SAIC Company) 2002. *Total System Performance Assessment-License Application Methods and Approach*. TDR-WIS-PA-000006 REV 00. Las Vegas, Nevada: Bechtel SAIC Company. ACC: MOL.20020923.0175.

161760 BSC (Bechtel SAIC Company) 2002. *Ventilation Model Report*. ANL-EBS-MD-000030 REV 02. Las Vegas, Nevada: Bechtel SAIC Company. ACC: MOL.20030102.0140.

160975 BSC (Bechtel SAIC Company) 2002. *Ventilation Model*. ANL-EBS-MD-000030 REV 01 ICN 01. Las Vegas, Nevada: Bechtel SAIC Company. ACC: MOL.20021106.0055.

162268 BSC (Bechtel SAIC Company) 2003. *Abstraction of Drift Seepage*. MDL-NBS-HS-000019 REV 00. Las Vegas, Nevada: Bechtel SAIC Company.

161773 BSC (Bechtel SAIC Company) 2003. *Analysis of Hydrologic Properties Data*. MDL-NBS-HS-000014 REV 00. Las Vegas, Nevada: Bechtel SAIC Company. ACC: DOC.20030404.0004.

160240 BSC (Bechtel SAIC Company) 2003. *Calibrated Properties Model*. MDL-NBS-HS-000003 REV 01. Las Vegas, Nevada: Bechtel SAIC Company. ACC: DOC.20030219.0001.

160109 BSC (Bechtel SAIC Company) 2003. *Development of Numerical Grids for UZ Flow and Transport Modeling*. ANL-NBS-HS-000015 REV 01. Las Vegas, Nevada: Bechtel SAIC Company. ACC: DOC.20030404.0005.

164285 BSC (Bechtel SAIC Company) 2003. *Drift Degradation Analysis*. ANL-EBS-MD-000027 REV 02. Las Vegas, Nevada: Bechtel SAIC Company. ACC: DOC.20030709.0003.

161530 BSC (Bechtel SAIC Company) 2003. *Drift-Scale Coupled Processes (DST and TH Seepage) Models*. MDL-NBS-HS-000015 REV 00. Las Vegas, Nevada: Bechtel SAIC Company. URN-1087

163506 BSC (Bechtel SAIC Company) 2003. *Drift-Scale Coupled Processes (DST and THC Seepage)*. MDL-NBS-HS-000001 REV 02C. Las Vegas, Nevada: Bechtel SAIC Company. ACC: MOL.20030507.0274. TBV-5120

164136 BSC (Bechtel SAIC Company) 2003. *Repository Design Project, RDP/PA IED Typical Waste Package Components Assembly (4)*. 800-IED-WIS0-00204-000-00A. Las Vegas, Nevada: Bechtel SAIC Company. ACC: ENG.20030702.0004.

164069 BSC (Bechtel SAIC Company) 2003. *Repository Design Project, Repository/PA IED Emplacement Drift Configuration 1 of 2*. 800-IED-EBS0-00201-000-00A. Las Vegas, Nevada: Bechtel SAIC Company. ACC: ENG.20030630.0002.

163226 BSC (Bechtel SAIC Company) 2003. *Seepage Model For PA Including Drift Collapse*. MDL-NBS-HS-000002 REV 02. Las Vegas, Nevada: Bechtel SAIC Company. ACC: DOC.20030709.0001.

161770 Canori, G.F. and Leitner, M.M. 2003. *Project Requirements Document*. TER-MGR-MD-000001 REV 01. Las Vegas, Nevada: Bechtel SAIC Company. ACC: DOC.20030404.0003.

154672 Chan, T.; Binnall, E.; Nelson, P.; Stolzman, R.; Wan, O.; Weaver, C.; Ang, K.; Braley, J.; and McEvoy, M. 1980. T*hermal and Thermomechanical Data from In Situ Heater Experiments at Stripa, Sweden*. LBL-11477. Berkeley, California: Lawrence Berkeley Laboratory. TIC: 211543.

101539 CRWMS M&O (Civilian Radioactive Waste Management System Management and Operating Contractor) 1997. *Ambient Characterization of the Drift Scale Test Block*. BADD00000-01717-5705-00001 REV 01. Las Vegas, Nevada: CRWMS M&O. ACC: MOL.19980416.0689.

146917 CRWMS M&O 1997. *Drift Scale Test Design and Forecast Results*. BAB000000-01717-4600-00007 REV 01. Las Vegas, Nevada: CRWMS M&O. ACC: MOL.19980710.0155.

103564 CRWMS M&O 1997. *Yucca Mountain Site Geotechnical Report*. B00000000-01717-5705-00043 REV 01. Two volumes. Las Vegas, Nevada: CRWMS M&O. ACC: MOL.19971017.0736; MOL.19971017.0737.

111115 CRWMS M&O 1998. *Drift Scale Test As-Built Report*. BAB000000-01717-5700-00003 REV 01. Las Vegas, Nevada: CRWMS M&O. ACC: MOL.19990107.0223.

102679 CRWMS M&O 1998. Ge*ology of the Exploratory Studies Facility Topopah Spring Loop*. BAB000000-01717-0200-00002 REV 01. Las Vegas, Nevada: CRWMS M&O. ACC: MOL.19980415.0283.

129261 CRWMS M&O 1999. *Single Heater Test Final Report*. BAB000000-01717-5700-00005 REV 00 ICN 1. Las Vegas, Nevada: CRWMS M&O. ACC: MOL.20000103.0634.

123916 CRWMS M&O 2000. *Abstraction of Drift-Scale Coupled Processes*. ANL-NBS-HS-000029 REV 00. Las Vegas, Nevada: CRWMS M&O. ACC: MOL.20000525.0371.

149040 CRWMS M&O 2000. *Calculation of Permeability Change Due to Coupled Thermal-Hydrological-Mechanical Effects*. CAL-NBS-MD-000002 REV 00. Las Vegas, Nevada: CRWMS M&O. ACC: MOL.20000711.0192.

138860 CRWMS M&O 2000. *Geologic Framework Model (GFM3.1)*. MDL-NBS-GS-000002 REV 00 ICN 01. Las Vegas, Nevada: CRWMS M&O. ACC: MOL.20000121.0115.

144454 CRWMS M&O 2000. *Mountain-Scale Coupled Processes (TH) Models*. MDL-NBS-HS-000007 REV 00. Las Vegas, Nevada: CRWMS M&O. ACC: MOL.19990721.0528.

153314 CRWMS M&O 2000. *Seepage Model for PA Including Drift Collapse*. MDL-NBS-HS-000002 REV 01. Las Vegas, Nevada: CRWMS M&O. ACC: MOL.20010221.0147.

154291 CRWMS M&O 2001. *Abstraction of Drift Seepage*. ANL-NBS-MD-000005 REV 01. Las Vegas, Nevada: CRWMS M&O. ACC: MOL.20010309.0019.

100439 de Marsily, G. 1986. *Quantitative Hydrogeology: Groundwater Hydrology for Engineers*. San Diego, California: Academic Press. TIC: 208450.

154365 Freeze, G.A.; Brodsky, N.S.; and Swift, P.N. 2001. *The Development of Information Catalogued in REV00 of the YMP FEP Database*. TDR-WIS-MD-000003 REV 00 ICN 01. Las Vegas, Nevada: Bechtel SAIC Company. ACC: MOL.20010301.0237.

100534 Hardin, E.L. and Chesnut, D.A. 1997. *Synthesis Report on Thermally Driven Coupled Processes*. Milestone SPL8BM4. Livermore, California: Lawrence Livermore National Laboratory. ACC: MOL.19980113.0395.

148865 Itasca Consulting Group 1998. *3DEC, 3 Dimensional Distinct Element Code, User's Guide (Version 2.00)*. Minneapolis, Minnesota: Itasca Consulting Group. TIC: 247503.

156788 Itasca Consulting Group. 1997. *FLAC {superscript 3D}, Fast Lagrangian Analysis of Continua in 3 Dimensions*. Version 2.0 Five volumes. Minneapolis, Minnesota: Itasca Consulting Group. TIC: 251273.

102010 Jury, W.A.; Gardner, W.R.; and Gardner, W.H. 1991. *Soil Physics*. 5th Edition. New York, New York: John Wiley & Sons. TIC: 241000.

100588 Leverett, M.C. 1941. "Capillary Behavior in Porous Solids." *AIME Transactions, Petroleum Development and Technology, Tulsa Meeting, October 1940. 142*, 152-169. New York, New York: American Institute of Mining and Metallurgical Engineers. TIC: 240680.

150092 Nelson, P.H.; Rachiele, R.; Remer, J.S.; and Carlsson, H. 1981. *Water Inflow into Boreholes During the Stripa Heater Experiments*. LBL-12574. Berkeley, California: Lawrence Berkeley Laboratory. TIC: 228851.

163274 NRC (U.S. Nuclear Regulatory Commission) 2003. *Yucca Mountain Review Plan, Final Report*. NUREG-1804, Draft Final Revision 2. Washington, D.C.: U.S. Nuclear Regulatory Commission, Office of Nuclear Material Safety and Safeguards. TIC: 254002.

154570 Paulsson, B.N.P.; King, M.S.; and Rachiele, R. 1980. *Ultrasonic and Acoustic Emission Results from the Stripa Heater Experiment*s. Parts 1 & 2. LBL-10975. Berkeley, California: Lawrence Berkeley National Laboratory. TIC: 211547.

160778 Pruess, K.; Oldenburg, C.; and Moridis, G. 1999. T*OUGH2 User's Guide, Version 2.0*. LBNL-43134. Berkeley, California: Lawrence Berkeley National Laboratory. TIC: 253038.

162589 Rejeb, A. 1996. "Mathematical Simulations of Coupled THM Processes of Fanay-Augères Field Test by Distinct Element and Discrete Finite Element Methods." *Developments in Geotechnical Engineering, 79*, 341-368. [New York, New York]: Elsevier. TIC: 254247.

162047 Rutqvist, J. 2002. UZ AMRs for SR - Thermal-Hydrological-Mechanical Effects. Scientific Notebook SN-LBNL-SCI-204-V1. ACC: MOL.20010518.0086; MOL.20020701.0135; MOL.20020724.0607.

162583 Rutqvist, J. and Stephansson, O. 2003. "The Role of Hydromechanical Coupling in Fractured Rock Engineering." *Hydrogeology Journal, 11*, ([1]), 7-40. [New York, New York]: Springer-Verlag. TIC: 254245.

162587 Rutqvist, J. and Tsang, C-F. 2002. "A Study of Caprock Hydromechanical Changes Associated with CO{subscript 2}-Injection into a Brine Formation." *Environmental Geology, 4*2, ([2-3]), 296-305. [New York, New York]: Springer-Verlag. TIC: 254244.

162584 Rutqvist, J. and Tsang, C-F. 2003. "Analysis of Thermal-Hydrologic-Mechanical Behavior Near an Emplacement Drift at Yucca Mountain." *Journal of Contaminant Hydrology, 62-63*, 637-652. New York, New York: Elsevier. TIC: 254205.

162586 Rutqvist, J.; Börgesson, L.; Chijimatsu, M.; Nguyen, T.S.; Jing, L.; Noorishad, J.; and Tsang, C.-F. 2001. "Coupled Thermo-hydro-mechanical Analysis of a Heater Test in Fractured Rock and Bentonite at Kamaishi Mine — Comparison of Field Results to Predictions of Four Finite Element Codes." *International Journal of Rock Mechanics & Mining Sciences, 38*, ([1]), 129-142. [New York, New York]: Pergamon. TIC: 254246.

162048 Rutqvist, J.; Wu, Y.-S.; Tsang, C.-F.; and Bodvarsson, G. 2002. "A Modeling Approach for Analysis of Coupled Multiphase Fluid Flow, Heat Transfer, and Deformation in Fractured Porous Rock." *International Journal of Rock Mechanics and Mining Sciences, 39*, (4), 429-442. [New York, New York]: Pergamon. TIC: 253953.

163202 Sobolik, S.R.; Finley, R.E.; and Ballard, S. 1999. "Thermal-Mechanical Measurements in the Drift Scale Test, Yucca Mountain, Nevada." *Rock Mechanics for Industry, Proceedings of the 37th U.S. Rock Mechanics Symposium, Vail, Colorado, USA, 6-9 June, 1999*. Amadei, B.; Kranz, R.L.; Scott, G.A.; and Smeallie, P.H.; eds. *2*, 735-742. Brookfield, Vermont: A.A. Balkema. TIC: 245246.

162049 Sobolik, S.R.; Finley, R.E.; and Ballard, S. 1998. "Post-Test Comparison of Thermal-Mechanical Measurements vs. Analyses for the In-Situ Single Heater Test, Yucca Mountain, Nevada." *International Journal of Rock Mechanics and Mining Sciences, 35*, (4-5), 649. New York, New York: Pergamon. TIC: 253944.

137577 Tsang, Y.W. and Birkholzer, J.T. 1999. "Predictions and Observations of the Thermal-Hydrological Conditions in the Single Heater Test." *Journal of Contaminant Hydrology, 38*, (1-3), 385-425. New York, New York: Elsevier. TIC: 244160.

160355 USGS (U.S. Geological Survey) 2001. S*imulation of Net Infiltration for Modern and Potential Future Climates*. ANL-NBS-HS-000032 REV 00 ICN 02. Denver, Colorado: U.S. Geological Survey. ACC: MOL.20011119.0334.

163532 Wagner, R.A.; Ballard, S.; Blair, S.C.; and Mukhopadhyay, S. 2001. "A Methodology for Validation of Process Models Used to Simulate Thermal Tests at Yucca Mountain." *Rock Mechanics in the National Interest, Proceedings of the 38th U.S. Rock Mechanics Symposium, DC Rocks 2001, Washington, D.C., USA, 7-10 July 2001*. Elsworth, D.; Tinucci, J.P.; and Heasley, K.A., eds. *Volume 1*, 631-636. Exton, Pennsylvania: A.A. Balkema. TIC: 250864.

162654 Wang, J.S. 2003. "Scientific Notebook Referenced in Model Report U0250, Drift Scale THM Model MDL-NBS-HS-000017 REV 00." Correspondence from J.S. Wang (BSC) to File, April 28, 2003, with attachment. ACC: MOL.20030505.0160.

123506 Witherspoon, P.A.; Wang, J.S.Y; Iwai, K.; and Gale, J.E. 1980. "Validity of Cubic Law for Fluid Flow in a Deformable Rock Fracture." *Water Resources Research, 16*, (6), 1016-1024. [Washington, D.C.]: American Geophysical Union. TIC: 220088.

145625 Zimmerman, R.M.; Blanford, M.L.; Holland, J.F.; Schuch, R.L.; and Barrett, W.H. 1986. *Final Report, G-Tunnel Small-Diameter Heater Experiments*. SAND84-2621. Albuquerque, New Mexico: Sandia National Laboratories. ACC: HQS.19880517.2365.

Software Cited

147562 LBNL (Lawrence Berkeley National Laboratory) 1999. *Software Code: EXT*. V1.0. Sun SPARC, UNIX OS, DEC ALPHA, UNIX OS. 10047-1.0-00.

147553 LBNL (Lawrence Berkeley National Laboratory) 1999. *Software Routine: 2KGRIDV1.F*. V1.0. Sun SPARC, UNIX OS, DEC ALPHA, UNIX OS. 10244-1.0-00.

154783 LBNL (Lawrence Berkeley National Laboratory) 2001. *Software Code: FLAC3D*. V2.0. PC. STN: 10502-2.0-00.

154791 LBNL (Lawrence Berkeley National Laboratory) 2001. *Software Routine: Delb.dat*. V1.0. PC. STN: 10507-1.0-00.

154792 LBNL (Lawrence Berkeley National Laboratory) 2001. S*oftware Routine: Gpzones.dat*. V1.0. PC. STN: 10509-1.0-00.

162038 LBNL (Lawrence Berkeley National Laboratory) 2002. *Software Code: Tin*. V1.1. PC Windows 98. 10899-1.1-00.

161491 LBNL (Lawrence Berkeley National Laboratory) 2003. *Software Code: TOUGH2*. V1.6. PC/MS-DOS under Windows 98, Sun UltraSparc OS 5.5.1, DEC-Alpha OSF1 V4.0. 10007-1.6-01.

9.2 CODES, STANDARDS, REGULATIONS, AND PROCEDURES

156605 10 CFR 63. Energy: Disposal of High-Level Radioactive Wastes in a Geologic Repository at Yucca Mountain, Nevada. Readily available.

AP-2.22Q, Rev. 0, ICN 1. *Classification Criteria and Maintenance of the Monitored Geologic Repository Q-List.* Washington, D.C.: U.S. Department of Energy, Office of Civilian Radioactive Waste Management. ACC: DOC.20030422.0009.

AP-SI.1Q, Rev. 5, ICN 1. *Software Management*. Washington, D.C.: U.S. Department of Energy, Office of Civilian Radioactive Waste Management. ACC: DOC.20030708.0001.

9.3 SOURCE DATA, LISTED BY DATA TRACKING NUMBER

148120 LB000300123142.001. Thermal-Hydrological Simulations of the Drift Scale Test. AMR N0000, Thermal Tests Thermal Hydrological Analysis/Model Report. Submittal date: 03/24/2000.

162179 LB0110AIRK0015.001. Developed Data for Air-K Tests. Submittal date: 11/12/2001.

159525 LB0205REVUZPRP.001. Fracture Properties for UZ Model Layers Developed from Field Data. Submittal date: 05/14/2002.

160897 LB0208AIRKDSTH.001. Air Permeability Data for the Heating Phase of the DST. Submittal date: 08/09/2002.

161243 LB0208UZDSCPMI.002. Drift-Scale Calibrated Property Sets: Mean Infiltration Data Summary. Submittal date: 08/26/2002.

160799 LB0210THRMLPRP.001. Thermal Properties of UZ Model Layers: Data Summary. Submittal date: 10/25/2002.

111475 LB990501233129.004. 3-D UZ Model Calibration Grids for AMR U0000, "Development of Numerical Grids of UZ Flow and Transport Modeling". Submittal date: 09/24/1999.

162183 LB991131233129.004. Modeling of Thermo-Hydrological Data to Simulate Flow, Transport, and Geothermal Conditions of the UZ Model. AMR U0050, "UZ Flow Models and Submodels". Submittal date: 03/11/2000.

142884 LL000114004242.090. TSPA-SR Mean Calculations. Submittal date: 01/28/2000.

147304 MO0002ABBLSLDS.000. As-Built Borehole Locations and Sensor Locations for the Drift Scale Test Given in Local (DST) Coordinates. Submittal date: 02/01/2000.

153848 MO0004RIB00035.001. Rock Thermal Expansion. Submittal date: 04/07/2000.

161129 MO0208RESTRDST.002. Restructured Drift Scale Test (DST) Heating Phase Power and Temperature Data. Submittal date: 08/06/2002.

161496 MO0301SEPFEPS1.000. LA FEP List. Submittal date: 01/21/2003.

103769 MO9901MWDGFM31.000. Geologic Framework Model. Submittal date: 01/06/1999.

148524 MO9911SEPGRP34.000. Geotechnical Rock Properties. Submittal date: 11/10/1999.

129272 MO9912SEPDOIHP.000. Determination of Outer/Inner Heater Power Ratio Using Heater Power Data. Submittal date: 12/16/1999.

162046 SN0207F3912298.037. Summary of Smoothed Measurements of Displacement Data for the Heating Phase of the Drift Scale Test (with Results from 12/3/1997 through 1/14/2002). Submittal date: 07/15/2002.

161876 SN0301F4102102.006. Rock Mass Mechanical Properties, Slot Test #3, Location 21+25 in the ECRB. Submittal date: 01/14/2003.

129168 SNL01B05059301.006. Laboratory Thermal Expansion Data for Boreholes UE25 NRG-4, NRG-5; USW NRG-6 and NRG-7/7A. Submittal date: 02/07/1996.

9.4 OUTPUT DATA, LISTED BY DATA TRACKING NUMBER

LB0306DRSCLTHM.001. Drift Scale THM Model Predictions: Simulations. Submittal date: 06/26/2003.

LB0306DRSCLTHM.002. Drift Scale THM Model Predictions: Summary Plots. Submittal date: 06/26/2003.

LB0306DSTTHMVL.001. DST and Niche THM Model Validation: Simulations. Submittal date: 06/26/2003.

LB0306DSTTHMVL.002. DST and Niche THM Model Validation: Summary Plots Values. Submittal date: 06/26/2003.

INTENTIONALLY LEFT BLANK

ATTACHMENT I—Calibration of α and b_{max}

The calibration of α and b_{max} in Section 6.4 was conducted using MS Excel 97 SR-2 spreadsheets. Two spreadsheets were constructed: (1) a spreadsheet to determine combinations of α and b_{max} satisfying $F_{kr} = 0.125$ (red line in Figure 6.4-3), and (2) a spreadsheet to determine combinations of α and b_{max} satisfying $F_{ke} = 9$ (blue line in Figure 6.4-3).

1. Spreadsheet for determining combinations of α and b_{max} satisfying $F_{kr} = 0.125$ (red line in Figure 6.4-3)

A spreadsheet was developed in MS Excel 97 SR-2 to calculate F_{kr} for fixed inputs of initial stresses, initial permeability, and fracture frequency, and for variable inputs of α and b_{max}. The spreadsheet has been submitted to TDMS Output–DTN: LB0306DSTTHMVL.002 file *dst_fkr.xls*. It performs calculations in the following steps:

1) Calculate initial fracture aperture (b_i) from initial permeability (k_i) and fracture frequency (f) according to:

$$b_i = \sqrt[3]{6 \times k_i / f} \qquad \text{(Eq. I-1)}$$

2) Calculate the residual fracture apertures (b_{1r}, b_{2r}, b_{3r}) for fractures belonging to set 1, 2, and 3, respectively, according to:

$$b_{1r} = b_i + b_{\max}\left[-\exp(\alpha\sigma_{xi})\right] \qquad \text{(Eq. I-2)}$$

$$b_{2r} = b_i + b_{\max}\left[-\exp(\alpha\sigma_{yi})\right] \qquad \text{(Eq. I-3)}$$

$$b_{3r} = b_i + b_{\max}\left[-\exp(\alpha\sigma_{zi})\right] \qquad \text{(Eq. I-4)}$$

where σ_{ix}, σ_{iy}, and σ_{iz} are initial stresses, in x, y and z direction. Equations (I-2) to (I-4) are derived from Equation (6.2-9), assuming that the current stress is infinitely high, and hence fractures are compressed to their residual stage.

3) Calculate initial-to-residual permeability correction factors, F_{kxr}, F_{kyr} and F_{kzr} for x, y and z permeability, respectively, according to:

$$F_{kxr} = \frac{b_{2r}^3 + b_{3r}^3}{2b_i^3},\ F_{kyr} = \frac{b_{1r}^3 + b_{3r}^3}{2b_i^3},\ F_{kzr} = \frac{b_{1r}^3 + b_{2r}^3}{2b_i^3} \qquad \text{(Eq. I-4)}$$

4) Calculate the geometric mean of the permeability changes as:

$$F_{kr} = \sqrt[3]{F_{kxr} \times F_{kyr} \times F_{kzr}} \qquad \text{(Eq. I-6)}$$

Fixed inputs are: σ_{xi} = -3.46e6 Pa, σ_{xi} = -2.89e6 Pa, σ_{zi} = -5.77e6 Pa, k_i = 1e-13 m^2, f = 4.32 m^{-1} (Initial stress at DST is according to Figure 7.3-1b, based on Assumtion 2 in Section 5; permeabilty and frequency are extracted from Table 4.1.3 for the Tptpmn unit).

Variable inputs are α (in Pa^{-1}) and b_{max} (in m)

Final output is F_{kr}, which should be matched to be close to 0.125.

A hard copy of the spreadsheet is provided below. In this case, b_{max} was varied between 1.0e-4 and 2.5e-4 m. For each b_{max}, the α value that gave the closest match of F_{kr} to 0.125 was determined by trial and error. This was conducted by entering different values in the α column until the best possible match of F_{kr} to 0.125 was obtained. The best match was determined for one decimal point of the α value.

Input	Input	Input	Input	Input	Varied	Calibrated
Sig_xi	Sig_yi	Sig_zi	k_i	freq	bmax	alpha
-3.46E+06	-2.89E+06	-5.77E+06	1.00E-13	4.32	1.000E-04	3.40E-07
-3.46E+06	-2.89E+06	-5.77E+06	1.00E-13	4.32	1.500E-04	4.50E-07
-3.46E+06	-2.89E+06	-5.77E+06	1.00E-13	4.32	2.000E-04	5.20E-07
-3.46E+06	-2.89E+06	-5.77E+06	1.00E-13	4.32	2.500E-04	5.80E-07
-3.46E+06	-2.89E+06	-5.77E+06	1.00E-13	4.32	3.000E-04	6.30E-07
-3.46E+06	-2.89E+06	-5.77E+06	1.00E-13	4.32	3.500E-04	6.70E-07
-3.46E+06	-2.89E+06	-5.77E+06	1.00E-13	4.32	4.000E-04	7.10E-07

(For visibility the spreadsheet in file *dst_fkr.xls* is spit into two tables on this page)

Calculated	Calculated	Calculated	Calculated	Calculated	Calculated	Calculated	Matched
b_i	b_r1	b_r2	b_r3	F_krx	F_kry	F_krz	F_ke
5.18E-05	2.09E-05	1.44E-05	3.77E-05	0.203953	0.226403	0.043741	0.1264
5.18E-05	2.02E-05	1.09E-05	4.06E-05	0.245749	0.270601	0.034248	0.1316
5.18E-05	1.87E-05	7.29E-06	4.18E-05	0.264955	0.287107	0.024937	0.1238
5.18E-05	1.82E-05	5.02E-06	4.30E-05	0.286405	0.307592	0.022095	0.1249
5.18E-05	1.79E-05	3.21E-06	4.39E-05	0.30413	0.324547	0.020656	0.1268
5.18E-05	1.73E-05	1.30E-06	4.45E-05	0.316321	0.335048	0.018743	0.1257
5.18E-05	1.75E-05	3.91E-07	4.51E-05	0.331039	0.350322	0.019284	0.1308

The values of b_{max} and α in the above table are plotted as the red line Figure 6.4-3. Note that the units for bmax and α are m and Pa^{-1}, in the above table, whereas the units in are respectively μm and MPa^{-1} in Figure 6.4-3.

The above spreadsheet has been submitted to TDMS Output-DTN: LB0306DSTTHMVL.002 file *dst_fkr.xls.*

2. Combinations of α and b_{max} satisfying F_{ke} = 9 *(blue line in Figure 6.4-3)*

A spreadsheet was developed in MS Excel 97 SR-2 to calculate F_{ke} for fixed inputs of pre-excavation (initial) stresses, post-excavation stresses, initial permeability, and fracture frequency, and for variable inputs of α and b_{max}. The spreadsheet has been submitted to TDMS Output-

DTN: LB0306DSTTHMVL.002 file *niche_fke.xls*. The spreadsheet performs calculations in the following steps:

1) Calculate initial fracture aperture (b_i) from initial permeability (k_i) and fracture frequency (f) according to Equation (I-1).

2) Calculate post-excavation fracture apertures (b_{1e}, b_{2e}, b_{3e}) for fractures belonging to set 1, 2, and 3, respectively, according to:

$$b_{1e} = b_i + b_{\max}\left[\exp(\alpha\sigma_{xe}) - \exp(\alpha\sigma_{xi})\right] \quad \text{(Eq. I-7)}$$

$$b_{2e} = b_i + b_{\max}\left[\exp(\alpha\sigma_{ye}) - \exp(\alpha\sigma_{yi})\right] \quad \text{(Eq. I-8)}$$

$$b_{3e} = b_i + b_{\max}\left[\exp(\alpha\sigma_{ze}) - \exp(\alpha\sigma_{zi})\right] \quad \text{(Eq. I-9)}$$

where σ_{ix}, σ_{iy}, and σ_{iz} are pre-excavation (initial) stresses and σ_{xe}, σ_{ye}, and σ_{ze} are post-excavation stresses, in x, y and z direction respectively. Equations (I-7) to (I-8) are derived from Equation (6.2-9) assuming that the current stress is the stress after excavation.

3) Calculate pre- to post excavation correction factors, F_{kxe}, F_{kye} and F_{kze} for x, y and z permeability, respectively according to:

$$F_{kxe} = \frac{b_{2e}^3 + b_{3e}^3}{2b_i^3},\ F_{kye} = \frac{b_{1e}^3 + b_{3e}^3}{2b_i^3}, F_{kze} = \frac{b_{1e}^3 + b_{2e}^3}{2b_i^3} \quad \text{(Eq. I-10)}$$

4) Calculate the geometric mean of the permeability changes as:

$$F_{ke} = \sqrt[3]{F_{kxe} \times F_{kye} \times F_{kze}} \quad \text{(Eq. I-11)}$$

Fixed inputs are: σ_{xi} = -3.19e6 Pa, σ_{xi} = -2.65e6 Pa, σ_{zi} = -5.31e6 Pa, σ_{xe} = -4.05e6 Pa, σ_{ye} = -1.88e6 Pa, σ_{ze} = -7.50e5 Pa, k_i = 1e-13 m^2, f = 4.32 m^{-1} (Stress values are given in Wang 2003 [162654], SN-LBNL-SCI-204-V2, p. 125, initial permeability is 1e-13 m^2 to be consistent with the initial permeability assumed for calibration against F_{kr} above, and fracture frequency is extracted from Table 4.1.3 for the Tptpmn unit).

Variable inputs are α (in Pa^{-1}) and b_{max} (in m)

Final output is F_{ke}, which should be matched to be close to 9.0

A hard copy of the spreadsheet is provided below. In this case, b_{max} was varied between 1.978e-4 and 2.5e-4 m. For each b_{max}, the α value that gave the closest match of F_{ke} to 9.0 was determined by trial and error. This was conducted by entering different values in the α column until the best possible match of F_{ke} to 9.0 was obtained. The best match was determined for one decimal point of the α value.

Input	Input	Input	Input	Input	Input	Input	Input
Sig_xi	Sig_yi	Sig_zi	Sig_xe	Sig_ye	Sig_ze	k_i	freq
-3.19E+06	-2.65E+06	-5.31E+06	-4.05E+06	-1.88E+06	-7.50E+05	1.00E-13	4.32
-3.19E+06	-2.66E+06	-5.31E+06	-4.05E+06	-1.88E+06	-7.50E+05	1.00E-13	4.32
-3.19E+06	-2.66E+06	-5.31E+06	-4.05E+06	-1.88E+06	-7.50E+05	1.00E-13	4.32
-3.19E+06	-2.66E+06	-5.31E+06	-4.05E+06	-1.88E+06	-7.50E+05	1.00E-13	4.32
-3.19E+06	-2.66E+06	-5.31E+06	-4.05E+06	-1.88E+06	-7.50E+05	1.00E-13	4.32
-3.19E+06	-2.66E+06	-5.31E+06	-4.05E+06	-1.88E+06	-7.50E+05	1.00E-13	4.32
-3.19E+06	-2.66E+06	-5.31E+06	-4.05E+06	-1.88E+06	-7.50E+05	1.00E-13	4.32
-3.19E+06	-2.66E+06	-5.31E+06	-4.05E+06	-1.88E+06	-7.50E+05	1.00E-13	4.32
-3.19E+06	-2.66E+06	-5.31E+06	-4.05E+06	-1.88E+06	-7.50E+05	1.00E-13	4.32
-3.19E+06	-2.66E+06	-5.31E+06	-4.05E+06	-1.88E+06	-7.50E+05	1.00E-13	4.32
-3.19E+06	-2.66E+06	-5.31E+06	-4.05E+06	-1.88E+06	-7.50E+05	1.00E-13	4.32
-3.19E+06	-2.66E+06	-5.31E+06	-4.05E+06	-1.88E+06	-7.50E+05	1.00E-13	4.32
-3.19E+06	-2.66E+06	-5.31E+06	-4.05E+06	-1.88E+06	-7.50E+05	1.00E-13	4.32
-3.19E+06	-2.66E+06	-5.31E+06	-4.05E+06	-1.88E+06	-7.50E+05	1.00E-13	4.32

(For visibility the spreadsheet file *niche_fke.xls* is split into two tables on this page)

Varied	Calibrated	Calculated	Calculated	Calculated	Calculated	Calculated	Calculated	Calculated	Matched
bmax	alpha	b_i	b_e1	b_e2	b_e3	F_kex	F_key	F_kez	F_ke
2.500E-04	9.20E-07	5.179E-05	4.45E-05	7.43E-05	1.75E-04	20.87	19.71	1.79	9.04
2.200E-04	7.30E-07	5.179E-05	4.18E-05	7.60E-05	1.74E-04	20.70	19.38	1.84	9.04
2.100E-04	6.50E-07	5.179E-05	4.05E-05	7.64E-05	1.74E-04	20.60	19.24	1.84	9.01
2.050E-04	6.00E-07	5.179E-05	3.96E-05	7.66E-05	1.74E-04	20.59	19.20	1.84	8.99
2.040E-04	5.80E-07	5.179E-05	3.92E-05	7.67E-05	1.74E-04	20.74	19.33	1.84	9.04
2.000E-04	5.20E-07	5.179E-05	3.81E-05	7.69E-05	1.75E-04	20.78	19.35	1.83	9.03
1.978E-04	4.60E-07	5.179E-05	3.69E-05	7.69E-05	1.75E-04	20.82	19.37	1.82	9.02
1.978E-04	4.60E-07	5.179E-05	3.69E-05	7.69E-05	1.75E-04	20.82	19.37	1.82	9.02
1.980E-04	4.20E-07	5.179E-05	3.61E-05	7.69E-05	1.75E-04	20.93	19.46	1.81	9.03
2.000E-04	3.70E-07	5.179E-05	3.50E-05	7.68E-05	1.75E-04	21.02	19.54	1.79	9.02
2.040E-04	3.30E-07	5.179E-05	3.42E-05	7.67E-05	1.76E-04	21.15	19.67	1.77	9.02
2.100E-04	2.90E-07	5.179E-05	3.34E-05	7.64E-05	1.76E-04	21.14	19.66	1.74	8.98
2.200E-04	2.50E-07	5.179E-05	3.26E-05	7.61E-05	1.76E-04	21.16	19.70	1.71	8.94
2.500E-04	1.90E-07	5.179E-05	3.12E-05	7.59E-05	1.77E-04	21.68	20.22	1.68	9.03

The values of b_{max} and α in the above table are plotted as the blue line in Figure 6.4-3. Note that the units for b_{max} and α are m and Pa $^{-1}$, in the above table, whereas the units are respectively µm and MPa^{-1} in Figure 6.4-3.

The above spreadsheet has been submitted to TDMS Output-DTN: LB0306DSTTHMVL.002 file *niche_fke.xls*.

ATTACHMENT II—Statistical Analysis of Displacement Data

A statistical evaluation of the predicted MPBX displacements was conducted using an MS Excel 97 SR-2 spreadsheet. The spreadsheet has been submitted to TDMS Output-DTN: LB0306DSTTHMVL.002 file *u0250_displacement_comparison_statistics.xls.* First, the calculated and measured values of displacement were extracted from the x-y plots shown in Figure 7.4.2-2. The values were extracted in TECPLOT V8.0 using the data/probe command for x values of 6, 12, 18, 24, 30, 36, 42 and 48 months. The extracted displacements (in mm) for each anchor were entered into the spreadsheet as shown below. Yellow column shows simulated data for upper vertical (UV), lower vertical (LV) or 60° inclined (INC) extensometers (See Figure 7.4.2-1). Blue columns show measured data extracted from Figure 7.4.2-2, with empty cells indicating missing or bad data. Labels 1, 2, 3, and 4 in the table heads indicate, Anchors 1, 2, 3, or 4. The numbers in the table below are considered as input to this statistical analysis. Values of displacement in column 2 to 14 are in mm.

	147-1	148-1	149-1	150-1	154-1	155-1	156-1	157-1	178-1	179-1	180-1	SIM UV-1	SIM LV-1	SIM INC-1
	INC-1	INC-1	UV-1	LV-1	INC-1	INC-1	UV-1	LV-1	INC-1	INC-1	UV-1	SIM UV-1	SIM LV-1	SIM INC-1
0														
6	1.98	1.5		2.76		2.53	2.38	2.08	0.51	1.3	1.47	1.03	2.01	0.92
12	2.57	1.8		2.08	2.95	3.12	2.88					1.47	2.9	1.37
18	3.42	2.45		2.83	4.37	3.84						1.93	3.78	1.73
24	4.12	2.9		3.33	6.06	4.45						2.26	4.45	2.03
30	4.41	3.25		3.26	7.48	4.85						2.48	4.82	2.32
36	4.57	3.4		3.66	5.89	5.02						2.61	5.33	2.36
42	4.73	3.54		3.72	5.85	5.09						2.76	5.61	2.52
48	4.84	3.65		3.96	6.02	5.32						2.78	5.62	2.52

	147-2	148-2	149-2	150-2	154-2	155-2	156-2	157-2	178-2	179-2	180-2	SIM UV-2	SIM LV-2	SIM INC-2
	INC-2	INC-2	UV-2	LV-2	INC-2	INC-2	UV-2	LV-2	INC-2	INC-2	UV-2	SIM UV-2	SIM LV-2	SIM INC-2
0														
6	2.51	1.52		2.75	2.02	3.04	2.73			2.32	1.45	1.2	2.33	1.43
12	3.25	1.8	2.68	3.95		3.55	3.32	3.3	2.62			1.92	3.51	2.08
18		2.33		4.4		4.54		4.02	3.16			2.52	4.58	2.66
24	5.14	2.87		5.11		5.2	5.89	4.9	3.57		2.41	3.05	5.38	3.18
30	5.67	3.4		5.75		5.64	7.32	5.6	3.9		2.78	3.46	5.82	3.62
36	5.96	3.74		6.21		5.85	8.12	6.02	4.04		3.02	3.73	6.56	3.86
42	6.1	3.98		6.42		5.73	8.57	6.27	3.54		2.45	4.01	6.9	4.15
48	6.25	4.16		6.75		6.09	8.97	6.6	4.07		3.06	4.09	6.94	4.23

	147-3	148-3	149-3	150-3	154-3	155-3	156-3	157-3	178-3	179-3	180-3	SIM UV-3	SIM LV-3	SIM INC-3
	INC-3	INC-3	UV-3	LV-3	INC-3	INC-3	UV-3	LV-3	INC-3	INC-3	UV-3	SIM UV-3	SIM LV-3	SIM INC-3
0														
6	2.61	2.63	2.99	3.06	3.25	3.13	2.28			2.09	2.34	1.62	2.45	1.77
12	3.56	3.43	4.12	4.95	2.43	3.96	3.08		3.63	2.64		2.82	4.06	2.95
18		4.31	5.05			4.97			4.42			3.68	5.48	3.81
24	5.41	4.98	5.81		3.7	5.81	4.21		5.14			4.36	6.51	4.49
30	6.02	5.46	6.49		4.22	6.33	4.45		5.77			4.92	7.09	5.09
36	6.51	5.81	6.9		4.53	6.73	4.68		6.15			5.3	7.96	5.51
42	6.72	6.14	7.2		4.8		4.91		6.68			5.8	8.36	6.02
48	7.01	6.51	7.49		5.03		5.19		6.96			6.05	8.43	6.25

	147-4	148-4	149-4	150-4	154-4	155-4	156-4	157-4	178-4	179-4	180-4	SIM UV-4	SIM LV-4	SIM INC-4
	INC-4	INC-4	UV-4	LV-4	INC-4	INC-4	UV-4	LV-4	INC-4	INC-4	UV-4	SIM UV-4	SIM LV-4	SIM INC-4
0														
6	2.54	1.9	1.89	2.15		2.22	2.4		2.3	1.97	1.43	0.3	1.36	0.85
12	4.07	3.32	3.45	4.05	3.38	3.08	3.29	3.2	3.49	3.42		1.58	3.01	2.36
18	5.63		4.72	5.08	5.37	4.03		4.28	4.68			2.7	4.63	3.69
24	7.07		5.97	6.27	7.12	4.82	6.6	5.24	6.03		4.97	3.95	6.17	5.04
30	8.32		7.06	7.64	8.64	5.44	8.35	6.16	7.29		6.01	5.6	7.36	6.13
36	8.49		7.88	8.54	9.58	5.98	9.3	6.54	8.21		6.66	6.14	8.74	7.3
42	7.06		8.42	8.95	10.21	5.96	10.1	6.81	9.35		7.41	7.09	9.61	8.2
48	7		8.96	9.37	10.76	6.5	10.82	7.28	8.72		7.98	7.79	10.23	8.97

As described in Section 7.4.2, the three statistical measures considered are: root-mean-square-difference (RMSD), mean-difference (MD) and normalized-absolute-mean difference (NAMD). The equations for calculating RMSD, MD, and NAMD are given in Section 7.4.2. The statistical evaluation was made for all anchor categories 1, 2, 3 and 4 separately, as well as for all anchors combined at 6,12, 18, 24, 30, 36, 42, and 48 months. As an example, the calculations of RMSD, MD, and NAMD at 12 months are given below (simulated and measured values are in mm):

SIM-1-12m	MEA-1-12m	sim-mea	(sim-mea)^2	abs((sim-mea)/mea)
1.47	2.88	-1.410	1.988	0.490
2.9	2.08	0.820	0.672	0.394
1.37	2.57	-1.200	1.440	0.467
1.37	1.8	-0.430	0.185	0.239
1.37	2.95	-1.580	2.496	0.536
1.37	3.12	-1.750	3.063	0.561
		MD	RMSD	NAMD
		-0.925	1.281	0.448
SIM-2-12m	MEA-2-12m	sim-mea	(sim-mea)^2	abs((sim-mea)/mea)
1.92	3.32	-1.400	1.960	0.422
3.51	3.3	0.210	0.044	0.064
3.51	3.95	-0.440	0.194	0.111
2.08	3.25	-1.170	1.369	0.360
2.08	1.8	0.280	0.078	0.156
2.08	3.55	-1.470	2.161	0.414
2.08	2.62	-0.540	0.292	0.206
		MD	RMSD	NAMD
		-0.522	0.933	0.247
SIM-3-12m	MEA-3-12m	sim-mea	(sim-mea)^2	abs((sim-mea)/mea)
2.82	4.12	-1.300	1.690	0.316
2.82	3.08	-0.260	0.068	0.084
4.06	4.95	-0.890	0.792	0.180
2.95	3.56	-0.610	0.372	0.171
2.95	3.43	-0.480	0.230	0.140
2.95	2.43	0.520	0.270	0.214
2.95	3.96	-1.010	1.020	0.255
2.95	3.63	-0.680	0.462	0.187
2.95	2.64	0.310	0.096	0.117
		MD	RMSD	NAMD
		-0.325	0.745	0.185
SIM-4-12m	MEA-4-12m	sim-mea	(sim-mea)^2	abs((sim-mea)/mea)
1.58	3.45	-1.870	3.497	0.542
1.58	3.29	-1.710	2.924	0.520
3.01	4.05	-1.040	1.082	0.257
3.01	3.2	-0.190	0.036	0.059
2.36	4.07	-1.710	2.924	0.420
2.36	3.32	-0.960	0.922	0.289
2.36	3.38	-1.020	1.040	0.302
2.36	3.08	-0.720	0.518	0.234
2.36	3.49	-1.130	1.277	0.324
2.36	3.42	-1.060	1.124	0.310
		MD	RMSD	NAMD
		-1.100	1.056	0.274
		MD-all	RMSD-all	NAMD-all
		-0.809	1.065	0.292

The values for MD-all, RMSD-all and NAMD-all on the previous page are the outputs for 12 months from this statistical analysis. The complete output from this analysis is listed below:

Time (months)	MD-all	RMSD-all	NAMD-all
6	-0.937	1.086	0.436
12	-0.809	1.065	0.292
18	-0.868	1.307	0.261
24	-0.946	1.597	0.251
30	-0.982	1.812	0.238
36	-0.611	1.928	0.252
42	-0.487	1.830	0.257
48	-0.494	1.898	0.236

Numbers in the table on this page define the curves in Figure 7.4.2-3. As shown in Figure 7.4.2-3 the units for MD-all, RMSD-all, and NAMD-all are mm, mm, and fraction (unitless), respectively.

The entire spreadsheet for this calculation has been submitted to TDMS Output DTN: LB0306DSTTHMVL.002 file *u0250_displacement_comparison_statistics.xls*

ATTACHMENT III—Calculated Permeability Change Ratio at Niche Tests

In Section 7.5 of this Model Report, the calibrated stress permeability function is tested against air-permeability measurements conducted at several niches over a range of initial permeability values. The UM calculated log permeability change ratio in Figures 7.5.1 and 7.5.2 was calculated using an MS Excel 97 SR-2 spreadsheet similar to the ones developed in ATTACHMENT I. The spreadsheet for this calculation has been submitted to TDMS Output-DTN: LB0306DSTTHMVL.002 file *u0250_niche_validation.xls.*

Inputs for this analysis are pre-excavation (initial) stresses, post-excavation stresses, initial permeability, fracture frequency, and the parameters α and b_{max}. The spreadsheet performs the calculations in the following steps:

1) Calculate initial fracture aperture (b_i) from initial permeability (k_i) and fracture frequency (f) according to Equation (I-1).

2) Calculate post-excavation fracture apertures (b_{1e}, b_{2e}, b_{3e}) for fractures belonging to set 1, 2, and 3, respectively, according to Equation (I-7).

3) Calculate pre- to post-excavation correction factors F_{ke1}, F_{ke2} and F_{ke1} for individual fractures belonging to fracture set 1, 2 and 3, respectively, according to:

$$F_{ke1} = \left(\frac{b_{1e}}{b_i}\right)^3,\ F_{ke2} = \left(\frac{b_{2e}}{b_i}\right)^3, F_{ke1} = \left(\frac{b_{e3}}{b_i}\right)^3 \qquad \text{(Eq. III-1)}$$

4) Calculate pre- to post excavation correction factors, F_{kxe}, F_{kye} and F_{kze} for x, y and z permeability, respectively according to Equation (I-10).

5) Calculate the geometric mean of the permeability changes according to Equation (I-11),

Fixed inputs are:

σ_{xi} = -3.19e6 Pa, σ_{xi} = -2.65e6 Pa, σ_{zi} = -5.31e6 Pa

(Source: Wang 2003 [162654], SN-LBNL-SCI-204-V2, p. 125)

σ_{xe} = -4.05e6 Pa, σ_{xe} = -1.88e6 Pa, σ_{ze} = -7.50e5 Pa

(Source: Wang 2003 [162654], SN-LBNL-SCI-204-V2, p. 125)

f = 4.32 m^{-1} (Extracted from Table 4.1.3 for the Tptpmn unit).

b_{max} = 200e-6 m, α = 0.52e-6 Pa^{-1} (Calibrated in Section 6.4)

Variable input is the initial permeability, k_i

A hard copy of the spreadsheet in file *u0250_niche_validation.xls* is provided on the next page.

Input	Input	Input	Input	Input	Input	Input	Input	Input	Varied	Calculated
Sig_xi	Sig_yi	Sig_zi	Sig_xe	Sig_ye	Sig_ze	freq	bmax	alpha	k_i	Log(k_i)
-3.19E+06	-2.65E+06	-5.31E+06	-4.05E+06	-1.88E+06	-7.50E+05	4.32	2.000E-04	5.20E-07	1.00E-08	-8
-3.19E+06	-2.66E+06	-5.31E+06	-4.05E+06	-1.88E+06	-7.50E+05	4.32	2.000E-04	5.20E-07	6.00E-09	-8.221849
-3.19E+06	-2.66E+06	-5.31E+06	-4.05E+06	-1.88E+06	-7.50E+05	4.32	2.000E-04	5.20E-07	2.00E-09	-8.69897
-3.19E+06	-2.66E+06	-5.31E+06	-4.05E+06	-1.88E+06	-7.50E+05	4.32	2.000E-04	5.20E-07	1.00E-09	-9
-3.19E+06	-2.66E+06	-5.31E+06	-4.05E+06	-1.88E+06	-7.50E+05	4.32	2.000E-04	5.20E-07	6.00E-10	-9.221849
-3.19E+06	-2.66E+06	-5.31E+06	-4.05E+06	-1.88E+06	-7.50E+05	4.32	2.000E-04	5.20E-07	2.00E-10	-9.69897
-3.19E+06	-2.66E+06	-5.31E+06	-4.05E+06	-1.88E+06	-7.50E+05	4.32	2.000E-04	5.20E-07	1.00E-10	-10
-3.19E+06	-2.66E+06	-5.31E+06	-4.05E+06	-1.88E+06	-7.50E+05	4.32	2.000E-04	5.20E-07	6.00E-11	-10.22185
-3.19E+06	-2.66E+06	-5.31E+06	-4.05E+06	-1.88E+06	-7.50E+05	4.32	2.000E-04	5.20E-07	2.00E-11	-10.69897
-3.19E+06	-2.66E+06	-5.31E+06	-4.05E+06	-1.88E+06	-7.50E+05	4.32	2.000E-04	5.20E-07	1.00E-11	-11
-3.19E+06	-2.66E+06	-5.31E+06	-4.05E+06	-1.88E+06	-7.50E+05	4.32	2.000E-04	5.20E-07	6.00E-12	-11.22185
-3.19E+06	-2.66E+06	-5.31E+06	-4.05E+06	-1.88E+06	-7.50E+05	4.32	2.000E-04	5.20E-07	2.00E-12	-11.69897
-3.19E+06	-2.66E+06	-5.31E+06	-4.05E+06	-1.88E+06	-7.50E+05	4.32	2.000E-04	5.20E-07	1.00E-12	-12
-3.19E+06	-2.66E+06	-5.31E+06	-4.05E+06	-1.88E+06	-7.50E+05	4.32	2.000E-04	5.20E-07	6.00E-13	-12.22185
-3.19E+06	-2.66E+06	-5.31E+06	-4.05E+06	-1.88E+06	-7.50E+05	4.32	2.000E-04	5.20E-07	2.00E-13	-12.69897
-3.19E+06	-2.66E+06	-5.31E+06	-4.05E+06	-1.88E+06	-7.50E+05	4.32	2.000E-04	5.20E-07	1.00E-13	-13
-3.19E+06	-2.66E+06	-5.31E+06	-4.05E+06	-1.88E+06	-7.50E+05	4.32	2.000E-04	5.20E-07	6.00E-14	-13.22185
-3.19E+06	-2.66E+06	-5.31E+06	-4.05E+06	-1.88E+06	-7.50E+05	4.32	2.000E-04	5.20E-07	2.00E-14	-13.69897
-3.19E+06	-2.66E+06	-5.31E+06	-4.05E+06	-1.88E+06	-7.50E+05	4.32	2.000E-04	5.20E-07	1.00E-14	-14
-3.19E+06	-2.66E+06	-5.31E+06	-4.05E+06	-1.88E+06	-7.50E+05	4.32	2.000E-04	5.20E-07	6.00E-15	-14.22185
-3.19E+06	-2.66E+06	-5.31E+06	-4.05E+06	-1.88E+06	-7.50E+05	4.32	2.000E-04	5.20E-07	2.00E-15	-14.69897
-3.19E+06	-2.66E+06	-5.31E+06	-4.05E+06	-1.88E+06	-7.50E+05	4.32	2.000E-04	5.20E-07	1.00E-15	-15

(For visibility, the spreadsheet in *u0250_niche_validation.xls.* is split into two tables on this page; some intermediate calculation columns are not shown)

Calculated	Calculated	Calculated	Calculated	Calculate	Calculated	Calculated
Log(F_k1e)	Log(F_k2e)	Log(F_k3e)	Log(F_kxe)	Log(F_kye)	Log(F_kze)	Log(F_ke)
-0.0075	0.0134	0.0649	0.0399	0.0302	0.0031	0.0244
-0.0089	0.0160	0.0766	0.0474	0.0360	0.0038	0.0290
-0.0128	0.0230	0.1091	0.0682	0.0524	0.0055	0.0420
-0.0161	0.0290	0.1360	0.0858	0.0666	0.0070	0.0531
-0.0191	0.0343	0.1598	0.1015	0.0795	0.0084	0.0631
-0.0277	0.0492	0.2246	0.1457	0.1165	0.0124	0.0915
-0.0350	0.0616	0.2772	0.1826	0.1486	0.0160	0.1157
-0.0416	0.0728	0.3227	0.2155	0.1777	0.0193	0.1375
-0.0604	0.1037	0.4434	0.3059	0.2608	0.0293	0.1987
-0.0766	0.1293	0.5376	0.3798	0.3310	0.0385	0.2498
-0.0914	0.1520	0.6169	0.4439	0.3935	0.0471	0.2948
-0.1339	0.2140	0.8179	0.6134	0.5628	0.0740	0.4167
-0.1711	0.2643	0.9669	0.7444	0.6964	0.0990	0.5133
-0.2055	0.3079	1.0878	0.8535	0.8083	0.1230	0.5949
-0.3078	0.4239	1.3789	1.1235	1.0867	0.1967	0.8023
-0.4013	0.5147	1.5831	1.3177	1.2866	0.2634	0.9559
-0.4916	0.5913	1.7430	1.4716	1.4445	0.3248	1.0803
-0.7868	0.7862	2.1108	1.8299	1.8104	0.4966	1.3790
-1.1030	0.9312	2.3576	2.0725	2.0567	0.6342	1.5878
-1.4730	1.0492	2.5456	2.2582	2.2446	0.7495	1.7508
-4.8940	1.3343	2.9648	2.6738	2.6638	1.0333	2.1236
	1.5351	3.2379	2.9454	2.9369	1.2339	2.3721

Numbers in the orange columns in the two tables of on this page define the lines of calculated log change ratio in Figures 7.5-1 and 7.5-2.

The entire spreadsheet for this calculation has been submitted to TDMS Output-DTN: LB0306DSTTHMVL.002 file *u0250_niche_validation.xls.*